To the Graduate Council:

I am submitting herewith a thesis written by Jeffrey F. Gratz entitled "Paragenesis and Evolution of Mineralizing Fluids, Gordonsville Mine, Central Tennessee Zinc District." I have examined the final copy of this thesis for form and content and recommend that it be accepted in partial fulfillment of the requirements for the degree of Master of Science, with a major in Geology.

Kula C. Misra

Kula C. Misra, Major Professor

We have read this thesis
and recommend its acceptance:

Otto C. Kopp

Kenneth R. Walker

Accepted for the Council:

Lew Minkel

Vice Provost
and Dean of the Graduate School

STATEMENT OF PERMISSION TO USE

In presenting this thesis in partial fulfillment of the requirements for a Master's degree at The University of Tennessee, Knoxville, I agree that the Library shall make it available to borrowers under rules of the Library. Brief quotations from this thesis are allowable without special permission, provided that accurate acknowledgment of the source is made.

Permission for extensive quotation from or reproduction of this thesis may be granted by my major professor, or in his absence, by the Head of Interlibrary Services when, in the opinion of either, the proposed use of the material is for scholarly purposes. Any copying of use of the material in this thesis for financial gain shall not be allowed without my written permission.

Signature Jeffrey Shultz

Date January 12, 1986

PARAGENESIS AND EVOLUTION OF MINERALIZING FLUIDS, GORDONSVILLE MINE, CENTRAL TENNESSEE ZINC DISTRICT

A Thesis

Presented for the

Master of Science

Degree

The University of Tennessee, Knoxville

Jeffrey F. Gratz

March 1986

ACKNOWLEDGEMENTS

This thesis was prepared under the supervision of Dr. Kula C. Misra, who provided advice and encouragement during all stages of the research. I am also grateful to Drs. Kenneth R. Walker and Otto C. Kopp for their critical review of the manuscript. I wish to thank the Jersey Miniere Zinc Company for allowing me access to the Gordonsville mine, and special thanks to Fred Smith and Tony Parker for their guidance through the mine, help in sample collection, and interesting discussion of many of the topics relevant to this paper. I wish to acknowledge financial support from the Department of Geological Sciences Discretionary Fund at The University of Tennessee and grants-in-aid of research from Sima Xi, The Scientific Research Society and AIME, the American Institute of Mining and Metallurgical Engineering. And finally, thanks go to many of my fellow students who helped make my time here that much more enjoyable and to my parents, for their continuing support.

ABSTRACT

The Gordonsville zinc mine is located in the Central Basin section of the Interior Lowlands Physiographic Province of Middle Tennessee. The Gordonsville mine, along with the nearby Elmwood mine, are the major producers of zinc ore in the Central Tennessee zinc district. Ore-grade mineralization is believed to be confined to dissolution cavities and collapse breccias in the Mascot Formation, the upper unit of the Upper Cambrian - Lower Ordovician Knox Group. Sphalerite is the only zinc ore mineral in the district. Associated gangue minerals include fluorite, barite, calcite, galena, minor dolomite and quartz. Approximately two hundred samples were collected from several stopes in the Gordonsville mine in order to: (1) establish mineral paragenesis within the mine and, (2) through fluid inclusion and chemical analyses, determine the nature of ore fluids.

From petrographic and field study the generalized sequence of ore and gangue mineralization is as follows: early, white calcite - sphalerite - galena - fluorite - main-stage, white to lavender calcite - barite - late-stage, clear to amber calcite. Textural evidence suggests that these minerals were, for the most part, in equilibrium with circulating fluids throughout the mineralization period. Based on fluid inclusion data, trace element data, and petrographic evidence, the three textural varieties of

sphalerite (disseminated, massive, and vug-filling) appear to belong to the same depositional episode. Electron microprobe analyses of minor element concentrations in all sphalerite types suggest that microscopic color regions in sphalerite (white to deep orange) may be due to variations in cadmium content. The whiter areas contain the highest concentrations of cadmium (0.25 - 0.75 wt.%). Main-stage, white to lavender calcite and late-stage, clear to amber calcite could not be differentiated by the trace elements analyzed although they differ in color, crystal habit, formational temperatures and salinities.

Fluid inclusion analyses on ore and gangue minerals suggest that the mineralizing fluid changed in temperature and salinity through time. Homogenization temperatures for all minerals fall within the general range of 90° to 130°C. A decrease in fluid temperature of approximately 6°C following sphalerite deposition may have been sufficient to cause precipitation of fluorite. A further decrease in fluid temperature is suggested by inclusions in amber calcite (and barite?). Freezing temperatures, which provide an estimate of fluid salinities, remained fairly constant through main-stage calcite deposition (-17° - -22°C, corresponding to 20 - 23 equiv. wt.% NaCl). Precipitation of barite and late-stage, amber calcite, however, was marked by a large decrease in fluid salinity (7 - 12 equiv. wt.% NaCl).

The consistency and narrowly defined range of paired homogenization and freezing temperatures for fluid inclusions in sphalerite suggest that the ore mineral precipitated from one fluid rather than by the mixing of two or more fluids. Metals may have traveled with partly oxidized sulfur, or as chloride or organometallic complexes with reduced sulfur. Precipitation of fluorite and main-stage calcite was brought about by temperature and, possibly, compositional changes in the ore fluid. Limited carbon and oxygen isotope analyses of the three calcite stages show only minor variation and all data fall in or near the region of marine carbonates. This suggests that the slight decrease in fluid temperature and the marked decrease in fluid salinity during late-stage mineral precipitation was not necessarily due to an influx of meteoric water, although a meteoric component cannot be ruled out.

TABLE OF CONTENTS

LIST OF TABLES

LIST OF FIGURES

FIGURE PAGE

FIGURE PAGE

CHAPTER 1

INTRODUCTION

Purpose of Study

The Gordonsville and Elmwood mines are located in the Central Tennessee zinc district. The district became the focus of exploration in 1963, when geologists suggested the area near Murfreesboro, the apex of the Nashville Dome, as favorable for zinc deposits in the subsurface Lower Ordovician carbonate formations. This suggestion was based on the evidence that these formations were host to sphalerite ore in East Tennessee and that oil well cuttings as well as surface veins in Middle Tennessee contained small amounts of sphalerite. Also, the Lower Ordovician carbonates in Middle Tennessee occur within 600 meters of the surface over a large area providing easy access for drilling and mining operations (Winslow and Hill, 1973; Callahan, 1977; Gaylord and Briskey, 1983). Exploratory drilling confirmed the presence of ore-grade sphalerite in breccias and altered limestone in 1967. Production began at the Elmwood mine in August, 1975. Continued exploration led to the opening of the Gordonsville mine in early 1982, and it is presently the major ore producer in the district (Gaylord and Briskey, 1983).

Ore-grade mineralization in the district is believed to be confined to stratabound collapse breccias and dissolution cavities in the Mascot Formation, the upper unit of the Upper

Cambrian - Lower Ordovician Knox Group. The nature of mineralization as well as mineral associations (galena, dolomite, calcite, fluorite, and barite) are similar to those of zinc (+lead) deposits in Missouri, Illinois, and Kentucky. These deposits, including those in the East Tennessee zinc district have usually been classified as Mississippi Valley-type deposits (Hoagland, 1976). The Central Tennessee zinc district, however, is distinctly different from the nearby East Tennessee districts. Compared to the East Tennessee zinc deposits, the Central Tennessee deposits (1) occur in a tectonically stable area whereas those in East Tennessee lie in thrust faulted terrain, (2) are located in a higher stratigraphic position than those of East Tennessee, (3) generally have calcite rather than dolomite as the predominant gangue mineral, (4) contain relatively large amounts of barite, fluorite, and galena, (5) are characterized by much darker colored sphalerite, and (6) show more intense silicification (Gaylord and Briskey, 1983). Thus, results of investigations on the East Tennessee zinc deposits are not necessarily applicable to those of the Central Tennessee zinc district.

The two main objectives of this study were to establish the mineral paragenesis within the Gordonsville mine and to determine the nature of ore fluids. Understanding the sequence of mineralization is paramount to an understanding of the changing characteristics of ore fluids through time.

The paragenesis was inferred mainly from textural relationships among the minerals, both in the mine exposures and specimens; an attempt was also made to discriminate among possible different stages of sphalerite and calcite from their trace element compositions. Fluid inclusion geothermometry was used to determine the homogenization and freezing temperatures of fluid inclusions within sphalerite, fluorite, calcite, and barite. From this data base, minimum temperatures and approximate compositions of mineralizing fluids were determined. A limited number of calcite samples were also analyzed for their oxygen and carbon isotope ratios to provide additional constraints on ore-fluid composition.

Previous Work

As mining in the Central Tennessee zinc district is a relatively recent venture, research in the area, understandably, has been limited. Prior to the drilling program, details of the Upper Cambrian - Lower Ordovician Knox Group, host to ore-grade zinc mineralization, were unknown as the Knox Group is not exposed in the district (except at two cryptoexplosive sites). Recently, with access to underground stopes and drill cores, researchers have been able to gather information regarding Knox stratigraphy and post-depositional processes such as brecciation and mineralization (Stagg and Fischer, 1970; Gilbert and Hoagland, 1970; Kyle, 1973; Callahan, 1977; Gorody, 1980).

Several authors have outlined the paragenetic sequence of ore and gangue minerals in the district (Kyle, 1973, 1976; Kearns and Campbell, 1978; Larsen, 1978; Ferguson, 1981; Gaylord and Briskey, 1983); however, their interpretations are somewhat contradictory, particularly with respect to the position of the several stages of calcite. This study has attempted to resolve these conflicts and clarify terminology which has presented problems in previous publications.

In the earlier studies, fluid inclusion geothermometry was performed mostly on minerals from surface veins and a few cores. DeGroodt (1973) found that fluid inclusions in fluorite from surface veins and cores yielded formational or homogenization temperatures between 100° and 125°C. Fluid inclusions in fluorite, calcite and barite studied by Roedder (1971) gave homogenization temperatures ranging from 80° to 120°C; freezing temperatures from inclusions in fluorite ranged from -8° to below -30°C. In both studies, however, measurements were mostly limited to fluid inclusions in samples from surface vein exposures of fluorite. Recently, Seal et al. (1985) studied several sphalerite and fluorite samples from the Gordonsville mine with results similar to those of Roedder (1971) and DeGroodt(1973). The present study is the first detailed fluid inclusion analysis to be done on subsurface ore and gangue minerals with the aim of tracing the change in mineralizing fluids through time.

Only limited data are available on minor and trace element contents of ore and gangue minerals. There has been some quantitative and qualitative work on the trace element composition of early calcite in the Elmwood mine (Larsen, 1978) and of sphalerite in surface veins (Jolly and Heyl, 1968). Minor element determination in sphalerite has been performed on samples from Elmwood and Gordonsville mines (Larsen, 1978; Craig et al., 1983; Seal et al., 1985). Recently, Sr isotope measurements were obtained from gangue minerals at the Gordonsville and Elmwood mines in order to understand the depositional history (Grant and Bliss, 1983).

CHAPTER 2

GEOLOGIC SETTING

Location

The Gordonsville mine is located in the northeastern corner of the Central Basin section of the Interior Lowlands physiographic province in Middle Tennessee (Figure 1). Geographically, it lies approximately 80km east of Nashville in Smith County (Kyle, 1976; Callahan, 1977). The Interior Lowlands are bounded to the east and west by the Highland Rim, a wide topographic shelf of up to 400m in relief. The transition zone between these two provinces, where the Gordonsville and Elmwood mines are located, is an area characterized by rough topography with relief of about 150m. Structurally, the Central Basin is a broad anticline known as the Nashville Dome, which is, in turn, the southern extension of the Cincinnati Arch, a northeast trending uplift with gentle dips away from the apex at 10m/km (Winslow and Hill, 1973; Gaylord and Briskey, 1983). The Gordonsville mine lies just east of the apex of the Nashville Dome.

Stratigraphy

The Gordonsville zinc deposit is hosted by the Mascot Formation, the youngest of four formations within the Upper Cambrian - Lower Ordovician Knox Group (Figure 2). The

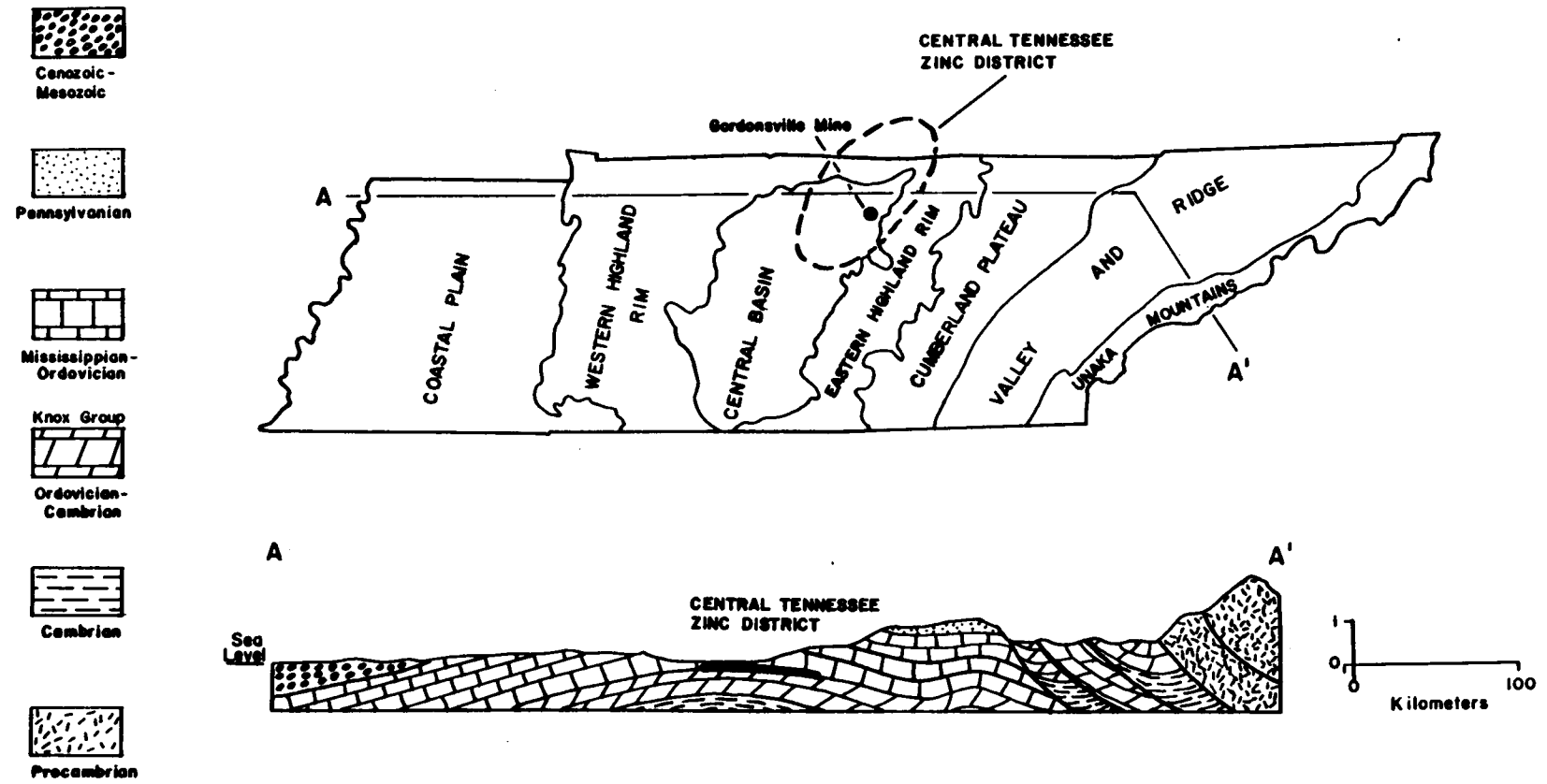

Figure 1. Location of Central Tennessee zinc district with respect to major physiographic provinces and geologic structures in Tennessee. Modified from Kyle (1976).

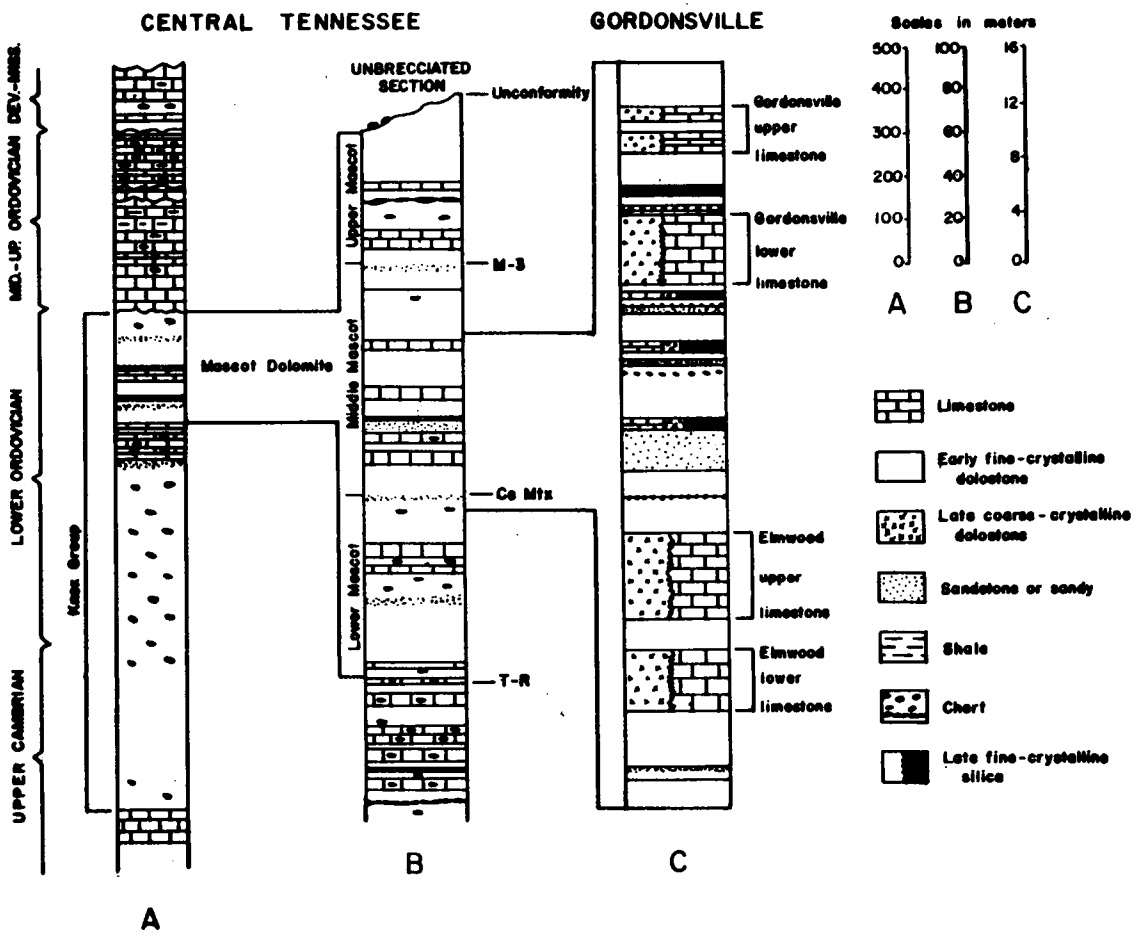

Figure 2. Generalized stratigraphic sections of Central Tennessee and the Gordonsville mine. The Gordonsville limestone (upper and lower) is the major ore horizon. Modified from Kyle (1976) and Gaylord and Briskey (1983).

Knox Group is 915m thick in the vicinity of the Gordonsville mine. Except at two small "cryptoexplosive" areas (Flynn and Wells Creek structures), the Knox Group is not exposed in Middle Tennessee. The Mascot Formation is characterized by light to medium gray and olive, finely crystalline dolostone, interbedded with limestone. Sedimentary features and fauna such as, oolite bars, scoured algal surfaces, and pelmatozoans indicate a shallow water depositional environment (Gorody, 1980). The top of the Mascot is truncated by a regionally extensive erosional unconformity (Harris, 1969, 1971) above which lies the Wells Creek Formation, the lowermost formation of the Middle Ordovician Stones River Group. Pre-Middle Ordovician relief on the unconformity was approximately 38m with shale and fine-grained dolomite and limestone of the Wells Creek Formation filling in the paleotopographic lows (Gilbert and Hoagland, 1970). Above this formation Middle Ordovician limestone lithologies show features indicative of normal, open marine environment (Gorody, 1980). In the Gordonsville mine area, the Knox Group is overlain by 335 to 410m of Middle Ordovician and younger rocks (Kyle, 1976). The thickness of the Mascot Formation, host to zinc mineralization, is 180 to 260m and is controlled primarily by the erosion which produced the post-Knox unconformity (Stagg and Fischer, 1970).

The Mascot Formation contains sand beds which have been used to subdivide the unit into upper, middle and lower members (Figure 2). The base of the Mascot Formation is defined by the T-R marker bed, a distinctive black-green shale horizon that forms the uppermost unit of the underlying Kingsport Formation (Kyle, 1976). In East Tennessee, the Kingsport Formation consists of limestone beds or their "dolomitized equivalents", interbedded with lesser amounts of finely crystalline dolostone (Harris, 1969). Because economic mineralization is primarily associated with the Mascot Formation in Middle Tennessee, drilling rarely penetrates the Kingsport or older formations; consequently, detailed stratigraphic information on the Kingsport and older formations is not available for Central Tennessee.

Brecciation and Mineralization

The mineralized interval in the Gordonsville mine is located in the middle portion of the middle member of the Mascot Formation (Figure 2). This interval lies stratigraphically above the mineralized zone in the Elmwood mine. While all ore occurs in association with brecciated and altered rock there are many breccia bodies devoid of mineralization (Kyle, 1976). It is generally believed that dissolution of the more soluble limestone beds ultimately caused the collapse and brecciation of the overlying dolostone beds, as has been proposed for the Mascot-Jefferson

City district (Wedow and Marie, 1964; Callahan, 1967; McCormick et al., 1971). The process is believed to have been initiated by the lateral movement of meteoric water through a paleoaquifer system. This water, undersaturated in $CaCO_3$, moved through passageways either along formational contact irregularities or joints and faults. As limestone was dissolved, large voids formed which, under great confining pressure, collapsed, forming breccias (Gaylord and Briskey, 1983). If brecciation occurred through successive limestone units it is termed a "breakthrough breccia". In the Gordonsville mine large vugs, collapse breccias (Figure 3), and breakthrough breccias are evident.

Two separate stages of brecciation have been suggested for the Central Tennessee zinc district (Kyle, 1973, 1976). The early stage of brecciation is represented by fine rock-matrix breccia at various intervals within the Mascot Formation and is usually unmineralized. A later breccia system overprints the earlier brecciation and extends from the Kingsport Formation to the post-Knox unconformity. Several breakthrough breccia bodies extend 60m into Middle Ordovician lithologies (Hoagland, 1973). This later breccia system, the host to sphalerite and related gangue mineralization, is characterized by two types of matrix. A "coarse rock-matrix breccia" is most common in the lower parts of the breccia system and contains coarsely crystalline material, mostly dolomite crystals and dolostone fragments

(a)

(b)

Figure 3. Photographs of mineralized collapse breccias in the Gordonsville mine. (a) Matrix composed of sphalerite, minor calcite; (b) heavily brecciated zone, matrix composed of sphalerite, calcite, minor fluorite.

along with a mixture of chert fragments, quartz sand and insoluble residue. The upper parts of the system, where most of the ore is located, contains "mineral matrix breccias". Here, the matrix is composed of calcite, sphalerite, and barite, with lesser amounts of fluorite, galena, pyrite and quartz (Kyle, 1976; Gaylord and Briskey, 1983). Technically, the term "matrix" refers to the finer grained material which surrounds coarser grains or rocks; however, in the district, mine geologists refer to matrix as any material surrounding the breccia fragments. The latter definition will be used throughout this paper.

There is much debate as to the timing of brecciation and its relationship to mineralization. In the East Tennessee districts, many geologists believe that most of the brecciation was due to karstification during the time of the post-Knox unconformity (Harris, 1969, 1971). However, some of the brecciation in East Tennessee zinc districts may have been synsedimentary, localized on subaerially exposed parts of the environmental complex (Churnet, 1979; Churnet et al., 1982; Churnet and Misra, 1983). Some of the breakthrough breccia bodies in the Central Tennessee district extend into the Middle Ordovician formations and thus this brecciation must post-date the post-Knox erosional event (Winslow and Hill, 1973; Hoagland, 1976; Kyle, 1976; Steinberg, 1981). These breccias may have formed during the Middle Ordovician or later through reactivation of the paleoaquifer (several

Middle Ordovician unconformities in the area attest to water level changes) (Gaylord and Briskey, 1983). The early breccias of both Central and East Tennessee districts probably formed the framework upon which the late, ore-hosting breccias could develop (Hoagland et al., 1965; Hill et al., 1971; Churnet and Misra, 1983; Gaylord and Briskey, 1983).

As there is no evidence of brecciated ore at Gordonsville (Gaylord and Briskey, 1983), it is believed that mineralization occurred after brecciation. Thus, mineralization must have occurred after some Middle Ordovician sediment had been deposited. Surface vein deposits of fluorite, barite, galena, and sphalerite in the district penetrate Lower Mississippian strata (Jewel, 1947). If these veins are connected to subsurface breccias, as is believed to be the case by several workers (DeGroodt, 1973; Gorody, 1980; Gaylord and Briskey, 1983; Fred Smith, pers. comm., 1985), ore mineralization in the Central Tennessee district may have occurred as late as Mississippian time.

Sphalerite is the only zinc ore mineral in the Central Tennessee zinc district. Most commonly it is dark-reddish brown and coarsely crystalline. Often it is intergrown with calcite, barite, fluorite, and galena. A light brown, disseminated sphalerite is also found in the district; however, in Gordonsville it is not common. Pyrite is frequently found as fine grains associated with early mineral

phases. While marcasite and celestite are rare, localized concentrations of these minerals are occasionally found in dissolution cavities (Kearns and Campbell, 1978). Bituminous material and liquid hydrocarbons are commonly associated with both ore and gangue minerals.

CHAPTER 3

PETROGRAPHY

Most of the samples for this study were collected from stopes in the Gordonsville mine which expose mineralized carbonate rocks at the stratigraphic equivalent of the Gordonsville Limestone (see Figure 4 for sample locations). The samples containing disseminated sphalerite were collected along haul lines at the periphery of stopes, and early calcite was acquired From an unknown location within the Elmwood mine. Out of a total of approximately 200 samples, 80 polished thin sections were prepared for a petrographic study of ore and gangue minerals (see Appendix A for petrographic descriptions). The mineralogy and textures of the samples were studied using transmitted-light and reflected-light microscopy. Cathodoluminescence petrography was used to help determine the paragenesis of the early-formed minerals, dolomite and quartz.

Dolomitization and Silicification

Dolomite is a major constituent of both gangue and host rock. Many of the dolostone breccia fragments contain a variety of dolomite crystal sizes from fine-grained (mostly .02-.05 mm) to coarse (mostly .1-.8 mm) (size groups used by Churnet et al., 1982). Most dolostone fragments are either finely to medium crystalline or medium to coarsely

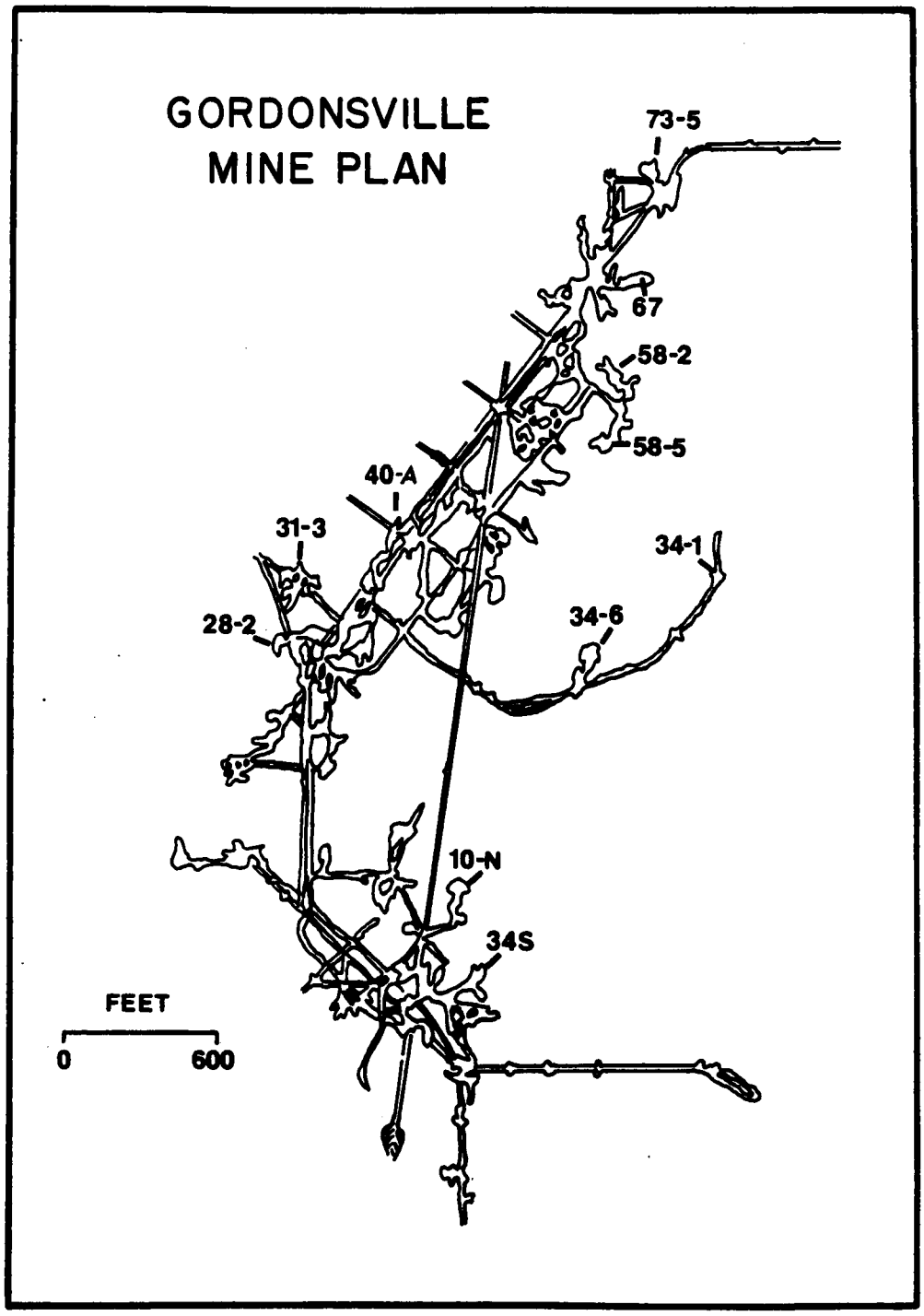

Figure 4. Sampling locations (stope numbers) at the Gordonsville mine. Modified from Gaylord and Briskey (1983).

crystalline. Rarely do fragments show a continuum from finely to coarsely crystalline. Texturally, the dolomite crystals within dolostone form an hypidiotopic to xenotopic and commonly porphyrotopic mosaic (texture terms as defined by Friedman, 1965). Medium- to coarse-grained dolostone fragments are comparable to dolostones of East Tennessee (Churnet et al., 1982). Their texture is usually porphyrotopic, and individual rhombs often display cloudy centers and clearer rims. Medium- to coarse-grained dolomite rhombs are also found as matrix in between rock fragments. Often rimming dolostone fragments are medium to very coarsely crystalline (≥5mm) dolomite rhombs which may or may not be zoned (cloudy centers, clearer rims). This "drusy" dolomite is also noted for its luminescent zonation (Figure 5). Drusy dolomite forms subsequent to brecciation and is usually surrounded by later minerals associated with sphalerite emplacement.

Silica is texturally complex, occurring as very fine-grained silica (chert), irregular silica masses and coarse-grained "drusy" quartz. Chert occurs as lenses, nodules, or layers, and is often fractured and brecciated. Many of the chert fragments seen in thin sections show well defined oolitic and pelloidal textures (Figure 6a). In fragments with no relict primary textures, silica forms very fine-grained, monotonous masses, or irregular masses where grain size is heterogeneous. These irregular masses may

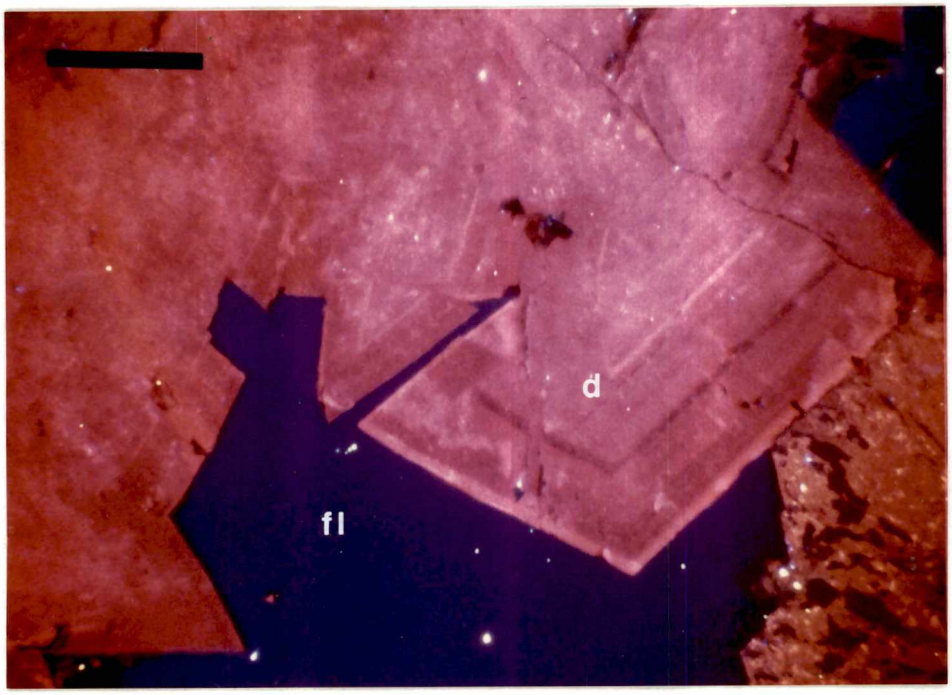

(a)

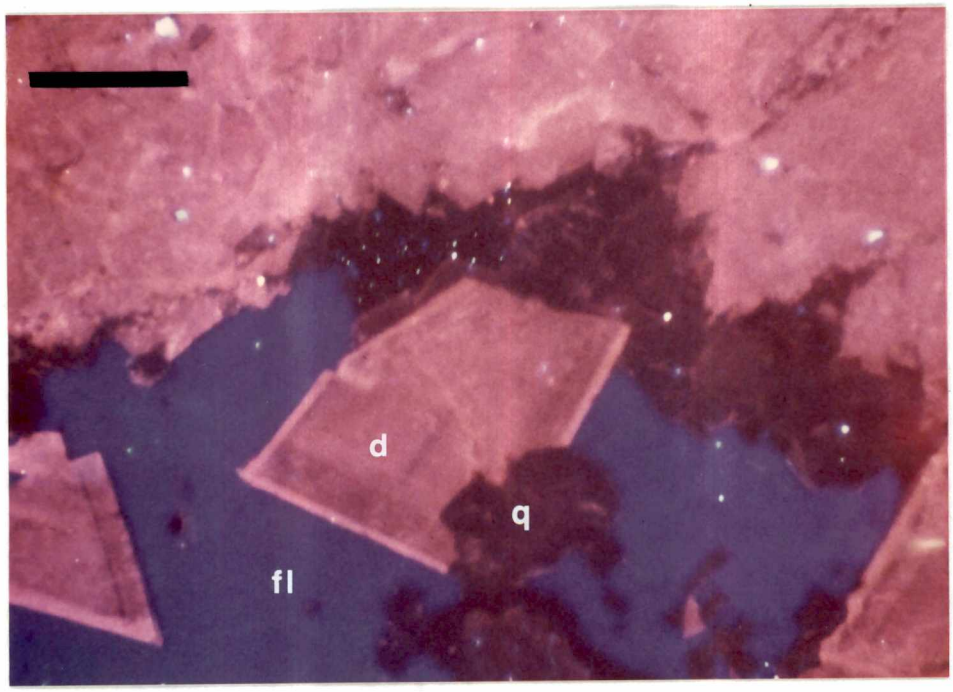

(b)

Figure 5. Photographs showing cathodoluminescent zonation in drusy dolomite (Sample 49e). In (b), note the quartz grains (q) embaying the earlier dolomite (d). Fluorite (fl) is the blue mineral. Bar scale represents 1mm.

Figure 6. Photomicrographs of silicification and dolomitization textures. Bar scale represents 0.5mm.

A. Silicified limestone fragment displaying relict oolitic texture. Note drusy quartz rim (q) and silica-filled, late stage fractures (Sample 29c).

B. Rind of drusy quartz (q) around fine-grained dolostone (dol) fragment. Matrix mineral is calcite (cal) (Sample 1b).

C. Rind of drusy dolomite (d) around fine-grained dolostone fragment (dol). Matrix mineral is sphalerite (sph) (Sample 1a).

D. Silicified limestone fragment partially dolomitized (top part of photomicrograph). Relict ooids are silicified (ch). Note aggregates of euhedral dolomite in the ooids (dol) (Sample 29b).

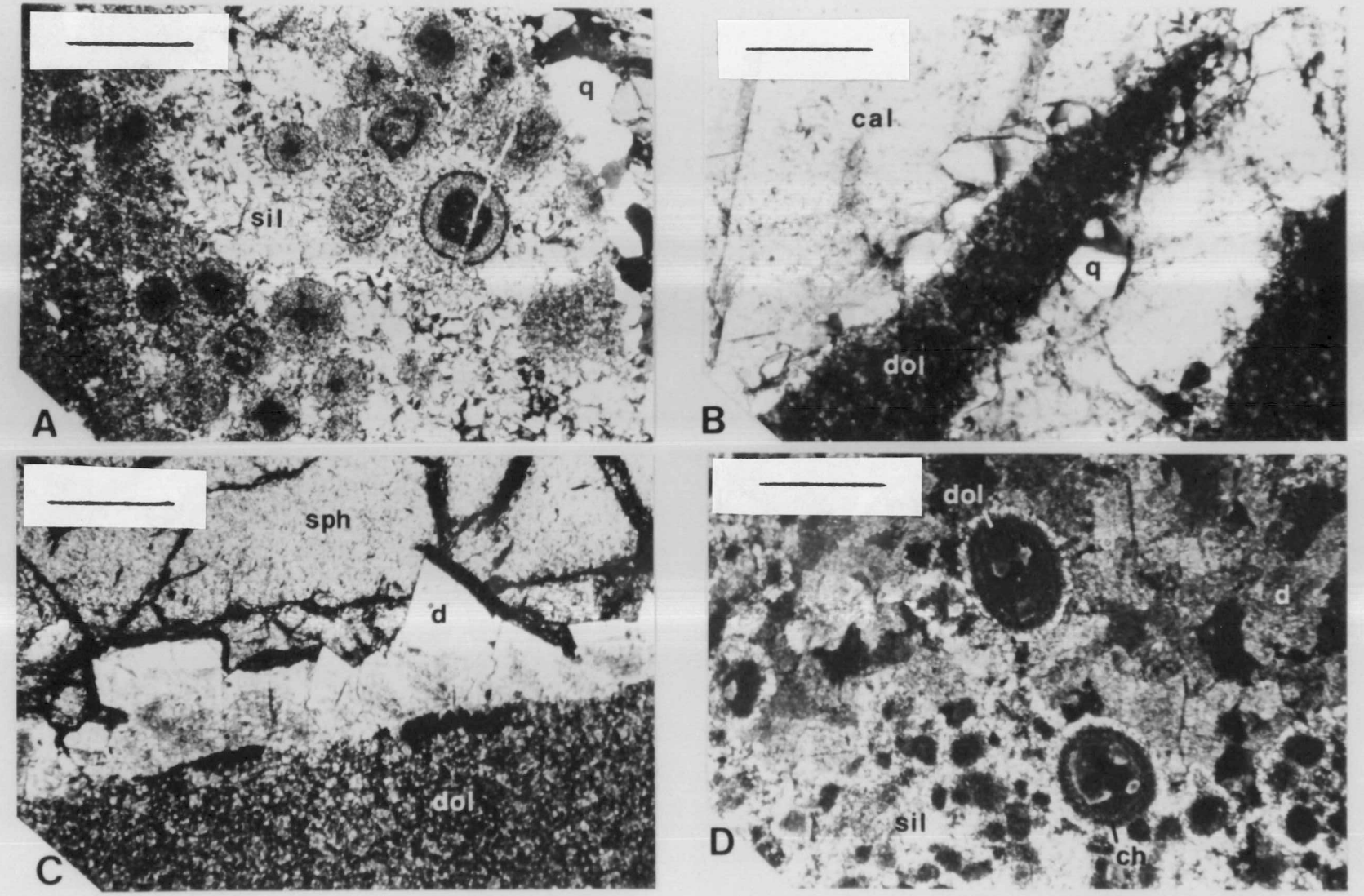
A
q
sil
B
cal
q
dol
C
sph
d
dol
D
dol
d
sil
ch

reflect inhomogeneity in the original limestone fabric. A fibrous variety of quartz may fill fractures or voids. Well rounded quartz grains are not uncommon in fragments containing dolomite and silica and may represent sand grains which were deposited along with the original limestone sediment. Drusy quartz is common around both chert and dolostone fragments and is often associated with very coarse-grained dolomite rhombs (Figure 6b,c).

Silicification and dolomitization are pervasive in the Gordonsville mine as in other mineralized areas in the Central Tennessee zinc district (Kyle, 1976; Craig, 1982). General field relations (Gorody, 1980; Craig, 1982), the persistence of primary fabric suggests that much of the silica and fine-grained dolomite was early diagenetic in origin. The observation that silicification and medium- to coarse-grained dolomitization is most intense in and around breccia systems, however, suggests that at least some silica and medium- to coarse-grained dolomite may have been precipitated by the same solutions which induced brecciation (Gaylord and Briskey, 1983). This would imply that silicification and dolomitization occurred well after sedimentation and lithification but prior to ore emplacement and gangue mineralization.

The relationship between silicification and dolomitization is complex. Silicified limestone is dolomitized to varying degrees. Often, euhedral dolomite

rhombs of the medium to coarse-grained variety are seen as aggregates in the center of relict ooids whereas the rest of the rock fragment is replaced and cemented by silica (Figure 6d). Dolomite rhombs may be randomly oriented single crystals in an otherwise cherty rock. Earlier studies (Dietrich et al., 1963) suggest that dolomitization began first and was "arrested" by the silicification process. Silicification was selective as it replaced $CaCO_3$ but not the already formed dolomite crystals. However, there are many examples of medium-grained dolomite rhombs being etched by the surrounding silica; while silicification is selective, it is not in total equilibrium with dolomite (Figure 7a). What are seen in the different rock fragments may be the result of the progressive stages of silicification arresting the dolomitization process. Several samples contain medium- to coarse-grained hypidiotopic to xenotopic dolomite in a matrix of "dirty" silica. This may represent an advanced stage of dolomitization. Similar features have also been observed in Knox Group carbonates in Burkesville, Kentucky (Craig, 1982) and Blacksburg, Virginia (Dietrich et al., 1963).

In summary, very finely crystalline dolomite is probably the earliest diagenetic feature of the observed rocks. This is followed by a complex history of dolomitization and silicification, the results of which are present to differing degrees in many of the samples studied. Subsequent to fracturing and brecciation, drusy quartz along with very

Figure 7. Photomicrographs of ore and gangue mineral textures. Bar scale represents 0.5mm.

A. Dolomite rhombs (d) in a silica matrix. Dolomite is etched by silica (Sample 4b).

B. Streaks of diffuse, bituminous material (bit) in sphalerite (Sample 22b).

C. White (w) and orange (or) coloration in sphalerite. Note that the bituminous inclusions are present in both color zones (Sample 68).

D. Sphalerite (sph), calcite (cal), and barite (bar), displaying sharp grain boundaries (Sample 11a).

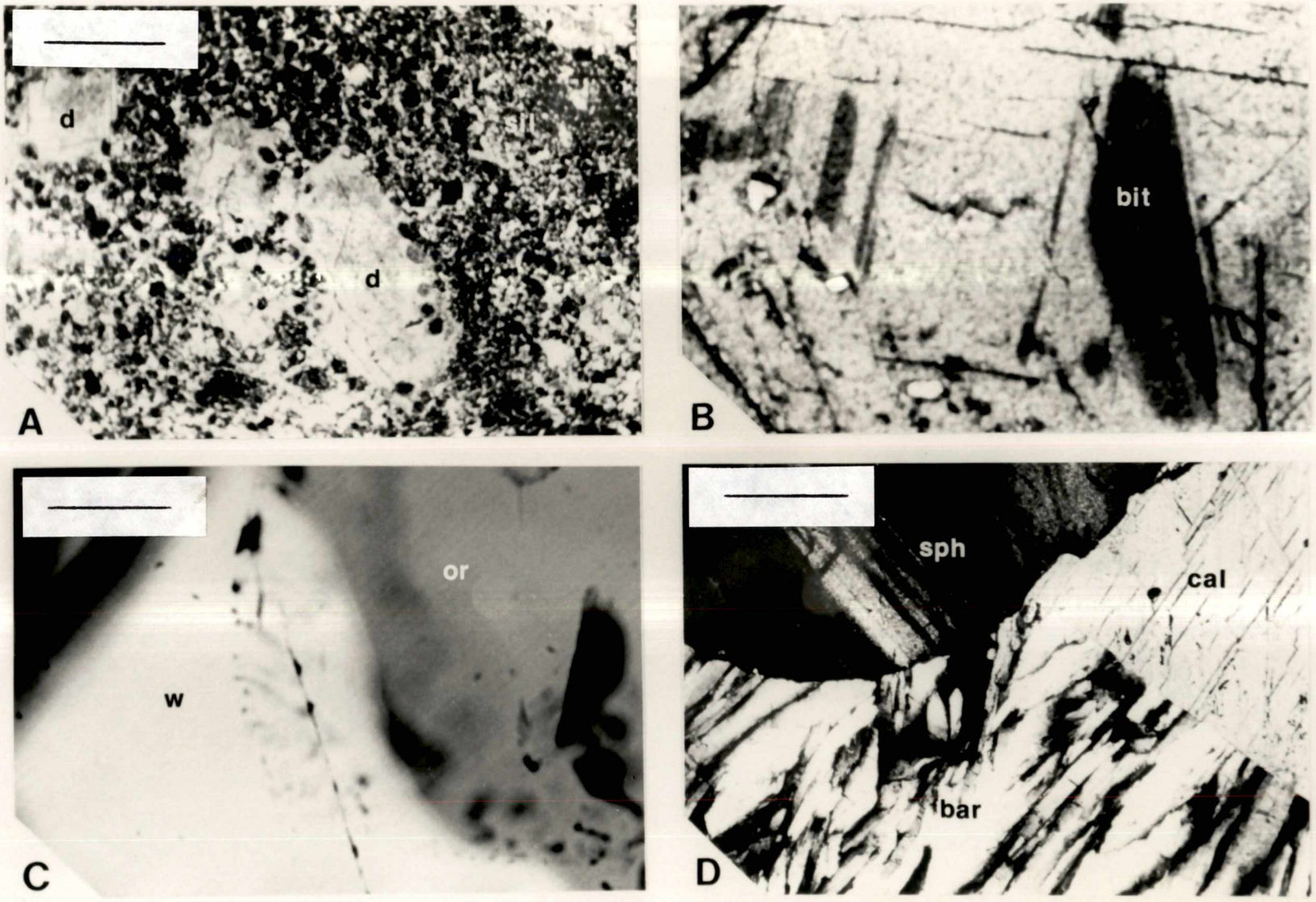
d
d
A
bit
B
or
w
C
sph
cal
bar
D

coarse grained dolomite formed as rinds on breccia fragments. Pyrite is found associated with dolostone and chert fragments and is especially apparent near the rims of fragments, in contact with the drusy quartz and dolomite. Pyritization probably occurred during early diagenesis and proceeded through late stage brecciation. No pyrite, however, is associated with later ore and gangue minerals.

Ore and Gangue Minerals

Sphalerite

Sphalerite is the only zinc ore mineral in the Central Tennessee zinc district. Three types of sphalerite, distinguished by texture and color, are present at the Gordonsville mine: massive, vug-filling, and disseminated. The most common variety is characterized by coarsely crystalline, dark reddish brown, resinous masses, often in mineralized matrix breccias either as single phase aggregates or intergrown with gangue minerals. This variety is referred to as "massive sphalerite". Vug-filling sphalerite is characterized by its large crystal size, dark brown to black color and ruby-red internal reflection (Figure 8a). Its crystals are commonly twinned. Disseminated, yellowish brown sphalerite is a less common variety and is usually found as small grains in altered limestone (Figure 8b).

In transmitted light, all varieties of sphalerite exhibit white to deep red coloration (Figure 7c). Unlike

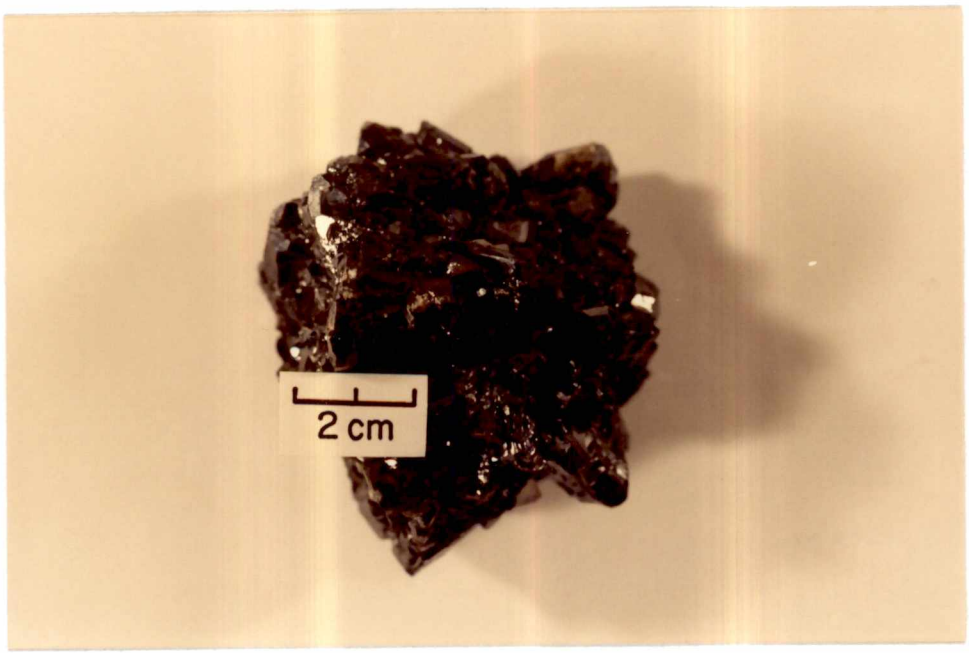

(a)

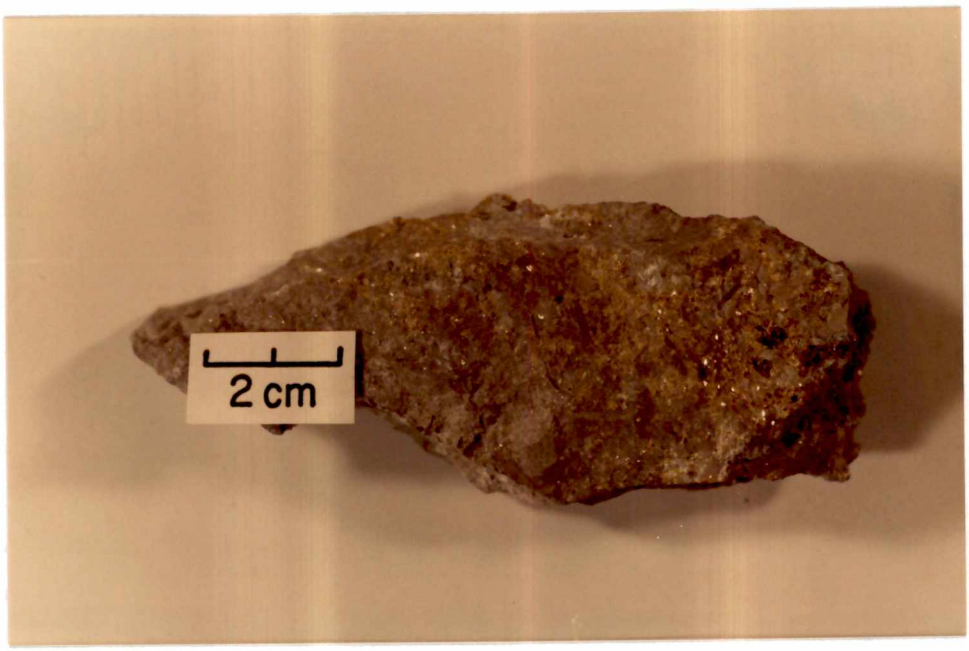

(b)

Figure 8. Photographs of specimens displaying different textural varieties of sphalerite. (a) Vug-filling sphalerite characterized by dark brown to black color and large crystal size; (b) light brown, fine-grained disseminated sphalerite.

samples from East Tennessee, these color zonations do not appear to express simple growth patterns (Craig et al., 1983); instead, they form a complex mosaic. Even in thin sections of vug-filling sphalerite which were cut perpendicular to growth direction, color zonations did not reflect growth direction. In fact, it is probably more appropriate to call them color "regions" rather than zonations as zonations tend to denote a semblance of order. These colors are visible in all three types of sphalerite: disseminated, massive, and vug-filling. Macroscopically, disseminated sphalerite is lighter in color than the other varieties. Yellow color is dominant under plain light in disseminated sphalerite; however, yellow and white are common under plain light in darker sphalerite as well. Disseminated sphalerite's lighter appearance may be due to its fine-grained nature, while the darker color of massive and vug-filling sphalerite may be the result of their coarse-grained characteristics.

Reasons for microscopic color variation are not readily apparent. Sphalerite is rich in hydrocarbon inclusions, both in solid and liquid phase. Bituminous material is often found in the form of diffuse streaks or blotches (Figure 7b). Whereas the darker color zones in East Tennessee sphalerite is attributed to changes in inclusion density (fluid, vapor, or solid) (Craig et al., 1983), this correlation is not evident in Central Tennessee. Sharp color

boundaries occur with no corresponding change in either inclusion density or hydrocarbon content (Figure 7c). The subject of microscopic color variation will be discussed in further detail in a later section concerning minor element analysis of sphalerite.

All types of sphalerite exhibit a distinct optical anisotropy. The fabric most closely resembles the "scotch-plaid" twinning of microcline. Recent work has attributed this characteristic to primary growth defects which are stabilized by high concentrations of cadmium and iron (Seal et al.,1985). Deformation twins, which may cause anisotropy, are not seen in the Central Tennessee sphalerite.

Paragenetically, sphalerite formed before most gangue minerals. While it most commonly fills large open spaces, it may contain inclusions of drusy quartz and dolomite. In most instances galena formed after sphalerite; however, a few cases have been documented in which sphalerite was later (Kearns and Campbell, 1978). An early calcite phase, which is rare in Gordonsville, is the only gangue mineral besides drusy quartz and dolomite to precipitate prior to sphalerite emplacement. Grain boundaries between sphalerite and other mineral phases are sharp suggesting equilibrium conditions during the deposition of all mineral phases (Figure 7d).

It has been suggested, based on texture and coloration, that the different sphalerite types may represent two or more different stages of deposition (Kyle, 1973; Gaylord and

Briskey, 1983; Seal et al., 1985). Petrographic information in this study does not warrant separation of massive and vug-filling sphalerite. Two generations of massive sphalerite based upon the abundance of carbonaceous inclusions have been proposed (Seal et al., 1985); in this study, however, these differences have not been recognized. Disseminated sphalerite is usually found at the periphery of breccia bodies in altered limestone and fine-grained dolostone. Rarely are disseminated and massive sphalerite found together, thus making paragenetic determinations difficult. Fluid inclusion and trace element data, presented later, will suggest that disseminated, massive and vug-filling sphalerite are all part of one major episode of mineralization.

Galena

Galena is only locally abundant in the Gordonsville mine. In some breccia bodies it is a common gangue mineral, whereas in others, galena is conspicuously absent. As mentioned previously, the paragenetic relationship between galena and sphalerite is complex; however, most galena appears to have precipitated after sphalerite. Galena is usually found as both crystalline masses commonly attached to sphalerite and/or the associated host rock and as large cubes on the same material (Figure 9).

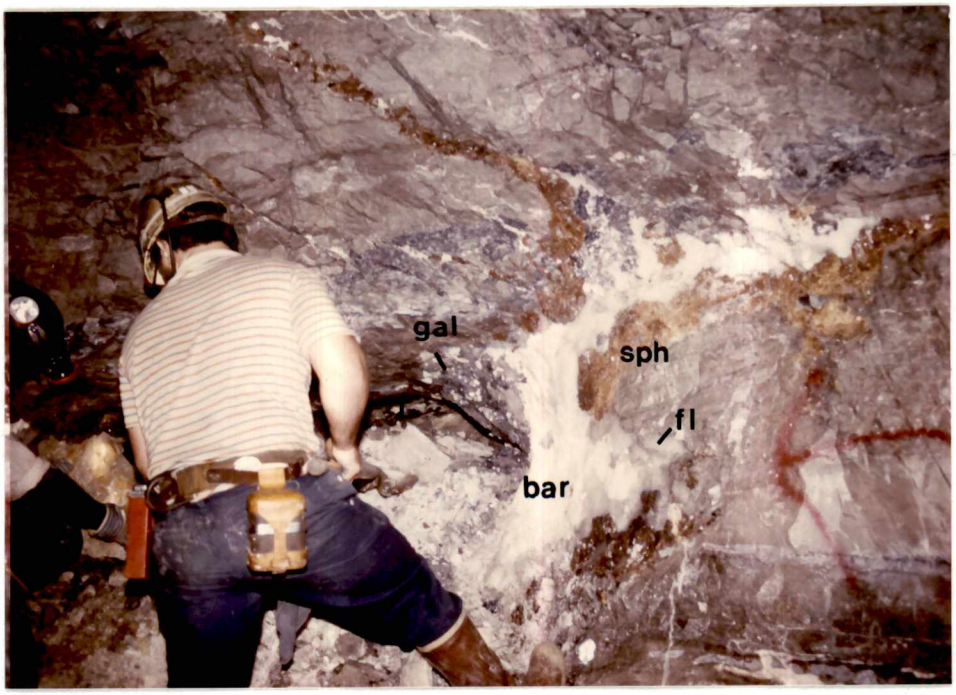

(a)

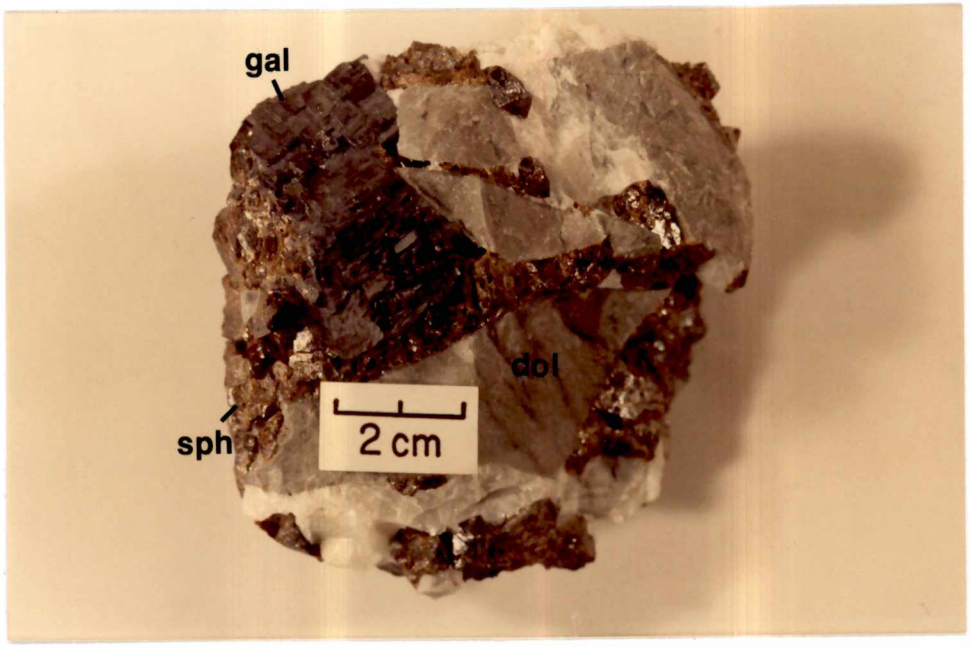

(b)

Figure 9. Photographs of locally abundant galena. (a) Associated with sphalerite (sph), barite (bar), and fluorite (fl) around vug (stope 58-5); (b) well-formed cubes in mineral matrix breccia along with sphalerite (sph) and dolostone (dol) fragments.

Fluorite

Fluorite, a common gangue mineral in the Gordonsville mine, is usually associated with mineralized breccias. Whereas there is only one textural variety of fluorite, it occurs in a variety of colors. Most fluorite is clear to purple but it can range in color from yellow and yellow-green to pink (Kearns and Campbell, 1978). The size of fluorite crystals also varies, from a few millimeters to several centimeters. Fluorite can be found in contact with all minerals. Often, it forms a rind over sphalerite in dissolution cavities (Figure 10a). Either calcite or barite may fill in the remainder of the cavity. There is no evidence of sphalerite forming after fluorite deposition. When fluorite crystals are broken, closer examination reveals that color is only superficial; fluorite is colorless internally (Figure 10b). The color may be the result of the interaction of crystal faces with later fluids of different compositions and/or temperatures. Boundaries between fluorite and other minerals are usually sharp (Figure 11a,b). Hydrocarbon inclusions are common in fluorite although not as ubiquitous as in sphalerite.

Calcite

It is difficult to place the gangue calcite in the paragenetic sequence as it precipitated during three different stages as well as in a variety of forms. Early

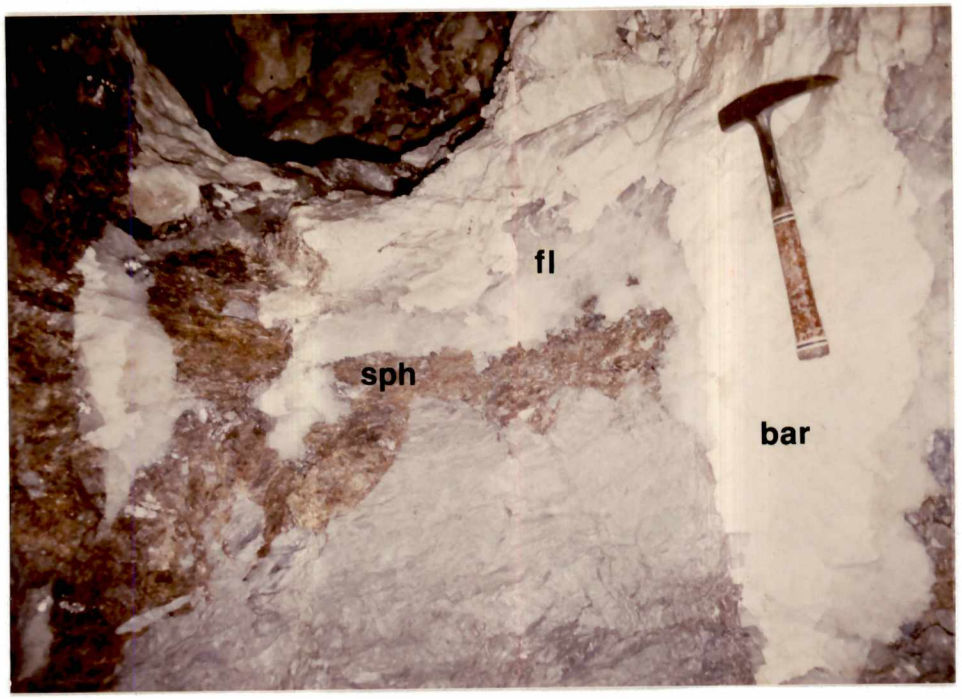

(a)

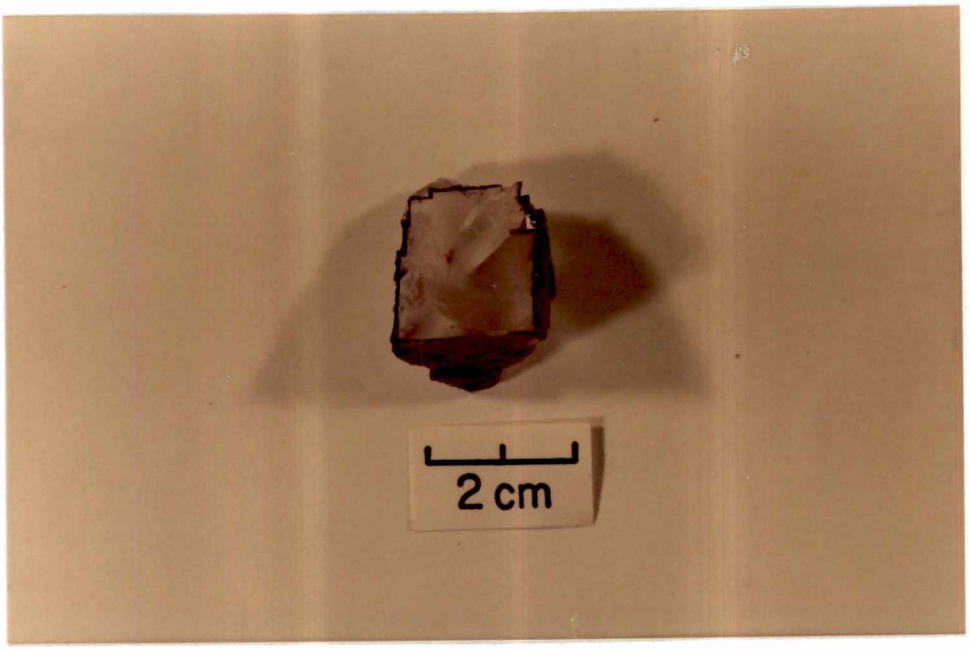

(b)

Figure 10. Photographs of clear to purple-colored fluorite (fl). (a) Forms rind around sphalerite (sph) at vug entrance (stope 58-5), associated with barite (bar); (b) slice through fluorite revealing that purple color is a surficial feature.

Figure 11. Photomicrographs of gangue mineral textures. Bar scale represents 0.5mm.

A. Sharp boundaries between drusy dolomite (d) and fluorite (fl), and barite (bar) and fluorite (Sample 52a).

B. Sharp boundaries between drusy dolomite (d), main-stage calcite (cal), and fluorite (fl) (Sample 49e).

C. Barite feathers (bar) penetrate main-stage calcite (cal). Barite - dolomite (d) boundary is sharp (Sample 49a-1).

D. Sharp boundary between barite (bar) and main-stage calcite (cal) (Sample 49a-2).

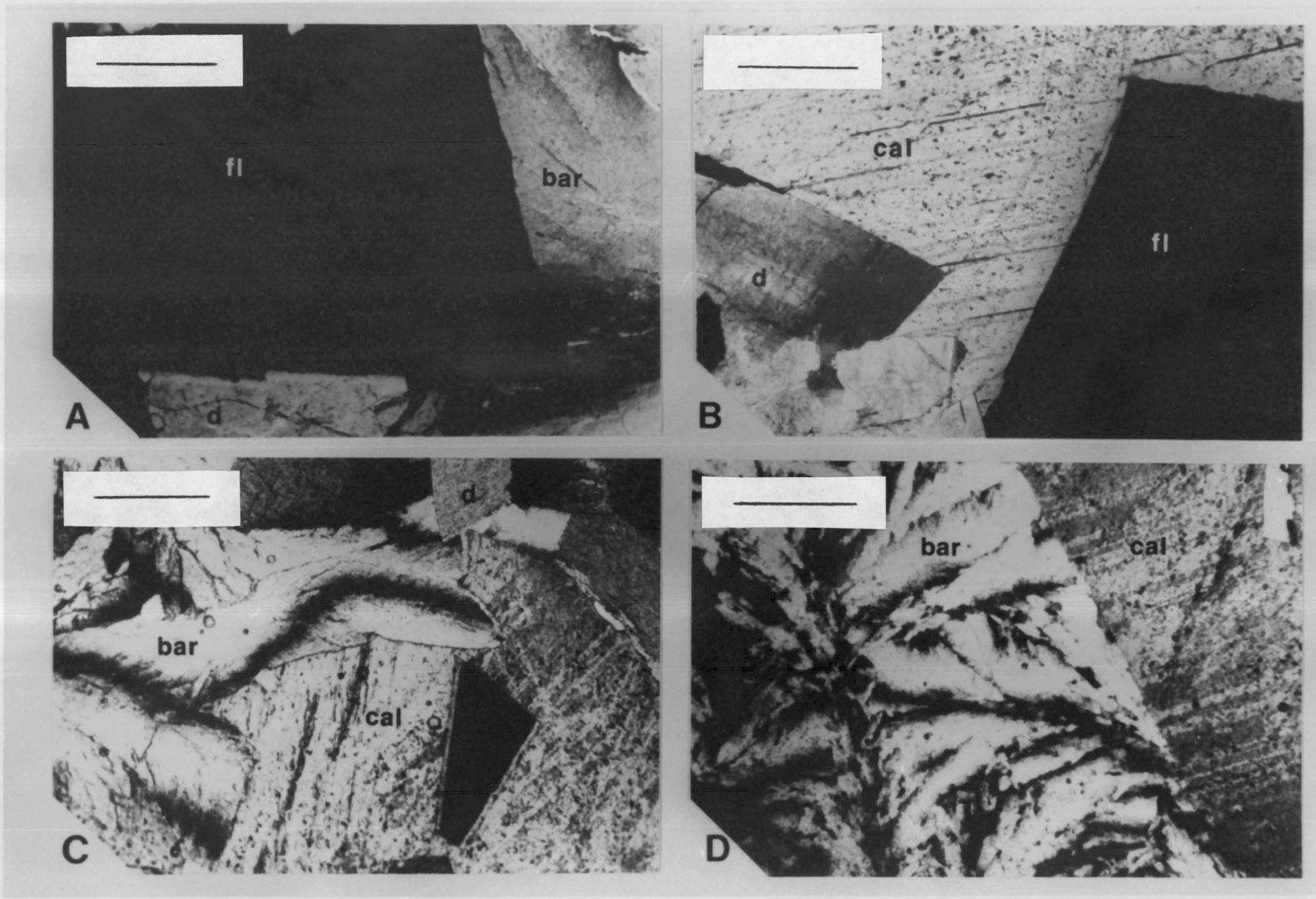
fl
bar
d
A
cal
d
fl
B
d
bar
cal
C
bar
cal
D

calcite, rarely found in Gordonsville, occurs as simple scalenohedrons on dolostone and silicified limestone before sphalerite mineralization (Figure 12a). In thin section, it is distinguished by its luminescent zonations which are absent in the later two phases of calcite mineralization (Larsen, 1978). Later calcites form after the precipitation of sphalerite and fluorite. Boundaries between early calcite and both sphalerite and fluorite are usually sharp.

The second phase of calcite deposition is characterized by blunt scalenohedrons which occur in a variety of colors. Second stage (or "main-stage") calcite has a grayish pink to lavender hue and is somewhat translucent or milky in appearance (Figure 12b). This type of calcite, the most prevalent of the calcite stages, makes up a large proportion of mineralized matrix breccias and is often associated with sphalerite, barite, and fluorite. Late-stage calcite is probably the last mineral to form within the mineralized zone. It is characterized by its transparent to amber color and its well-developed, generally twinned, scalenohedrons. Amber calcite is often attached to vug-filling sphalerite or isolated fluorite cubes. It may have formed directly on the drusy rind of dolostone and/or chert fragments. Bituminous material is commonly found either inside the amber calcite crystals or attached to the surface of crystal faces (Figure 13a).

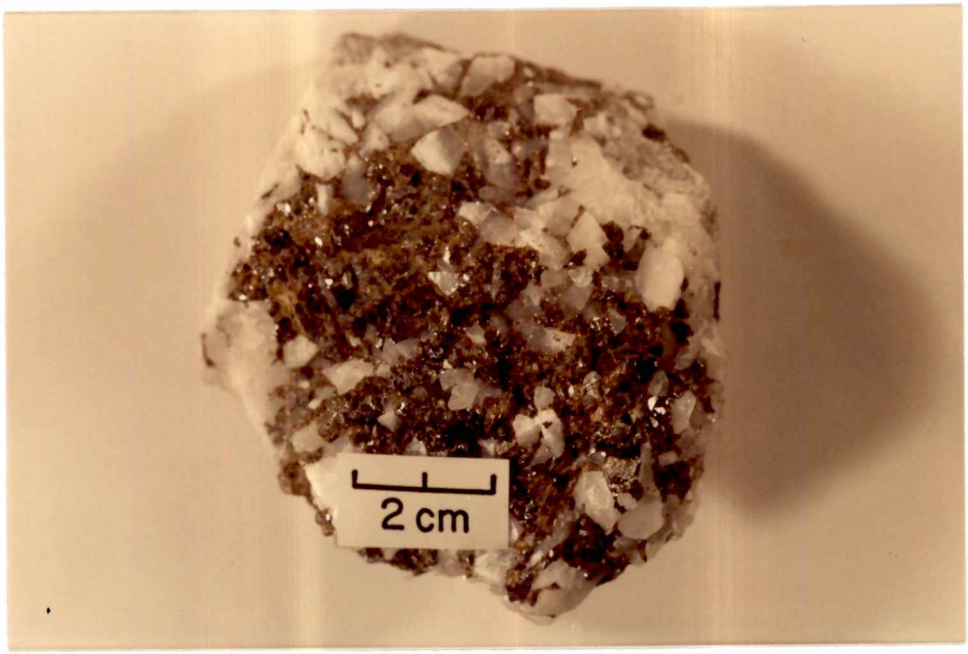

(a)

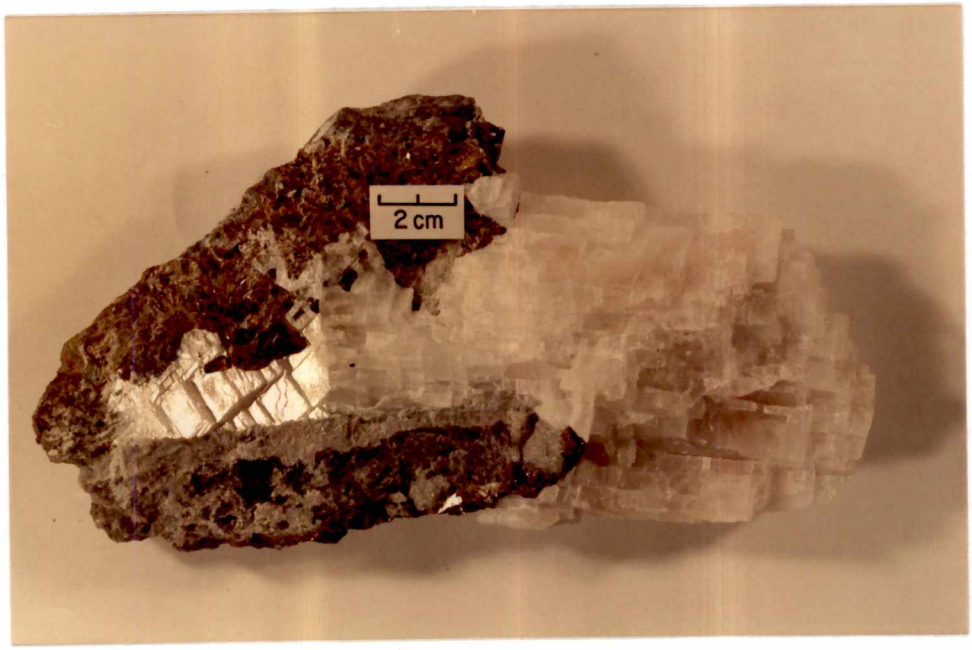

(b)

Figure 12. Photographs of two stages of calcite. (a) Early white calcite from Elmwood mine surrounded by later sphalerite; (b) main-stage white to lavender calcite as matrix between two silicified limestone fragments.

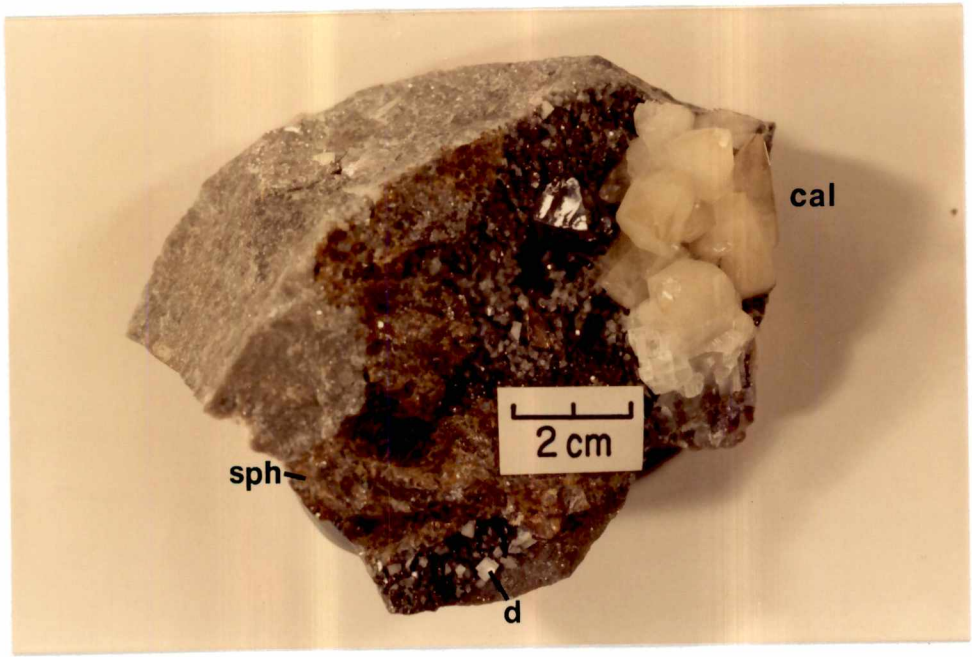

(a)

(b)

Figure 13. Photographs of late-stage gangue minerals. (a) Complex scalenohedrons of amber calcite (cal) on silicified limestone fragment. Associated with sphalerite (sph) and drusy dolomite (d); (b) barite "balls" surround fluorite cube. Specks of bitumen are trapped on feathery barite surface.

Barite

Barite occurs as breccia matrix and as barite "balls" in vugs. As matrix fill, its color is usually white to creamy; in vugs it may be almost yellow in appearance. The balls often form around sphalerite or fluorite cubes, sometimes reaching over 30cm in diameter (Kyle, 1976). As with amber calcite, bituminous material is commonly associated with barite, forming interstitially in breccia matrix or as globules on the surface of barite balls. Bitumen is easily trapped in barite due to barite's feathery, highly porous, growth texture (Figure 13b).

The textural relationship between barite and second-stage calcite is complex. Megascopically, both at outcrop and hand sample scale, their paragenetic relationship is ambiguous. Microscopically, barite feathers can be seen penetrating calcite which would imply that calcite precipitated first. However, in the same sample, fragments of barite feathers are surrounded by calcite which would denote the opposite. Often their mutual boundary is sharp and straight. In the majority of the thin sections studied, barite appears to have formed after second or main-stage calcite. Thus, paragenetically, while there was some overlap in their timing, much of the main-stage calcite has been interpreted to have formed before barite (Figure 11c,d).

Clear to amber calcite scalenohedrons appear to have formed after barite. It is not certain as to whether there

was continuous calcite precipitation from main-stage (white to lavender) calcite through late-stage (clear to amber) calcite. There is no evidence of erosional boundaries in barite or main-stage calcite to suggest disequilibrium or a depositional hiatus. Field observations, however, do not show a growth trend from white and lavender calcite to clear and amber calcite. The late-stage calcite is usually present as discrete crystals in vugs. Fluid inclusion studies give further insight as to the relative timing of barite and multiple stage calcite precipitation. A generalized paragenetic sequence of ore and gangue mineralization, based on the fabric relationships discussed above, is presented in Figure 14.

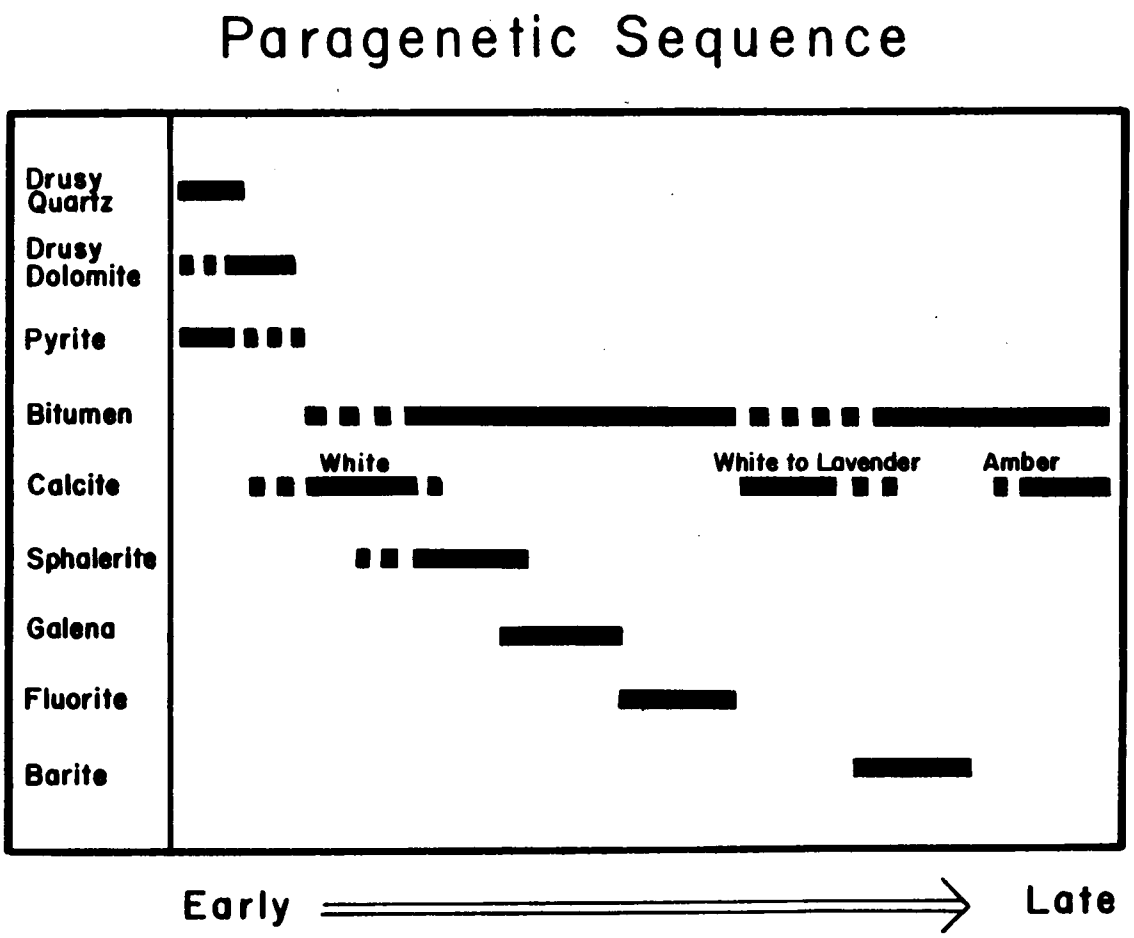

Figure 14. Sequence of ore and gangue mineral precipitation following brecciation in the Gordonsville zinc mine.

CHAPTER 4

FLUID INCLUSIONS

Introduction

Fluid inclusions can be grouped into three categories: primary, secondary, and pseudosecondary. Primary inclusions are those which formed while the mineral grew. The homogenization temperature (minimum temperature of trapping) and freezing temperature (salinity) of a primary inclusion should approximate the temperature and salinity of the fluid from which the mineral formed. Secondary inclusions are those which formed after the mineral was deposited. They relate to a later event; thus fluid inclusion data may or may not represent conditions of formational fluids. Because of the uncertainty, secondary inclusions are usually not used; however, with care they may give information regarding age relationships with other minerals. Pseudosecondary inclusions occur in fractures which formed during crystal growth. These fractures terminate while the crystal grows so that inclusions trapped in the fracture are actually of primary origin. For the composition and characteristics of even a primary inclusion to be considered to reflect that of the surrounding mineral, however, several assumptions must be made (Roedder, 1984):

1) The fluid trapped when the inclusion was sealed was a single homogeneous phase.

2) The cavity in which the fluid was trapped does not change in volume.

3) Nothing is added or lost from the inclusion after sealing.

4) Pressure effects are insignificant or are known.

5) The origin of the inclusion is known (primary, secondary, pseudosecondary).

Because these assumptions are difficult to prove, geologists still argue over the validity of fluid inclusion data; nevertheless, the data has increasingly become the basis for many interpretations in all sectors of geology. The study of Mississippi Valley-type deposits is no exception. Roedder (1971) studied minerals in five mines in East Tennessee zinc districts and found that most primary inclusions in sphalerite, fluorite, dolomite and quartz homogenized at 82°-149°C and contained strongly saline brines (>20 equivalent wt.% NaCl). Detailed studies on fluorite and sphalerite in the Mascot-Jefferson City district (Taylor et al., 1983) and the Sweetwater district (Zimmerman and Kesler, 1981) of East Tennessee showed that cooling and fluid mixing were possible causes for ore and gangue mineral deposition.

In the Central Tennessee zinc district, there has been limited research using fluid inclusions. Analyses of fluid inclusions in calcite and fluorite from near-surface veins and from cores in ore bodies by Roedder (1971) revealed homogenization temperatures slightly below those of East

Tennessee (90°-120°C). Only salinity values for inclusions in fluorite were determined and these range from 3% (equiv. wt.% NaCl) to greater than 23%. DeGroodt (1973) recorded homogenization temperatures of fluorite primarily from surface veins along with a few samples in the Elmwood mine. Homogenization temperatures in surface veins ranged from 64°-151°C while those from mine samples ranged from 99°-126°C. The current study examines inclusions in calcite, fluorite, sphalerite, and barite, all from within the Gordonsville mine (only three kilometers west of the Elmwood mine). In the following discussion on fluid inclusions, several abbreviations will be used:

T_h - homogenization temperature of the liquid and vapor phase

T_m - melting point of ice (freezing temperature)

T_e - eutectic melting temperature of saline solution (temperature at which ice-hydrate begins to melt)

Sample Preparation

Samples were selected for fluid inclusion analysis after the paragenetic sequence was established during the detailed petrographic study of all thin sections. Petrographic study of polished thin sections also allowed a cursory search for suitable inclusion-rich samples for analysis.

Fifty-five doubly polished thin sections were prepared for fluid inclusion study. The first cut on rock samples

was made with an Isomet slow speed saw with a very thin 5 inch diameter blade. Great care was taken in keeping temperatures and pressures affecting the rocks to a minimum. Cold water carborundum abrasives were used in the initial polishing. Final polishing was done on a horizontal lap using successive diamond grit sizes of 9, 6, 3, and 1μ. As this procedure could induce elevated temperatures within samples, the slowest speed setting was used and downward directed pressure on the lap wheel was kept to a minimum. After polishing, samples were mounted on frosted petrographic slides with a low temperature-setting, cyanonitrile-type cement ("super glue"). This type of mounting material was ideal because of its solubility in acetone and low setting temperatures. After the rock chip hardened to the slide, thick slices were cut, once again using the slow speed saw. The same polishing process was repeated until doubly polished specimens with good optical properties were obtained. The thickness to which sections were cut depended upon the opaqueness of the mineral being observed. Sphalerite, generally dark in appearance, was cut a little thicker than standard thin section size (40-50μm). Fluorite, usually transparent, was cut thicker (up to 1mm). The thicker the cut, the greater was the potential of finding suitable inclusions. Specimens were removed from slides by dissolving the adhesive in acetone. Chips were then wiped clean of any residue and placed in plastic vials.

Measurements

A modified U.S.G.S. gas-flow heating/freezing system marketed by Fluid Inc. was used for this investigation. Thermal gradients were minimized by two methods: (1) continuous flow of N_2 gas or compressed air around the sample and (2) direct contact of the thermocouple with the sample.

Homogenization temperatures were reached by passing heated, compressed air over the sample. By quickly heating and cooling the inclusion near the homogenization temperature ("temperature cycling" - Roedder, 1984) a precise T_h reading could be assured. If T_h was reached, the bubble would reappear upon cooling, usually at a considerably lower temperature. If T_h was not reached, the bubble would reappear and increase in size immediately upon cooling. Heating runs were conducted at the rate of 5°C per minute to approximately 15°C below T_h at which point the rate was reduced to 1° to 2°C per minute until T_h was reached.

Freezing temperatures were acquired by passing cooled N_2 gas directly over the sample. The inclusion had to be supercooled, usually well below its true freezing point, before the inclusion actually froze. Upon freezing, the slight volume change resulted in either a "jerk" by the vapor bubble or its complete collapse. As the inclusion

warmed, discrete ice crystals nucleated, usually turning the inclusion a brownish color. With continued warming, ice crystals coalesced. Finally, when the last ice crystal disappeared, the melting temperature (T_m) was reached. The same cycling technique for pinpointing T_h was used around the apparent T_m for more exact determinations. A summary of inclusion data is presented in Table 4-1. Detailed tables of all inclusion data can be found in Appendix B, and a list of sample numbers and corresponding stope locations is in Appendix C.

Pressure Correction

A maximum pressure correction can be applied to fluid inclusion homogenization temperatures if the amount of overburden at the time of ore deposition is known. This determination is difficult at the Gordonsville mine since it is not certain if the surface veins (as young as Mississippian age) are connected to the subsurface, ore-bearing breccia bodies. If they are, then overburden may have been greater than 500 m at the time of ore deposition. The many fractures and joints in the host rock suggest that the pressure during mineralization was close to hydrostatic, which would correspond to 47 and 52 bars at 10 and 25 wt.% NaCl respectively (derived from data of Haas, 1971). Based upon data from the system NaCl-H_2O presented by Potter (1977) the corresponding pressure corrections for

Table 4-1. Homogenization Temperatures (T_h), Freezing Temperatures (T_m), and Salinity Data from Fluid Inclusions of Ore and Gangue Minerals from the Gordonsville Mine.

Sample Number	Homogenization Temperatures			Freezing Temperatures			Average Salinity (eq. wt. % NaCl)
	No. of Incl.	Range (°C)	Average Temperature (°C)	No. of Incl.	Range (°C)	Average Temperature(°C)	
Sphalerite							
23	9	104.0 - 129.5	115.1	9	-21.2 - -22.3	-21.8	23.9
25	16	107.0 - 145.0	123.2	10	-21.9 - -22.3	-23.0	24.7
31	12	96.0 - 123.0	105.9	12	-20.2 - -23.5	-21.7	23.8
41	14	95.0 - 128.5	110.7	12	-14.5 - -22.8	-18.6	21.6
62	3	105.0 - 120.0	113.3	3	-22.5 - -23.2	-22.8	24.6
68	18	111.5 - 133.0	121.0	18	-20.4 - -23.6	-21.8	23.9
75	8	108.5 - 118.0	113.7	8	-14.3 - -21.0	-18.0	21.2
27A1	5	112.0 - 137.5	124.8	5	-21.2 - -22.5	-22.0	24.0
38A1	12	102.5 - 138.0	112.1	7	-21.8 - -23.3	-22.6	24.4
71A1	12	93.0 - 106.3	101.1	12	-18.5 - -22.1	-18.9	21.9
75A1	10	105.2 - 113.7	116.6	10	-15.3 - -21.3	-16.8	20.3
81A1	5	100.0 - 107.0	102.3	4	-18.0 - -20.0	-18.5	21.6
2-45	10	96.0 - 128.3	112.8	10	-22.1 - -23.5	-22.4	24.3
2-49	10	107.0 - 132.2	120.8	10	-21.7 - -23.0	-22.4	24.3
2-63	12	107.5 - 127.0	119.9	13	-16.0 - -22.5	-21.0	23.4
2-69	10	117.0 - 152.7	128.9	10	-18.4 - -21.0	-19.5	22.3
2-79	3	115.2 - 116.0	115.5	3	-18.4 - -18.5	-18.5	21.6
2-81	8	108.5 - 133.3	112.6	8	-14.0 - -20.8	-16.7	20.2
2-83	5	106.0 - 127.0	114.1	5	-17.2 - -20.6	-19.1	22.0
All Sph	182	95.0 - 152.7	115.8 (σ = 10.9)	169	-14.0 - -23.6	-20.7 (σ = 3.1)	22.9 (σ =1.5)
Fluorite							
55	11	102.7 - 113.4	108.5	11	-15.6 - -19.6	-17.8	21.0
81	21	100.5 - 116.3	112.8	20	-14.6 - -21.4	-17.0	20.4
86	7	91.5 - 101.7	95.7	7	-21.5 - -22.0	-21.8	23.9
38A1	2	99.7 - 103.6	101.9	2	-21.8 - -22.0	-21.9	24.0
48A1	11	92.3 - 113.7	102.0	12	-10.9 - -22.7	-18.4	21.5
2-22	18	112.2 - 122.7	116.2	20	-17.0 - -18.5	-17.9	21.1
2-31	20	101.0 - 116.7	107.7	19	-18.1 - -23.0	-21.8	23.9
2-50	16	106.7 - 120.4	116.0	16	-6.6 - -17.2	-14.0	17.9
2-52	35	105.6 - 118.5	114.7	35	-12.4 - -19.2	-15.0	18.8
All Fl	141	91.5 - 122.7	110.5 (σ = 7.9)	142	-6.6 - -23.0	-19.7 (σ = 3.3)	20.9 (σ = 2.1)

Table 4-1. - (Continued)

Sample Number	Homogenization Temperatures			Freezing Temperatures			Average Salinity (eq. wt. % NaCl)
	No. of Incl.	Range (°C)	Average Temperature (°C)	No. of Incl.	Range (°C)	Average Temperature(°C)	
Early Calcite							
E-1	20	80.3 - 106.5	97.5	20	-16.0 - -20.7	-19.2	22.1
Main-Stage Calcite							
12	10	112.8 - 147.2	131.8	10	-15.1 - -21.0	-18.1	21.3
16	10	132.0 - 148.2	141.1	10	-18.5 - -22.7	-20.3	22.9
35	9	120.4 - 158.0	140.4	8	-21.7 - -22.0	-21.9	24.0
2-3	8	105.0 - 120.9	113.4	8	-20.9 - -21.3	-21.2	23.5
2-22	5	128.0 - 157.9	147.6	5	-20.6 - -22.0	-21.6	23.8
2-70	12	117.1 - 160.0	138.2	12	-17.0 - -24.0	-21.1	23.4
2-72	15	101.6 - 156.6	122.6	15	-4.2 - -20.9	-17.9	21.1
3-13	6	127.7 - 150.4	137.4	6	-14.1 - -20.5	-19.0	21.9
All Cal	75	101.6 - 160.0	131.8 (σ = 15.6)	74	-4.2 - -24.0	-19.7 (σ = 3.4)	23.0 (σ = 1.0)
Late-Stage Calcite							
2-19	21	77.2 - 102.0	92.1	21	-5.0 - -8.1	-5.8	8.9
74	16	76.5 - 115.0	97.8	--	-----	--	--
2-54	8	78.5 - 108.3	97.0	8	-2.2 - -3.5	-2.6	4.3
19A1	10	85.5 - 115.5	99.7	10	-2.3 - -7.1	-4.6	7.3
2-28	4	72.1 - 105.5	92.5	4	-3.0 - -6.2	-4.6	7.4
75A2	--	-----	--	12	-3.0 - -5.0	-4.2	6.7
All Cal	59	72.1 - 115.5	95.3 (σ = 9.5)	55	-2.2 - -8.1	-4.3 (σ = 1.6)	7.4 (σ = 1.5)
Barite							
7A	--	-----	--	9	-4.3 - -5.6	-4.9	7.7
25	--	-----	--	7	-3.0 - -6.5	-4.4	7.0
27	--	-----	--	1	-----	-7.8	11.5
36	--	-----	--	14	-2.4 - -9.1	-7.0	10.5
53	--	-----	--	4	-4.4 - -4.6	-4.5	7.1
2-36	10	116.0 - 127.7	121.6	10	-3.2 - -6.3	-4.6	7.3
2-46	--	-----	--	7	-4.0 - -8.0	-6.6	10.0
2-60	2	120.5 - 124.2	122.4	11	-7.0 - -11.8	-8.9	12.8
2-69	--	-----	--	5	-3.6 - -7.6	-4.8	7.6
All Bar	12	116.0 - 127.7	121.6 (σ = 3.0)	68	-2.4 - -11.8	-5.8 (σ = 2.2)	8.9 (σ = 2.1)

fluid inclusion homogenization temperatures would be +5° to +10°C. This correction could be higher if the overburden was greater. Boiling is not evident in any of the fluid inclusions analyzed even though fluid temperatures may have reached 160°-170°C. Therefore, a minimum depth to ore emplacement must be that at which fluid pressure is sufficient to prevent boiling. These temperatures correspond to a minimum overburden of 70 meters for a 10 wt.% NaCl solution. Due to projected low values, the pressure correction was not applied to the data collected in this study.

Nature of Fluid Inclusions

Fluid inclusions examined in this study were of the liquid + vapor type and typically less than 30μm in size. Often large clusters of inclusions were filled by a single fluid with no visible vapor bubble; these were assumed to be "necked down" from oddly shaped, larger inclusions nearby. Daughter minerals were not observed. Equant inclusions situated away from clusters were interpreted as primary. Irregularly shaped inclusions were also interpreted as being primary. All other inclusions were assumed to be secondary unless some other feature proved them to be otherwise. Other inclusion characteristics are associated with certain minerals and will be discussed in the appropriate sections.

In this study, almost all data have been acquired from what are believed to be, based on the above descriptions, inclusions of primary origin. Pseudosecondary inclusions were rarely used as they may have been mistaken for secondary inclusions. Secondary inclusions were sometimes studied to see if later fluids affected earlier formed minerals. These inclusions, however, were used only for qualitative purposes.

Results

Sphalerite

Fluid inclusion measurements were made on all three types of sphalerite (disseminated, massive, and vug-filling), although most of the data were from the more massive variety. The most abundant inclusions were those which contained bituminous material, including solid, liquid, and liquid + vapor filled, ranging in size from <2μm to >100μm. At 460X magnification, the very small inclusions appeared as "dirt" specks. There seemed to be minimal correlation between sphalerite color and the concentration of dark inclusions. Clear, liquid + vapor inclusions were less common but occurred in a variety of sizes (from <2μm to >50μm); their shapes range from individual oval to square inclusions to flat, interconnected masses (Figure 15a,b).

Homogenization and freezing temperature pairs were obtained from inclusions in 20 samples. Homogenization

Figure 15. Photomicrographs of fluid inclusions in sphalerite and fluorite. Bar scale represents 0.5mm.

A. Plane of secondary, hydrocarbon inclusions in sphalerite (Sample 68).

B. Primary inclusions and inclusions in the process of "necking down" in sphalerite (Sample 68).

C. Primary inclusion in fluorite (Sample 2-22).

D. Plane of secondary inclusions in fluorite (Sample 2-22).

A
B
C
D

temperatures ranged from 80.0°C to 153.0°C with an average of 115.8°C (σ = 17.0). Most measurements clustered between 100° and 125°C. Problems during homogenization were minimal; replicate measurements were reproducible to ±0.3°C.

Freezing temperatures (disappearance of the last ice crystal, T_m) had a mean of -20.7°C (σ = 2.9) and ranged from -14.0° to -23.8°C. The NaCl-H_2O system has a eutectic (temperature at which ice first begins to melt, T_e) at -20.5°C and a metastable eutectic at approximately -28°C. T_e for sphalerite inclusions ranged from -75° to -45° indicating the presence of salts other than NaCl in the inclusion fluids (Roedder, 1963; Crawford, 1981) or the presence of undetected organic compounds (Leach, 1980). These eutectic temperatures suggest that $CaCl_2$ (and/or $MgCl_2$) is probably a major component in the system (Crawford, 1981). The freezing temperatures correspond to an average salinity of 22.9 equivalent wt.% NaCl (using the equation: wt.% NaCl equivalent = $1.76958\Theta - 4.2384 * 10^{-2}\Theta^2 + 5.2778 * 10^{-4}\Theta^3 \pm 0.028$ [$\Theta = 0 - T_m$]; Potter et al., 1978). Although the inclusions do not contain a pure NaCl solution, the salinity calculations are probably still valid based on the similarity of freezing point depression curves for different NaCl, KCl, $CaCl_2$, and $MgCl_2$ solutions (Crawford, 1981). Cotectic melting temperatures (the temperature at which $NaCl \cdot 2H_2O$ disappears) were not

determined in this study due to the difficulty in finding large inclusions of high optical quality.

Histograms of homogenization and freezing temperatures are presented in Figure 16. A graph of freezing temperatures against homogenization temperatures for the three sphalerite varieties shows no particular trend (Figure 17). Vug and massive sphalerite all plot in the same area. There is a slight deviation of disseminated sphalerite towards the higher freezing temperature (lower salinity) range while homogenization temperatures remain similar to those of the other varieties. This deviation, however, does not reflect two discrete populations as there is considerable overlap between the two sets.

Fluorite

Fluorite samples were the easiest to work with as they contained abundant, clear and large liquid + vapor inclusions. Planes of secondary inclusions were numerous; often, lower power objectives had to be used to insure that an inclusion that appeared to be isolated was actually not part of a fracture plane. Most inclusions were fairly large (30μm) and round to oval in shape (Figure 15c,d).

For fluorite, 124 heating and freezing pairs were run. Homogenization temperatures for primary inclusions ranged from 91.5° to 122.7°C with an average of 110.5°C (σ = 7.9). Freezing temperatures ranged between -23.0° and -4.0°C with

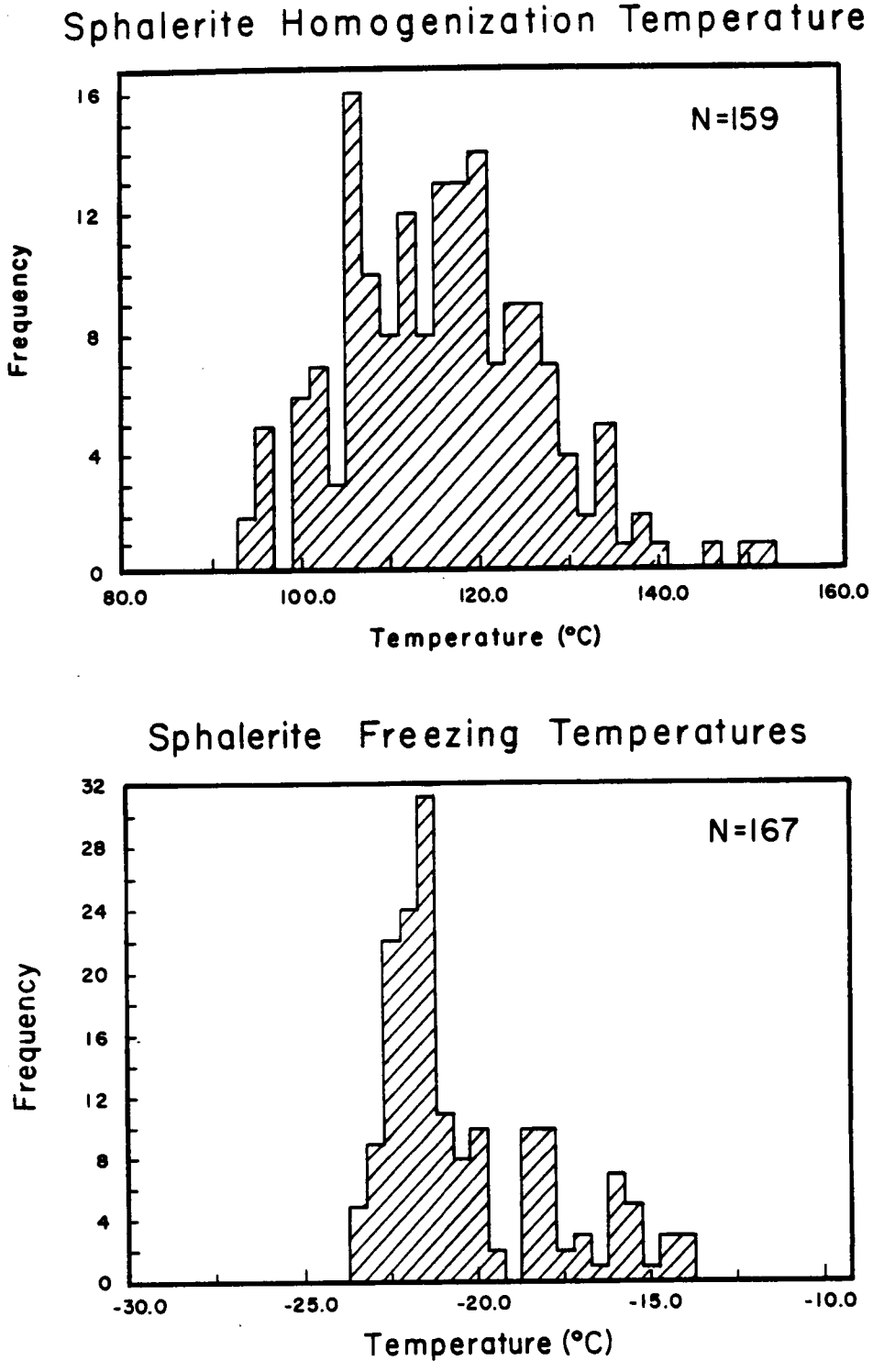

Figure 16. Histograms of homogenization and freezing temperatures for fluid inclusions in sphalerite from the Gordonsville zinc mine.

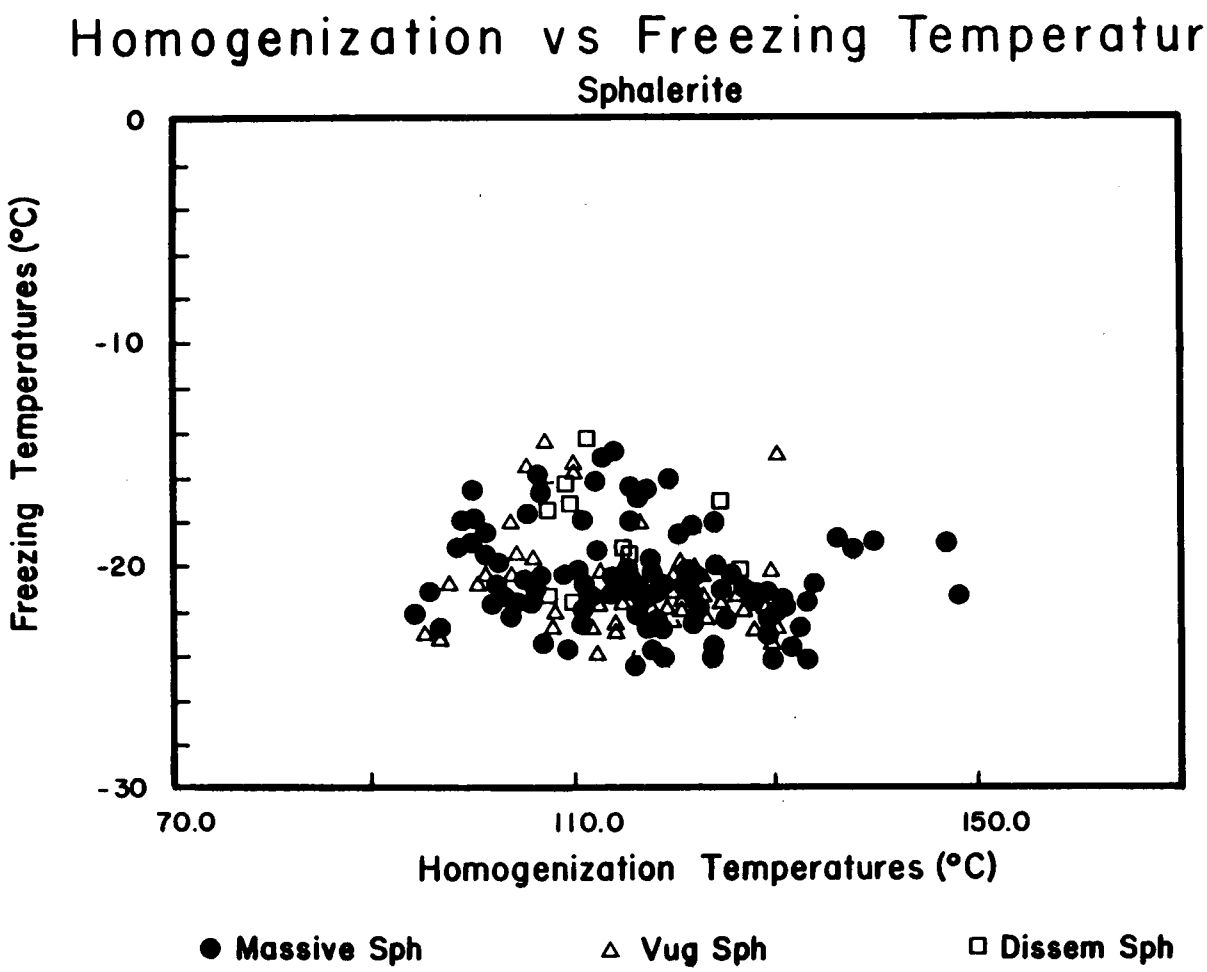

Figure 17. Homogenization vs freezing temperature for fluid inclusions in the three textural varieties of sphalerite from the Gordonsville zinc mine.

the majority occurring between -23° and -12°C. The average T_m was -17.5°C (σ = 3.2) (Figure 18). Only 3 inclusions had a T_m which was higher than -12.0°C. Both homogenization temperatures and calculated salinities fall below those of sphalerite. The variable peak heights on the histograms are probably due to sample bias; more data were collected from some samples than from others. Weighted averages of fluorite data (and of all mineral data) are within 0.5°C of uncorrected averages; thus, the averages recorded are believed to be valid.

A plot of homogenization temperature vs freezing temperature shows that data pairs fall in a restricted range (Figure 19). There is suggestion of a trend in the data from low T_m, low T_h to high T_m, high T_h. Linear and nonlinear regression analyses performed on all data and on sample averages yielded low R values of less than 0.6. The significance of a "best fit line", therefore, would be low.

The homogenization temperatures for both fluorite and sphalerite are believed to be fairly accurate, i.e., not anomalously high due to stretching and/or leakage. Great care was taken not to overheat samples. Studies by Bodnar and Bethke (1984) on fluorite and sphalerite found that there was no stretching upon overheating inclusions 30°-40°C past their homogenization temperatures. It is believed that in this study, if overheating did occur, the temperature fell well below these bounds.

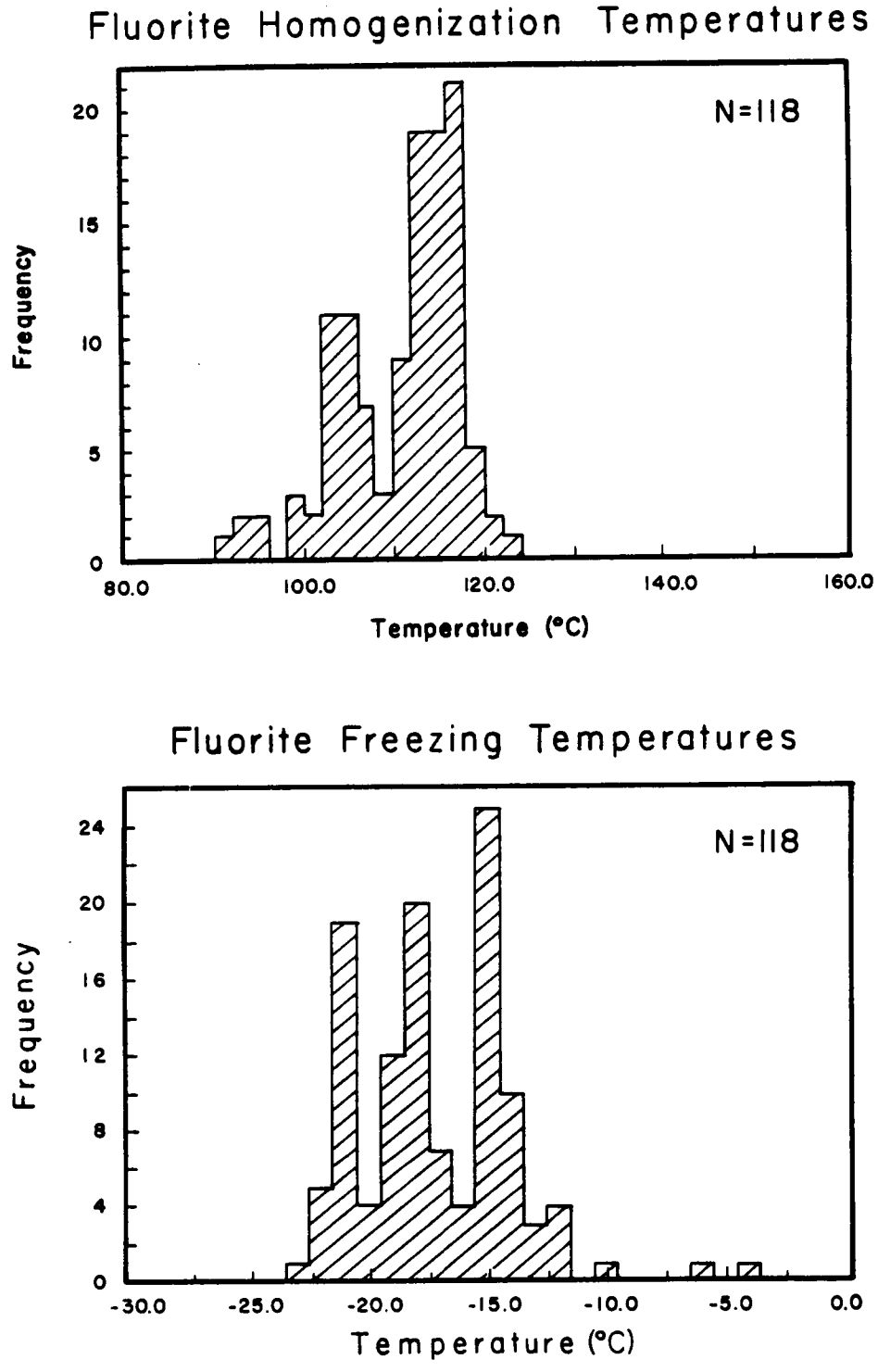

Figure 18. Histograms of homogenization and freezing temperatures for fluid inclusions in fluorite from the Gordonsville zinc mine.

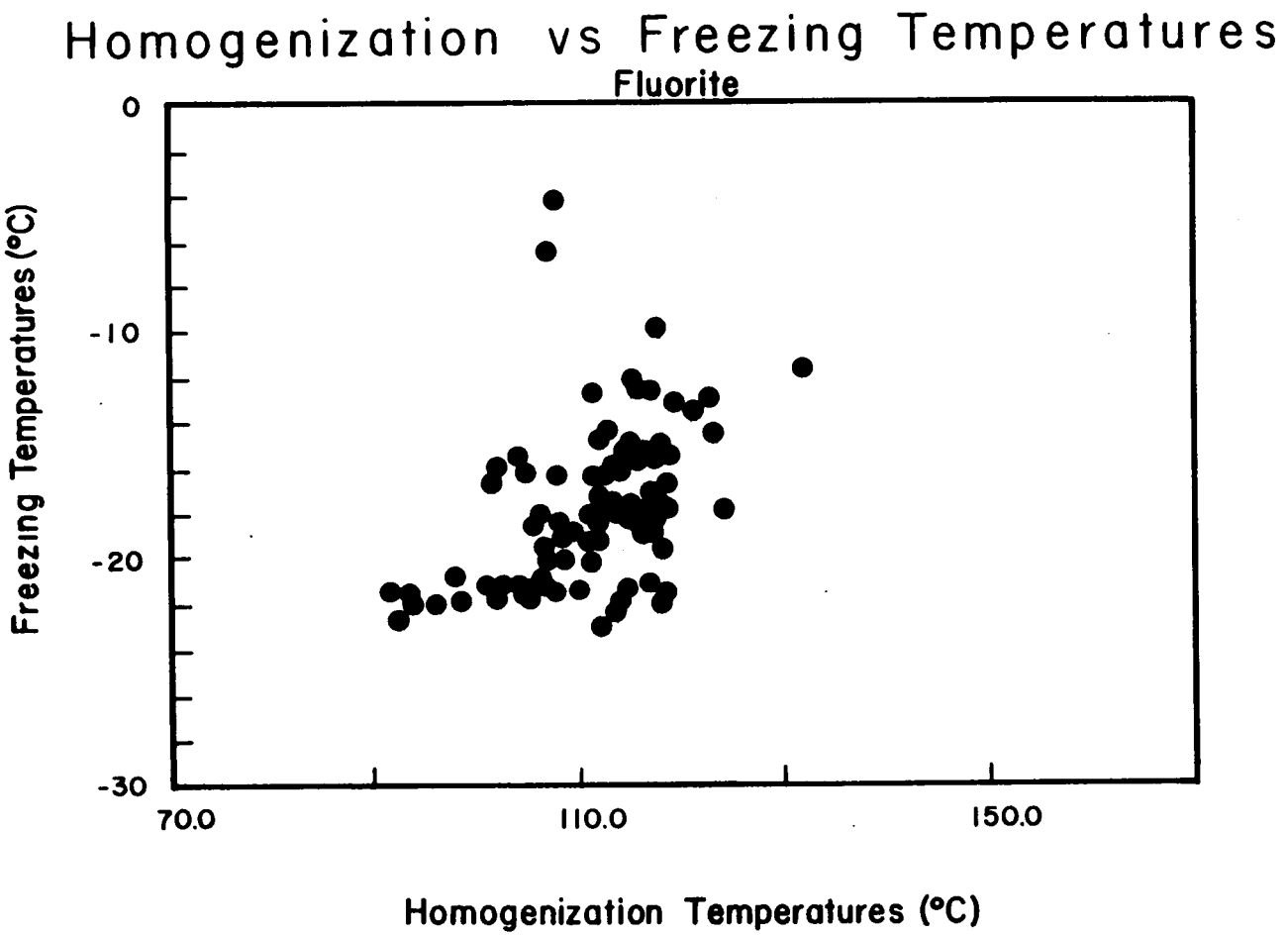

Figure 19. Homogenization vs freezing temperature for fluid inclusions in fluorite from the Gordonsville zinc mine.

Calcite

Measurements were made on calcite crystals of three different generations: early white calcite, post-sphalerite main-stage calcite, and late amber calcite. The homogenization temperatures of fluids in early calcite ranged between 80.3° and 106.5°C with an average of 97.5°C (σ = 7.6). Freezing temperatures ranged from -16.0° to -21.0°C with an average of -19.2°C (or 22.1 equivalent wt.% NaCl) (σ = 1.5). Liquid + vapor type fluid inclusions were numerous; rarely were dark inclusions (solid or liquid) apparent. These data, unfortunately, were collected from only one sample (from the Elmwood mine) as early calcite is rarely observed in the Gordonsville mine.

Main-stage calcite, white to lavender in color, is prevalent in the mine; thus, the majority of the determinations were made on this generation of calcite. The fluid inclusions contained in these crystals homogenized between 101.6° and 160.0° with an average of 131.8°C (σ = 24.3). Freezing temperatures of -4.2 to -24.0 (average -19.7°C, σ = 3.5) were obtained. Most measurements, however, were between -18° and -22°C (Figure 20). This calcite generation contained inclusions which showed remarkable consistency in salinity values (22.5 equivalent wt.% NaCl) yet varied significantly with respect to T_h. Compared to early calcite, main-stage calcite contained

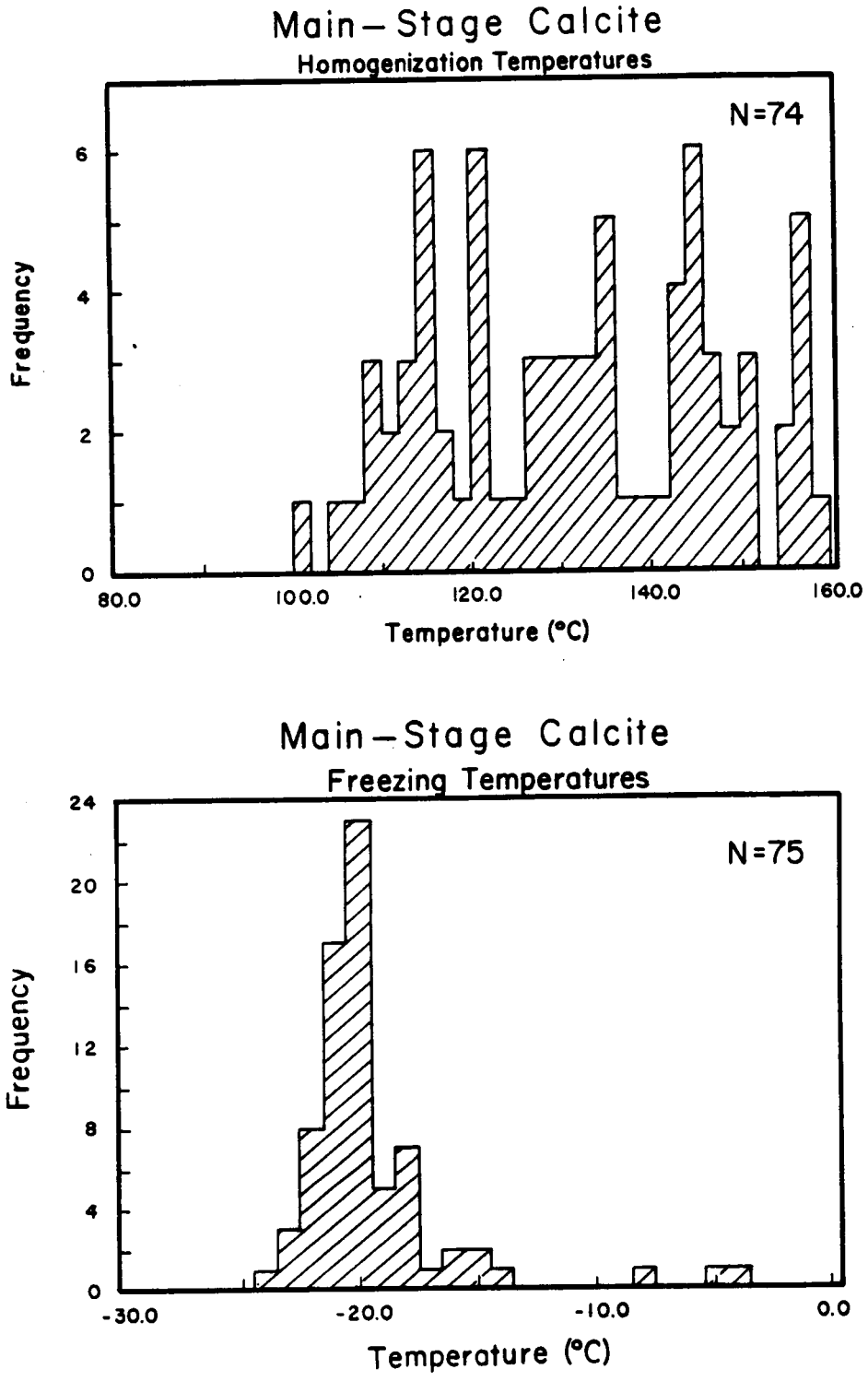

Figure 20. Histograms of homogenization and freezing temperatures for fluid inclusions in main-stage calcite from the Gordonsville zinc mine.

fewer inclusions but more dark inclusions and bituminous material. However, the quantity of dark, hydrocarbon inclusions is much less than that of sphalerite.

Clear to amber colored, late-stage calcite is rich in dark inclusions, presumably hydrocarbons (Figure 21a,b). The amber color may be a result of the higher density of dark inclusions as these inclusions are not as prominent in the clearer areas. Homogenization temperatures for fluids of vapor + liquid type inclusions ranged from 70.6° to 115.5°C with an average of 95.3°C (σ = 12.4). The range of freezing temperatures was quite narrow, between -2.2° and -9.3°C. The average T_m was -4.7°C (σ = 1.5) (7.4 equivalent wt.% NaCl) (Figure 22). There were no differences in homogenization or freezing temperatures between clear and amber colored areas of the calcite, therefore the color change probably does not represent a change in fluid temperature. Both homogenization temperatures and fluid salinities appear to be markedly different than those of the main-stage calcite. Early calcite and late calcite contain fluids of very different salinities while their respective homogenization temperatures are similar (Figures 23,24).

Amber calcite caused problems during the early stages of the fluid inclusion study. The initial determinations gave high T_h values, with an average of 170°C. Upon closer scrutiny, it was realized that, on any given chip, homogenization temperatures rose to the temperature to which

Figure 21. Photomicrographs of fluid inclusions in late-stage amber calcite and barite. Bar scale represents 0.5mm.

A. Dark, presumably hydrocarbon-rich inclusions in amber calcite (Sample 2-19).

B. Dark inclusions along with liquid/vapor inclusions in amber calcite (Sample 2-19).

C. Primary inclusion in barite. They are susceptible to leakage upon heating (Sample 36).

D. Primary inclusion in barite (Sample 36).

A
B
C
D

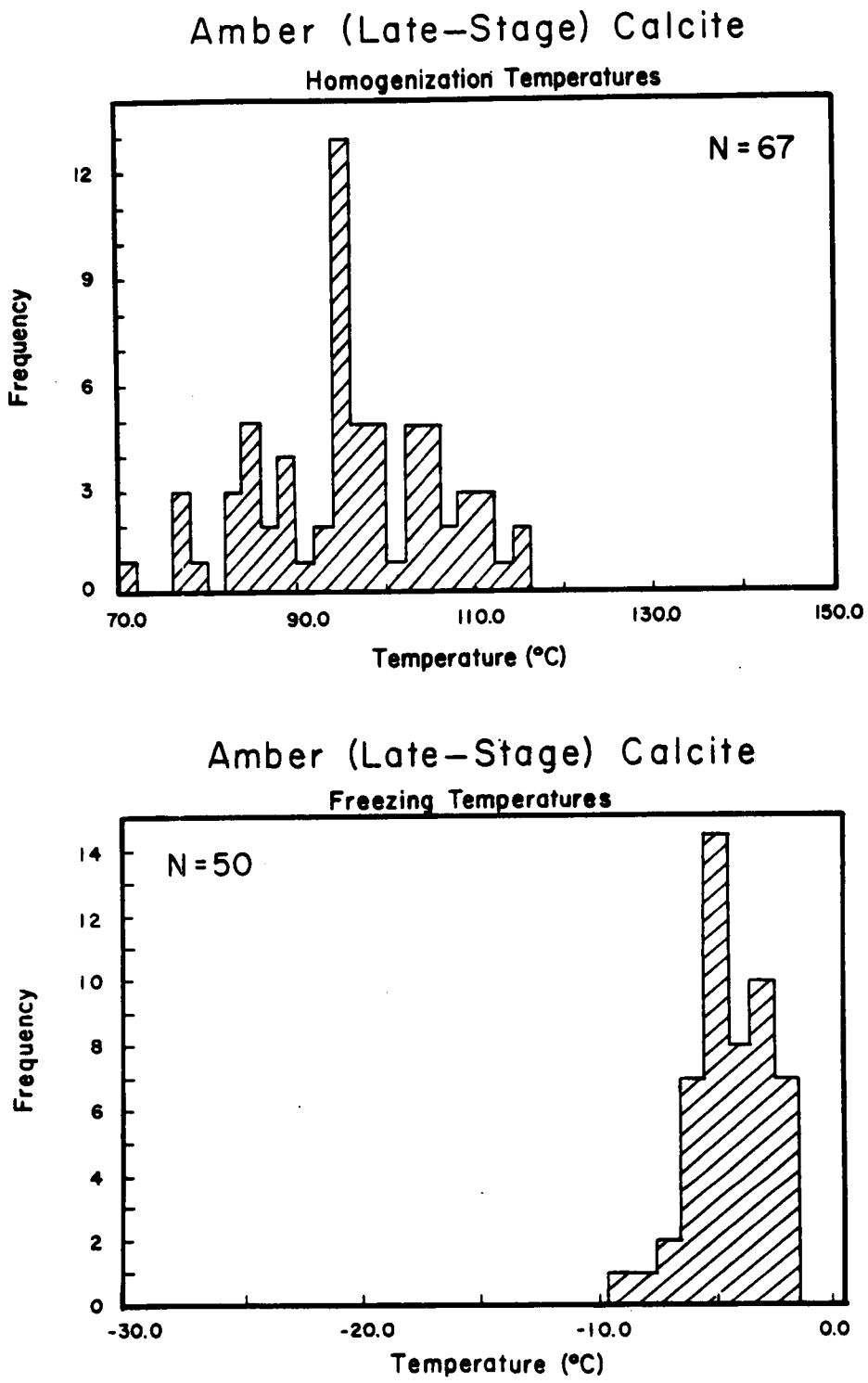

Figure 22. Histograms of homogenization and freezing temperatures for fluid inclusions in late-stage amber calcite from the Gordonsville zinc mine.

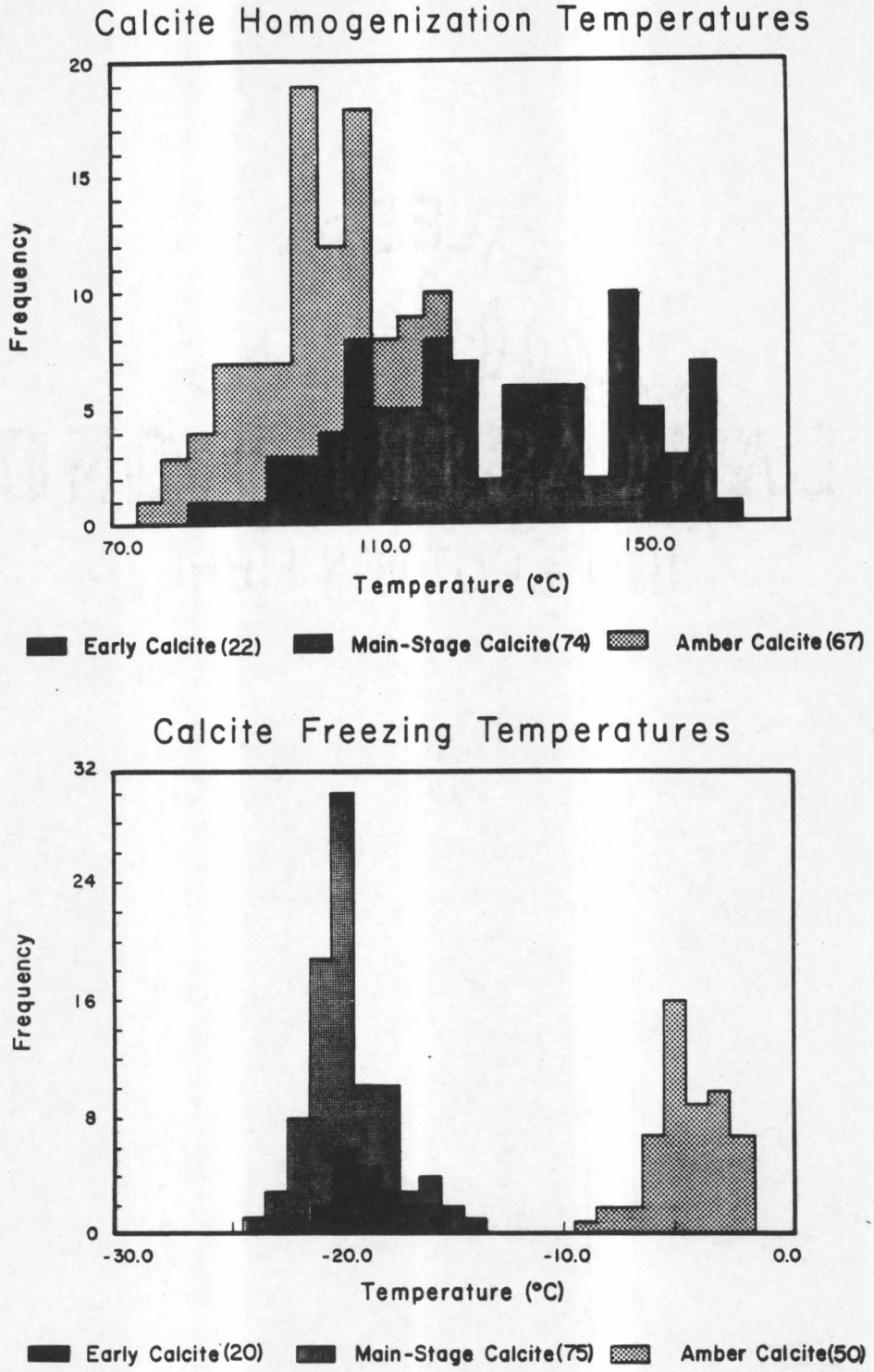

Figure 23. Stacked histograms displaying homogenization and freezing temperatures for fluid inclusions in the three different generations of calcite at the Gordonsville zinc mine.

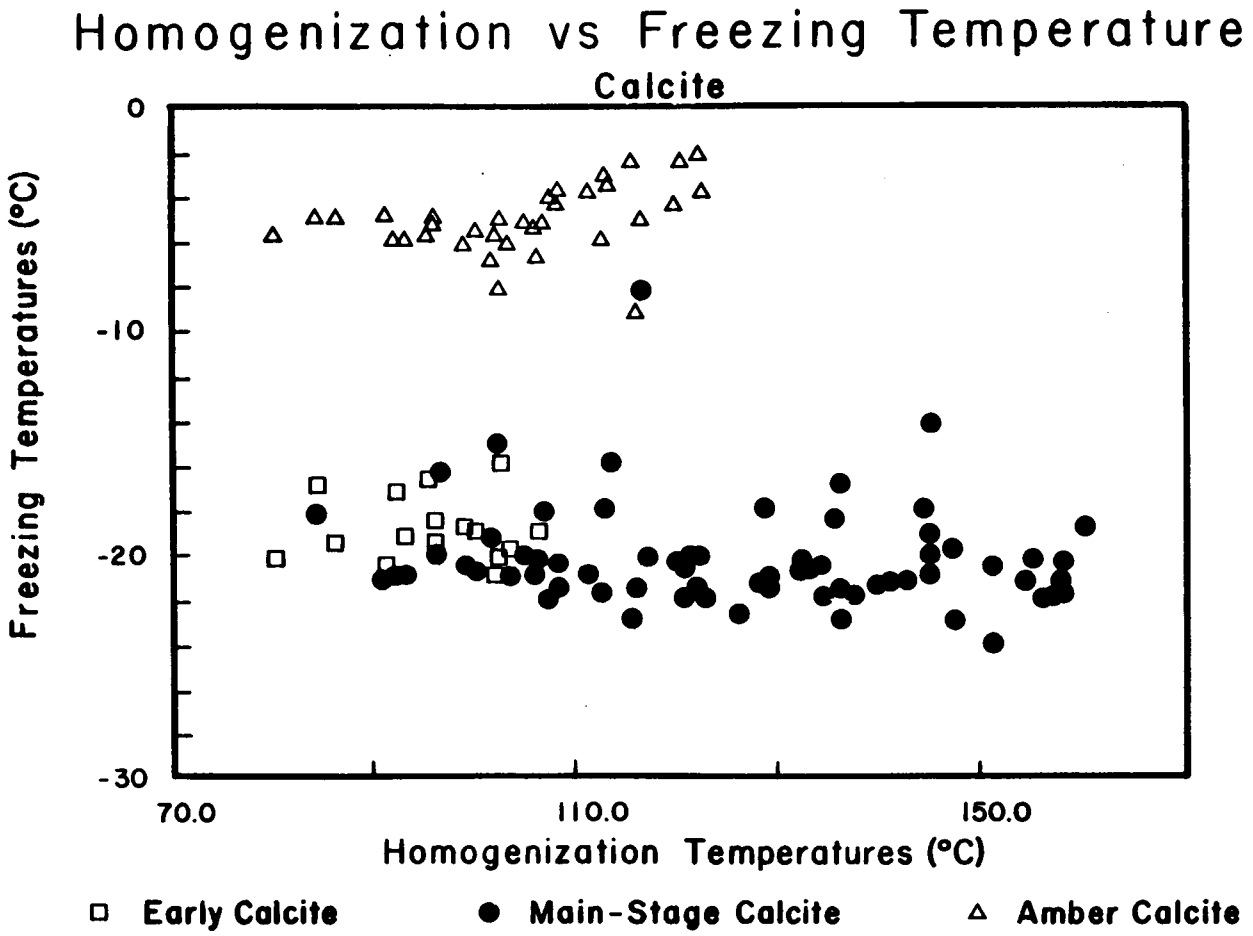

Figure 24. Homogenization vs freezing temperature for fluid inclusions in the three different generations of calcite from the Gordonsville zinc mine.

the chip was subjected, or higher. Inclusions which originally homogenized at low temperatures (100°), when subjected to higher temperatures, homogenized at those higher temperatures. The data were often consistent and reproducible, yet incorrect.

Presumably, the low-temperature inclusions leaked and/or were stretched due to overheating past their original T_h (Roedder, 1981). The high-temperature inclusions which usually contained large vapor bubbles are enigmatic, however. They may have stretched or leaked before their homogenization temperatures were reached. This proved to be true with barite. They may be inclusions which had earlier necked down; this might account for their variable vapor/liquid ratio. Another possibility is that these are inclusions of primary origin from an inhomogeneous liquid (Roedder, 1984). This would pose a problem by introducing sampling bias (throwing out good data from primary inclusions which deviate from expected results). The high temperature (170°C+) inclusions in this study are believed to be "anomalous" and hence should be eliminated from the data group for several reasons:

1) Vapor/liquid ratios were high. This could indicate necking down or leakage.

2) Lower temperature inclusions, after being subjected to overheating revealed approximately the same vapor/liquid ratios as the high temperature inclusions.

3) Some calcite fluid inclusions were similar in shape, size, and liquid/vapor variability to inclusions in barite whose vapor bubbles shrank as the temperature rose and then suddenly expanded, presumably due to leakage. The inclusions would either homogenize at a high temperature or not at all.

Another possible reason for the existence of these "anomalous" inclusions may be the presence of methane, often undetectable within the bubble phase of an inclusion. Its presence may increase the homogenization temperature by more than 30°C (Hanor, 1980). Why leakage is so common in this later calcite stage is uncertain. It may be due, again, to the introduction of methane. Leakage is aggravated by the presence of methane as the gas induces a build up in pressure within the inclusion, pressure greater than that of a normal inclusion with a water vapor bubble. The effect of methane on salinity values is minimal. Throughout all experimental work with amber calcite, the salinities determined remained fairly constant. These values are believed to be valid.

Barite

Fluid inclusions in barite homogenized between 85° and >200°C. These measurements are not as reliable as those for previous minerals because of the nature of the inclusions. Inclusions are highly variable in size and vapor/liquid ratios. Often inclusions are intricately connected with

each other (Figure 21c,d). Many inclusions leaked before their homogenization temperature was reached. Vapor bubbles would decrease in size, to a temperature of 80° to 110° and then rapidly increase in size, and often never disappear (or homogenize) upon continued heating. In several instances, the bubble would not renucleate upon cooling. Similar problems with fluid inclusions in barite have also been described by other workers (Leach, 1980; Bodnar and Bethke, 1984; Richardson and Pinckney, 1984).

Freezing temperature measurements were much more consistent in barite fluid inclusions. Even after an inclusion's homogenization temperature changed by over 100%, its determined salinity remained constant. It is believed that leaking did not affect salinity measurements appreciably. Freezing temperatures for 73 inclusions in 9 samples ranged from -2.0° to -11.8°C with an average of -5.8°C (σ = 2.0). This corresponds to a salinity of 7.7 equivalent wt.% NaCl (Figure 25). Twelve inclusions, which appeared to give valid results, homogenized between 116.0° and 127.7°C. There is a marked similarity between the low salinities of inclusions in barite and those in the late amber calcite; whereas their low salinities contrast sharply to the high salinities of inclusions in sphalerite, fluorite and the earlier two generations of calcite. Problems incurred upon freezing included failure to freeze and failure to renucleate. The failure to freeze may have been

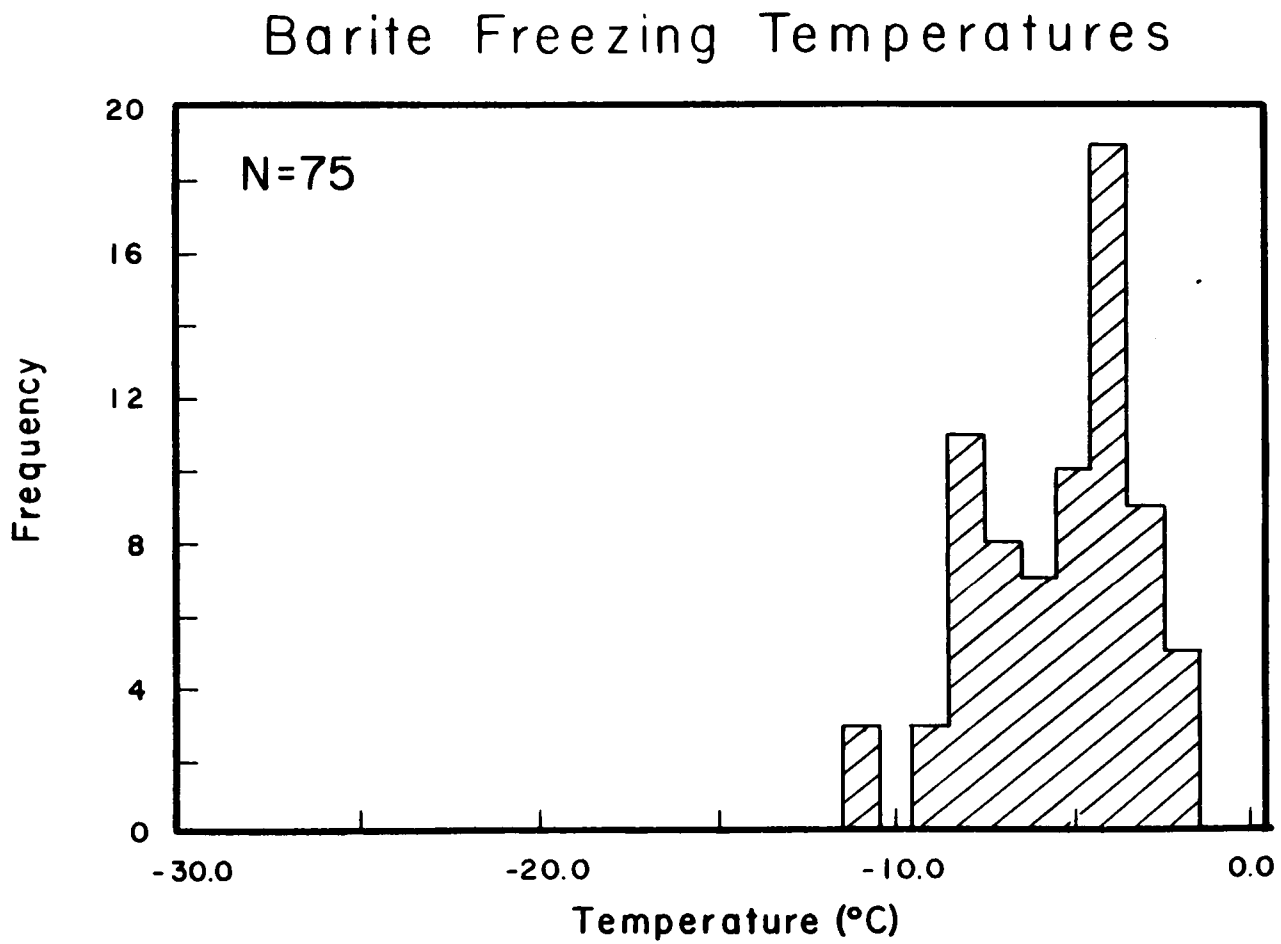

Figure 25. Histogram of freezing temperatures of fluid inclusions in barite from the Gordonsville zinc mine.

due to soluble or colorless hydrocarbons within the inclusions. Their presence would cause significant freezing point depression; however, it is improbable that the hydrocarbons existed as a liquid phase. The absence of suitable nuclei for the formation of ice would also inhibit freezing (Leach, 1980).

Interpretations

Fluid inclusion measurements have defined changes in temperature and salinity of the ore fluid through time. These changes are recorded graphically in Figure 26. The range of homogenization temperatures in this detailed study agrees with preliminary investigations by other workers in the Central Tennessee zinc district (Roedder, 1971; DeGroodt, 1973). Homogenization temperatures ranged from 75° to 160°C for all stages of gangue and ore deposition. A wide range of salinity values were recorded, from 3 equivalent wt.% NaCl for barite and late stage, amber calcite, to well over 23% for sphalerite and early calcite.

Early calcite is the first mineral in the paragenetic sequence from which formational temperatures and salinities have been derived. This generation of calcite was formed from a fluid of relatively low temperature (avg. 98°C) and high salinity (22%). Sphalerite, the only zinc ore mineral at Gordonsville, was deposited next. Sphalerite precipitation was marked by a slight increase in

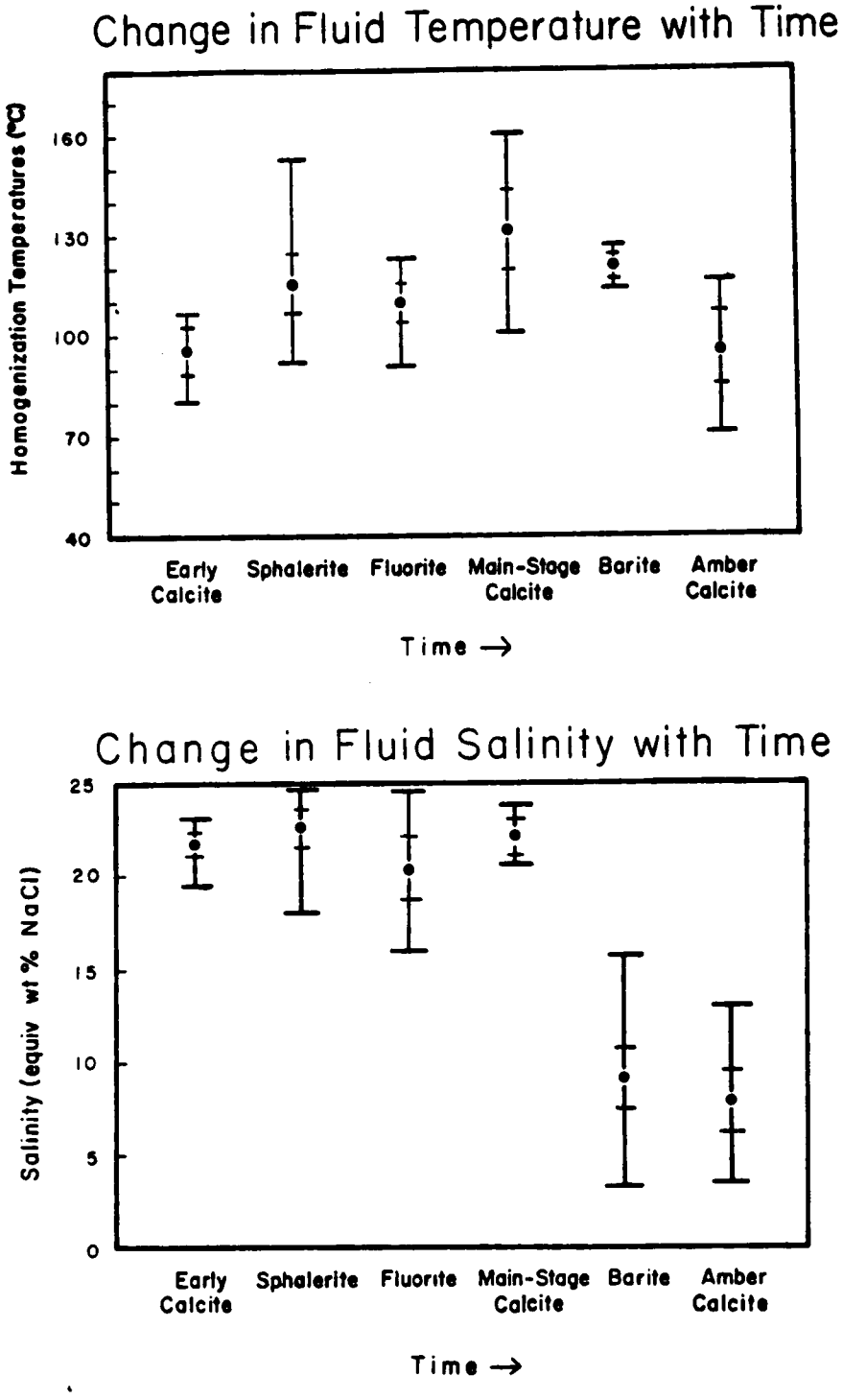

Figure 26. Change in fluid temperature and salinity with time as interpreted from fluid inclusion data, Gordonsville zinc mine (outer bar = total range, dot = average, inner bar = st. dev.).

temperature, from 80°-110°C to 100°-125°C. Unfortunately, early calcite data is from only one sample (from the Elmwood mine); thus, the validity of this temperature rise is uncertain. Sphalerite data have been grouped together since fluid inclusion evidence does not necessitate the separation of sphalerite into two or three stages. Fluid salinity remained essentially constant from early calcite through sphalerite deposition. The narrow range of sphalerite fluid inclusion data does not allow recognition of a trend in the temperature and salinity of depositional fluids cited by others as evidence for fluid mixing (Zimmerman and Kesler, 1981; Taylor et al., 1983). Sphalerite deposition marked a period of increased hydrocarbon presence as sphalerite contains diffuse bituminous material and a high density of hydrocarbon inclusions.

Hydrocarbon density decreased with the commencement of fluorite deposition; fluid temperatures and salinities, however, did not change dramatically. A decrease in temperature (from an average of 116° down to 110°C) was noted. The change in salinity was minimal (from an average of 23 to 21%) and probably insignificant. It is uncertain whether this decrease in temperature could account for the cessation of sphalerite deposition and the precipitation of fluorite. A change in fluid composition may have been a factor. Had this change in temperature accounted for the change in mineral deposition, one might expect an overlap or

fluctuation in sphalerite and fluorite mineralization. There is no evidence, however, that any sphalerite formed after fluorite.

Main-stage, white to lavender calcite is the next mineral phase in the paragenetic sequence. Fluids responsible for main-stage calcite precipitation were characterized by variable but higher temperatures (100°-160°C) than those responsible for deposition of the preceding minerals. Salinities, however, remained relatively high.

Fluid salinity was markedly lower during the precipitation of barite. Salinity decreased from 20-23% for earlier minerals to an average of 8% for barite. The latest stage mineral, amber calcite also precipitated at a relatively low salinity (7.5%), very close to that of barite. Homogenization temperatures were low (95°C), lower than formational temperatures for sphalerite, fluorite, and main-stage calcite. The few inclusions suitable for heating indicate that barite precipitated at a higher temperature than amber calcite but not as high as main-stage calcite. The validity of these measurements is questionable; however, based upon the bimodal distribution of salinity data, it is believed that barite and amber calcite precipitated from a similar fluid characterized by low salinities and temperatures.

Fluid salinity was nearly constant (20-23%) throughout most of the mineralization period. The low eutectic temperature (-45° - -60°C) of fluid inclusions suggests that fluids were NaCl - $CaCl_2$ rich. Oil inclusions, especially ubiquitous in sphalerite, indicate that the fluid migrated through, or was deposited in an area rich in organic matter. These observations imply that depositional fluids through much of the mineralizing sequence were connate or basin brines (White, 1974). During the later stages of mineralization, fluid inclusion data suggest that there was a large drop in fluid salinity along with a smaller decrease in temperature indicating the possible influx of cooler, more dilute fluids into the system.

In an earlier discussion on petrography, the relationship between main-stage calcite and barite, in some thin sections, was described as ambiguous, although the majority of the observations favored calcite deposition before barite. The precipitation of barite before main-stage calcite does not seem plausible in light of fluid inclusion evidence. If barite had precipitated first, there would have been a "seesaw" in fluid salinities, from high salinities in sphalerite, to very low salinities in barite, to high salinities and high temperatures in calcite, to low salinities and low temperatures for amber calcite. With this in mind, it must be concluded that some of the petrographic data is ambiguous. Seemingly fragmented barite

blades in main stage calcite may be represented in the third dimension by barite penetrating calcite (thus, barite post-dates the calcite).

CHAPTER 5

TRACE ELEMENT AND STABLE ISOTOPE STUDIES OF ORE AND GANGUE MINERALS

Atomic Absorption

A Varian Series 475 Absorption Spectrophotometer was used to analyze the minor and trace elements of sphalerite and gangue calcite. Dissolution of calcite and sphalerite followed the procedural outlines suggested by Pinta (1975) and McLaren (1978) respectively. The operating conditions for the atomic absorption spectrophotometer were as recommended in the Varian 475 Series Operating Manual. Precision estimates were calculated from sets of triplicate analyses. They are estimated to be ±2% for Fe, ±1% for Mg, ±1% for Mn,and ±1% for Sr in calcite, and ±2% for Cd, ±5% for Pb, ±5% for Mn, ±2% for Fe, ±5% for Mg, ±6% for Ni, and ±1% for Cu in sphalerite.

Calcite

Six samples of main-stage, white to lavender calcite and eight samples of late-stage, clear to amber calcite were analyzed for the trace elements Sr, Mn, and Fe, and the minor element Mg. Main-stage calcite and late-stage amber calcite cannot be differentiated by these four trace elements as their concentrations remained relatively constant during both phases of calcite deposition. Results from this study,

presented in Table 5-1, are similar to those for amber calcite by Larsen (1978); Mn concentration for amber calcites in this study, however, are somewhat lower. There is also no differentiation among trace elements in clear and amber colored (both late-stage) calcite. Instead, the color differences among white, clear, and amber calcite appear to be due to the density of fluid inclusions and hydrocarbon inclusions. Larsen (1978), however, believed the amber color to be caused by a combination of trace elements which would include Fe, Mn, and Yb. Data from the present study refute his conclusion, at least relative to the former two elements. Trace element data suggest that mineralizing fluids did not change in composition appreciably with respect to the four elements analyzed in this study.

Sphalerite

Thirteen samples of sphalerite were analyzed for Fe, Cd, Cu, Mg, Pb, Mn, and Ni, to determine whether or not the precipitation of the three textural varieties could be differentiated based on their trace element contents. Main stage and vug-filling sphalerite could not be differentiated by any of the seven trace elements. Disseminated sphalerite, however, is slightly deficient in the elements Fe and Cd, although this deficiency does not appear great enough to distinguish between disseminated sphalerite and the other two varieties. Bulk sphalerite analysis revealed Fe and Cd

Table 5-1. Trace Element Analyses (in ppm) of Calcite Samples from the Gordonsville Mine (values are averages from three replicate analyses).

Sample	Calcite Type	Mg	Fe	Sr	Mn
9	main-stage	2207	233	218	*
11	main-stage	1584	183	151	96
12	main-stage	1885	132	171	*
2-72	main-stage	1517	209	148	50
3-2	main-stage	1161	157	191	52
3-3	main-stage	1078	96	129	41
15	main-stage	1006	44	131	31
73	main-stage	887	113	165	28
74A	late-amber	1394	139	66	53
74C	late-clear	2034	118	156	122
2-29A	late-amber	1294	47	113	48
2-29C	late-clear	1299	298	176	30
2-56	late-amber	796	16	127	46

* - not determined

concentrations as high as nearly 2,500 ppm and Cu concentrations of up to 900 ppm. Pb and Mg concentrations varied from 10 to 20 ppm, while Mn and Ni concentrations average less than 1 ppm. These data, presented in Table 5-2, are consistent with analyses by Jolly and Heyl (1968) on sphalerite in surface veins although Fe, Cd, and Cu concentrations in this study are somewhat lower.

Electron Microprobe Analysis

An automated M.A.C. 400S electron microprobe was used to analyze sphalerite samples in order to determine whether or not white to orange color zones are caused by variations in the proportions of the elements Cd and Fe. Corrections for matrix effect were calculated using the method described by Ziebold and Ogilvie (1964). Corrections for background, drift and deadtime were performed by a Krisel Control Automation Program (on a D.E.C. PDP 11-15 computer). Because of the low concentrations of each element, background counts were taken at each analysis point to insure accuracy. However, because of the limitations of the instrument, values below 0.2 wt.% should only be regarded as qualitative determinations. Standards used for the sphalerite analysis included ZnS for Zn, Fe_2O_3 for Fe, and CdS for Cd.

Three polished thin sections were prepared from three samples of sphalerite (massive and vug-filling) for microprobe analysis. Two to three traverses were made across

Table 5-2. Trace Element Analyses (in ppm) of Sphalerite Samples from the Gordonsville Mine (values are averages from three replicate analyses).

Sample	Sph Type	Fe	Cd	Cu	Mg	Pb	Mn	Ni
2-83	dissem	1186	949	855	10	13	1	1
2-77	dissem	1115	914	871	16	14	1	1
45	dissem	1620	997	429	10	*	*	*
18	massive	2460	2154	851	3	*	*	1
23	massive	1794	1056	519	7	11	1	1
37	massive	1465	1426	469	20	19	1	1
2-45	massive	2306	2406	899	27	31	1	1
2-60	vug-fill	1917	1333	714	--	8	1	1
41	vug-fill	1868	1181	431	--	10	1	1
68	vug-fill	2251	1613	335	24	10	1	1
2-11	vug-fill	*	*	*	*	24	1	1
2-49	vug-fill	1947	954	625	4	14	1	1
2-62	vug-fill	1716	1103	557	22	21	1	1

* - not determined

several areas in each thin section. At different points along the traverses, color and Fe, Cd, Zn concentrations along with Fe/Cd ratios were noted. A total of 110 point analyses were preformed. A representative traverse is illustrated in Figure 27. Representative analyses are presented in Table 5-3; a list of all analysis results is given in Appendix Table D. Fe concentrations ranged from 0.10 wt.% to 0.53 wt.%, while Cd concentrations ranged from below the instrument's detection limit to 0.76 wt.%. According to the spot analyzed, Fe and Cd concentrations were placed in three color groups: orange, yellow, and white. It was found that, generally, white areas contain higher concentrations of Fe and Cd than orange areas and that the Fe/Cd ratio increases in orange areas. To see if this differentiation among color groups is statistically valid, an ANOVA statistical test was performed on the data. The purpose of an ANOVA test is to determine whether there is enough variation among the means of data sets to divide them into distinct populations, i.e., is the variance among data sets greater than within data sets. In this study, ANOVA demonstrated that color groups could be differentiated by the concentrations of the elements Fe and Cd (see Table 5-4). The average Cd concentration in white areas is 0.52 wt.% while that in orange areas averages 0.15 wt.%.

The general range of Cd and Fe concentrations is consistent with previous studies (Larsen, 1978; Craig et al.,

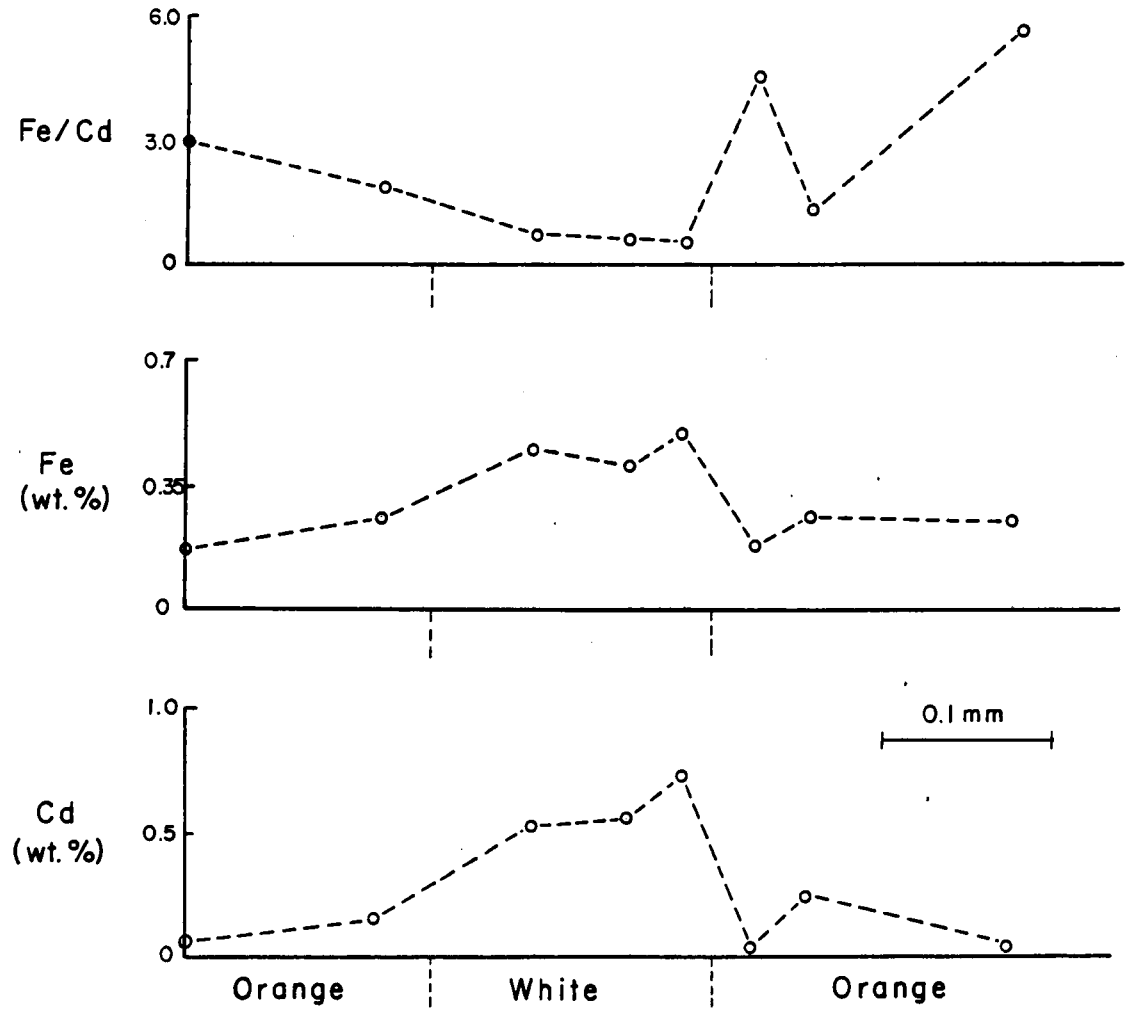

Figure 27. Electron microprobe traverse showing the variations of iron and cadmium contents in sphalerite (sample 18, traverse 5).

Table 5-3. Metal Content Averages (wt. % ± σ) from Color Zones in Three Samples of Massive and Vug-filling Sphalerite (110 Analyses).

Color	Fe	Cd	Zn	Fe/Cd
orange	0.26 ± 0.06	0.15 ± 0.13	66.70 ± 0.64	2.22 ± 1.68
yellow	0.27 ± 0.09	0.20 ± 0.19	66.89 ± 0.74	1.65 ± 1.09
white	0.36 ± 0.10	0.52 ± 0.15	66.34 ± 0.87	0.70 ± 0.17

Table 5-4. Summary Tables for Analysis of Variance (ANOVA) of Trace/Minor Element Compositions for Orange to White Coloration in Sphalerite.

Cadmium:

Source of Variation	Sum of Squares	Degrees of Freedom	Mean Squares	F Test
Among Samples	3.17	2	1.58	66.97*
Within Replications	2.51	106	0.02	
Total Variation	5.67	108		

Iron:

Source of Variation	Sum of Squares	Degrees of Freedom	Mean Squares	F Test
Among Samples	0.22	2	0.11	16.52*
Within Replications	0.73	110	0.01	
Total Variation	0.95	112		

Fe/Cd:

Source of Variation	Sum of Squares	Degrees of Freedom	Mean Squares	F Test
Among Samples	43.80	2	21.90	14.96*
Within Replications	131.73	90	1.46	
Total Variation	175.53	92		

* Significant at the .01 level of confidence

1982; Seal et al., 1985) although the interpretations are different. Larsen (1978) concluded that the dark areas in sphalerite are not due to compositional variations in Zn, Fe, Mn, Cd. Craig et al. (1983) found that areas rich in hydrocarbons contain relatively high Fe concentrations and high, but variable, Cd concentrations. Recently, Seal et al. (1985) noticed that zones of high birefringence mark areas high in Cd and Fe. Findings in this study suggest that the dark and light zones may be due to compositional variations in sphalerite. While both Fe and Cd appear to increase in concentration in whiter zones, the correlation of high Cd and whiter areas is statistically most valid (it has the highest F-statistic). Many of the white zones correspond to areas showing anisotropy; thus, the present data appears to support those of Seal et al. (1985).

Carbon and Oxygen Isotopic Analysis

Five samples of calcite were selected for isotopic analysis: one sample of early calcite, two of main-stage calcite, and two of amber calcite. Samples were checked for purity; as all samples were large and coarse-grained, contamination is believed to have been negligible. At Krueger Enterprises, Inc. in Cambridge, Massachusetts, samples were finely ground and reacted with 100% phosphoric acid at 50°C. After liberated CO_2 gases were withdrawn, isotopic analyses were performed on an Isogas 903

triple-collecting mass spectrometer. Isotopic analyses are reported as variation in per mil relative to the PDB standard for carbon and the SMOW standard for oxygen. Reproducibility is about 0.1 per mil for both carbon and oxygen.

Carbon and oxygen isotope data are given in Table 5-5. Both isotopic ratios fall in a narrow range for all five samples. Carbon isotopic ratios (-2.4 to -4.6 per mil) are characteristic of normal marine carbonate compositions while oxygen isotopic ratios (19.0 to 21.9 per mil) are slightly lighter than marine carbonates which average 24 to 26 per mil (Hall and Friedman, 1969). Although there is no evidence of a distinct trend in isotope pairs through the different stages of calcite deposition, there is a slight shift in ^{13}C values from -3.5 for early calcite to -2.4 and -2.5 for main-stage calcite to -3.9 and -4.6 for late-stage, amber calcite. The decrease in ^{13}C coupled with a decrease in salinity for late fluids suggests that the isotopically light carbon was introduced by dilute waters, possibly with a meteoric component; meteoric waters commonly have ^{13}C values of -7 to -18 per mil (Hall and Friedman, 1963). However, an influx of meteoric water would also be characterized by a decrease in ^{18}O values (Hannah and Stein, 1984). This change in ^{18}O has not been observed. Because of the independent variation of ^{13}C and ^{18}O isotope ratios, it must be concluded that fluids responsible for ore and gangue

Table 5-5. Calcite Isotope Compositions.

No.	Calcite Stage	Sample	$\delta^{18}O$	$\delta^{13}C$
1	early calcite	E-1	+19.0	-3.5
2	main-stage	12	+20.2	-2.4
3	main-stage	3-2	+20.5	-2.5
4	late-amber	75	+21.9	-4.6
5	late-amber	2-19	+19.8	-3.9

mineralization changed composition through time; whether or not meteoric water played a role is uncertain.

Precipitation of late-stage calcite (and possibly early calcite) was associated with the introduction of ^{13}C-depleted fluid into the system. On the other hand, ^{13}C-depleted fluids may have been indigenous to the area. The precipitation of main-stage calcite may have marked the entrance of ^{13}C-rich fluids, which also may have been associated with the precipitation of fluorite and sphalerite ore. This line of thought has been considered by Grant and Bliss (1983) who believe that sphalerite was associated with the arrival of fluids with elevated $^{87}Sr/^{86}Sr$ ratios, and that the mixing of these fluids with already existing fluids caused sphalerite precipitation. Fluid inclusion data, however, does not support fluid mixing at the site of deposition as a method for precipitating sphalerite.

CHAPTER 6

DISCUSSION

Transportation and Deposition of Sphalerite

A major problem concerning the genesis of Mississippi Valley-type deposits is the transport of metals and reduced sulfur to the site of mineralization and the subsequent deposition of sulfide minerals such as sphalerite and galena. Three models have been proposed for the transportation and precipitation of base metals and sulfur in Mississippi Valley-type deposits. In the first model, zinc and reduced sulfur are transported together in the same solution to the area of deposition. This has often been called the single solution model (Barnes, 1983). In the second model, two solutions, one containing reduced sulfur and the other containing zinc and/or lead with little sulfur, travel independently to a site where mixing occurs and sulfides precipitate. This has been appropriately named the fluid-mixing model (Anderson, 1975, 1983). An intermediary model involves the transport of metal together with sulfate (Skinner, 1967; Barton, 1967) or a partly oxidized sulfur species which is then reduced by organic matter at the site of deposition (Spirakis, 1983). There is no concensus as to which model is correct. In fact, Ohle (1980) and Sangster (1983) have conceded that no one particular model is suffice

to explain all Mississippi Valley-type deposits and that perhaps these deposits, in terms of their genesis, should be noted more for their dissimilarities than for their similarities.

The following outline will review the salient features of the models, their variations, and applications to the characteristics observed at Gordonsville. In the single solution model, reduced sulfur and base metals are transported together in approximately equal concentrations (Sverjensky, 1981). Precipitation is caused by pH change, cooling, or dilution (Anderson, 1983). The major problem with this model is that sphalerite solubilities are too low to allow transport at realistic pH values. Inorganic and organic complexes have been called upon to aid in metal and reduced sulfur transport. Bisulfide complexes were initially emphasized by Barnes (1967); however, later work (McLimans, 1977; Giordano and Barnes, 1979) concluded that zinc bisulfide complexing was not an effective method for transporting zinc and reduced sulfur below 200°C. Chloride complexing is another mechanism which has received a great deal of attention. Once again, however, there are disagreements as to its viability. McLimans (1977) and Barnes (1983) argue that in order for chloride complexing to be an effective transporting mechanism for metals and reduced sulfur the solution must be at a pH less than four (Barrett and Anderson, 1982). They contend that these conditions are

too acidic for the fluid to coexist with limestone or dolostone host rock during transport. Sverjensky (1981, 1984), however, argues that brines could carry metals as chloride complexes with reduced sulfur at pH's within two units of neutral, high enough to keep the solution from reacting with the country rock, by changing several parameters. Parameters which change include salinity (from $3m_{Cl^-}$ to $4.1m_{Cl^-}$), metal concentrations, activity coefficients, and the amount of dissolved CO_2. Under these conditions metals can travel with reduced sulfur in a solution with a pH above 4.4, the minimum level at which the ore-forming solution could remain in equilibrium with dolomite at 100°C (Sverjensky, 1981). Thus, mildly acidic conditions do not neccessitate the dissolution of carbonate. For those who find both chloride and bisulfide complexing as untenable processes but still hold to the single solution model, other mechanisms of ore transport have been sought. Although there has been little work in the area, organic complexing has been proposed as a mechanism by which to transport metals and sulfide in solution (Giordano and Barnes, 1981; Barnes, 1983).

The opposing model (mixing model) contends that basinal fluids derive metals through leaching of country rock, transport them as chloride or organic complexes, and precipitate them as sulfides when H_2S is encountered (Jackson and Beales, 1967; Beales, 1975; Anderson, 1975). Skinner

(1967) suggested that the source of reduced sulfur comes from the thermal degradation of petroliferous material. The amount of oil required, however, is improbably large (Spirakis, 1983). H_2S production may come about through sulfate-reducing bacteria and suitable organic nutrients (Anderson, 1983). This reduction process takes place outside the zone of ore deposition as the temperatures involved in the ore forming process (>100°C) are too high for bacterial life. This implies that reduction occurs away from the brine solution pathway and that H_2S travels by diffusion or fluid flow to a site where it mixes with metal-bearing brine and precipitates ore.

The third model involves the transport of base metals in solution with sulfate (Barton, 1967) or a partly oxidized sulfur species (Spirakis, 1983) with deposition being initiated by the increase in the activity of sulfide sulfur. Barton (1967) proposed that the sulfate in the ore solution is reduced due to the oxidation of organic matter or methane. The reduction of sulfate by non-biogenic organic matter, however, has been known to be a slow process below 300°C (Touland, 1960). Recently it has been found that partly oxidized sulfur species (native sulfur or S^{1-}) can be reduced by organic matter very quickly (Ohmoto and Rye, 1979; Spirakis, 1983). The partly oxidized (or partly reduced) species can be formed from an initial ore solution containing reduced sulfur or one containing sulfate. Reduced sulfur can

be partly oxidized by ferric iron in minerals such as pyrite (Spirakis, 1983). Upon incountering organic accumulations the partly oxidized form of sulfur will be reduced back to sulfide. In an initially sulfate solution, the sulfate undergoes partial reduction (by the reaction: $2H^+ + SO_4^{2-} + 3H_2S = 4S + 4H_2O$) and, at the site of ore deposition, undergoes total reduction by organic material.

The models presented to explain fluid transport and ore deposition are proposed by their respective authors to fit various Mississippi Valley-type deposits. How well these models fit is governed by the characteristics of each deposit including mineralogy, chemistry, and ore textures. This is no different with the Central Tennessee zinc district and specifically, the Gordonsville mine. Several observations put constraints upon the chemical environment of ore and gangue mineral deposition. Calcite formed before and after sphalerite deposition, and there is little evidence that the early calcite, most prevalent in the Elmwood mine, was etched by the ore solution (Kyle, 1976; Larsen, 1978). There is only minor evidence of replacement of host rock by sphalerite, and more importantly, brecciation and concommitant dissolution of carbonate occurred before ore and gangue mineralization took place. These observations clearly indicate that the ore solution was in equilibrium with carbonate host rock and gangue minerals,at least during mineralization.

The precipitation of ore minerals is inherently an acid-producing reaction ($Zn^{2+} + H_2S = ZnS + 2H^+$) in both the fluid-mixing and single solution models. This reaction is thought to aid in brecciation and dissolution; however, at Gordonsville, brecciation occurred before mineralization. Thus, either the acid solution was not strong enough to dissolve the host rock during mineral deposition or some other model for transport and deposition of sulfides must be invoked. If the metals are transported in a solution containing sulfate, the H^+ released will be used up by sulfate reduction ($SO_4^{2-} + 2H^+ + CH_4 = H_2S + CO_2 + 2H_2O$) thereby minimizing the acidity of the solution. While organic matter is abundant at the Gordonsville mine and may, indeed, be able to effectively reduce the incoming sulfates, this model is not favored. Barite is a major sulfate gangue mineral which occurs after sphalerite deposition. Ba^{2+} and SO_4^{2-} are highly insoluble in the same solution (Holland and Malinin, 1979) and would be expected to precipitate barite long before barite is seen in the paragenetic sequence. Possibly, then, Ba^{2+} content increased late in the mineralization sequence with an influx of barium-rich waters. However, the two stages of barite deposition observed in the Wisconsin zinc-lead district (McLimans et al., 1980) could only be explained by two periods of mixing of a Ba^{2+}-rich fluid with the ore fluid. It is much more likely that SO_4^{2-} or oxidant content changed through time rather than Ba^{2+} content.

As mentioned previously, invoking fluid-mixing and single solution models leads to problems if one is to believe that acid producing reactions, inherent to both models, will lead to further dissolution and brecciation. Oil-field brines, thought to be the precursors of ore-forming solutions (Carpenter et al., 1974; White, 1974, 1981; Sverjensky, 1981, 1984), are shown to have pH values as low as 4.3 (Sverjensky, 1984) and still remain in equilibrium with the surrounding limestone. Thus, the relationship between pH at which transported minerals are deposited and the minimum pH of calcite and dolomite stability is complex. Neither model can be discarded or proven by observations that brecciation and mineralization were not concurrent. It is also uncertain whether the mineralizing solution first caused dissolution and then mineralization or that dissolution/brecciation had already taken place, providing favorable sites for later ore and gangue mineral deposition.

Recently, fluid inclusion data have been used to support or reject the single solution or fluid-mixing models (Taylor et al., 1981; Zimmerman and Kesler, 1983; Richardson and Pinckney, 1984). A disparity among two or more solutions may generate a trend of temperatures and salinities such as the one proposed for sphalerite deposition in the Mascot-Jefferson City district (Taylor et al., 1983) and for fluorite deposition in the Sweetwater district (Zimmerman and Kesler, 1981), both in East Tennessee. On the other hand, a

clustering of fluid inclusion data and a lack of correlation between freezing and homogenization temperatures may be characteristic of one fluid thus supporting the single solution model.

While fluid inclusion data do appear to be a good test as to the validity of the two models, two factors which may complicate matters must be considered. First, an underlying assumption in using fluid inclusion data is that, if there are two fluids, their respective temperatures and salinities must be reflected in the data. If unequal quantities of fluids are mixed, a trend may be hidden by the characteristics of the fluid of the greatest volume. Thus, while a distinct trend of temperatures and salinities may be good evidence for fluid mixing, a cluster of freezing and homogenization temperature data, by itself, does not disprove mixing. Secondly, are the trends used by some authors to support a mixing model real or are they just an artifact of data manipulation? Graphs of homogenization and freezing temperature pairs for fluid inclusions may be made by plotting (1) individual inclusions, (2) the averages of fluid inclusion data from individual chips, or (3) the averages of fluid inclusion data from individual samples. In the fluid inclusion study of sphalerite in the Mascot-Jefferson City district, individual inclusions were plotted. Plotting by chip or by sample may be a better way of representing the data. For example, if 30 temperature-salinity pairs from one

sample are plotted with 10 temperature-salinity pairs from four samples, sample bias is introduced. An apparent trend may be the result of temperature-salinity fluctuations in one sample. Correlation coefficients of these "trends" are low (less than 0.65) when freezing and homogenization temperature data from the Mascot-Jefferson City district (from data of Taylor et al., 1983) are grouped, instead, by sample. While fluorite fluid inclusion data from the southeast belt of the Sweetwater district (from data of Zimmerman and Kesler, 1981) do show a trend when plotted by sample, the sample population is quite low (8 chips from 4 samples). Thus, these temperature-salinity trends, supposed proof of the fluid mixing hypothesis, may not be that apparent.

The consistency and narrowly defined range of paired homogenization and freezing temperature pairs in sphalerite lend support to the single solution model. While homogenization and freezing temperature pairs were plotted by individual inclusions, statistical data were collected by chip and by sample. No trends were observed; correlation coefficients were all below 0.70. On a larger scale, the uniformity of temperatures and salinities within ore producing districts supports derivation of mineralizing fluids from regional sources rather than from a mixing of different water types (Hanor, 1979). Also it has been suggested that the mixing of fluids would precipitate sphalerite rapidly, producing a fine-grained ore texture not

observed at Gordonsville (Mclimans and Barnes, 1980). Thus, while fluid inclusion results do not disprove fluid mixing, they, along with other observations, support the single solution model.

A diagram displaying the stability of some mineral and aqueous species as a function of oxygen fugacity and pH places constraints on the general range of conditions for which the transport of equal amounts of zinc and sulfur in one solution can produce a sizeable ore deposit (Figure 28). Using data compiled by Sverjensky (1981, 1984), an ore solution with a pH of approximately 5 to 5.5 can contain greater than 1 ppm Zn, the minimum concentration neccessary to form a major ore deposit (Roedder, 1976) and remain saturated with respect to both dolomite and calcite. Sphalerite precipitation ends as a result of a pH increase, oxygen fugacity increase, and/or temperature decrease. Fluid inclusion homogenization temperatures in fluorite suggest that a temperature decrease may have caused the termination of sphalerite mineralization. There was a subsequent rise in temperature, however, during main-stage calcite mineralization with no accompanying reoccurrence of sphalerite. Thus, either a pH increase and/or an oxygen fugacity increase must also have taken place to inhibit a second phase of sphalerite mineralization, or zinc was depleted from the mineralizing fluid. Barite remained soluble during sphalerite, fluorite and main-stage calcite

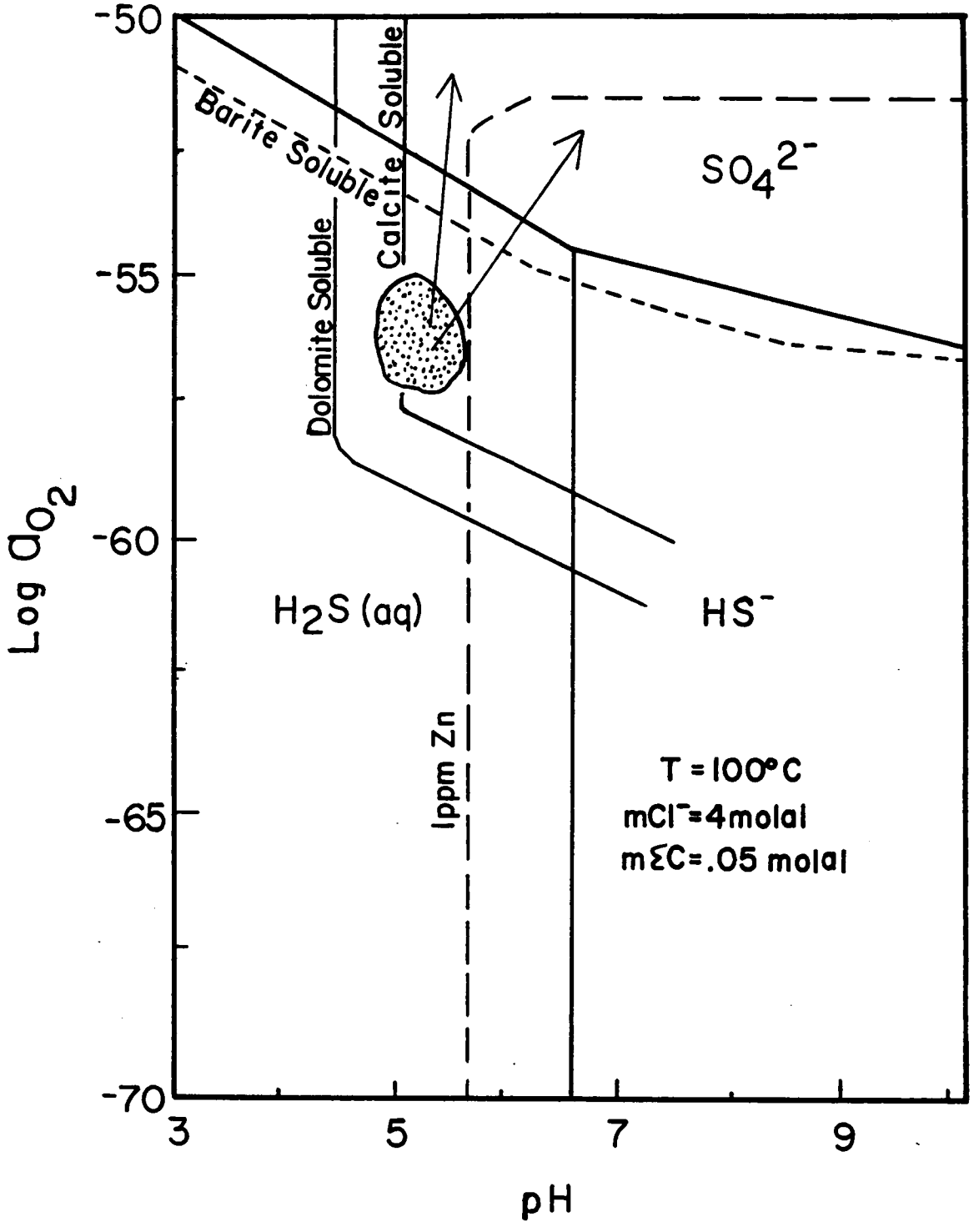

Figure 28. Mineral and aqueous species stability as a function of oxygen activity (fugacity) and pH. From calculations of McLimans (1977), Sverjensky (1981, 1984) and Giordano and Barnes (1981) (stippled region represents ore fluid).

mineralization. A rise in the oxygen fugacity or sulfate content of the system caused barite to precipitate. Amber calcite was also able to form; thus, pH either increased or remained constant.

The possibility that ore fluids transported sulfur in a partly oxidized state has not been ruled out. The flanks of structural highs in the Mascot formation could have acted as hydrocarbon traps providing sites for reduction and precipitation of sphalerite (Braun, 1983; Gaylord and Briskey, 1983). Breccia bodies containing ore-grade mineralization are often found on the flanks of the structural highs, while the highest areas are devoid of appreciable mineralization (Fred Smith, pers. comm., 1985). Gas (methane ?) may have been trapped in localized structural highs causing mineralizing fluids to flow along the periphery of domal areas where ore was precipitated. Bituminous material is abundant in the mine and is associated with both ore and gangue minerals.

Transportation and Deposition of Gangue Minerals

The fluids responsible for the precipitation of post-ore fluorite, barite, and calcite were, for the most part, in equilibrium with sphalerite, early calcite, and dolomite. The solubility of fluorite is affected by temperature, pressure, pH, and the ratio of the concentration of calcium and magnesium to that of fluoride ion in solution (Holland

and Malinin, 1979; Nordstram and Jenne, 1977). A study of fluorite solubility by Richardson and Holland (1979) concludes that simple cooling of ore fluids may be the most effective way to precipitate fluorite. Indeed, a 5-20°C drop in temperature after sphalerite deposition, neccessary for the precipitation of fluorite, is indicated by the fluid inclusion study. Once again, mixing of two fluids is a possible mechanism, but the narrow range of temperatures and salinities suggests this did not occur. An increase in the pH of the solution from below 3 to a pH of 5 or 6 also induces fluorite precipitation, but these conditions are inconsistent with the probable pH of the ore fluids of Mississippi Valley-type deposits.

A rise in temperature, as shown by calcite fluid inclusions, may explain the cessation of fluorite deposition and the precipitation of calcite. The solubility of calcite decreases with increasing temperatures while that of fluorite increases. The amount of calcium ions present in solution may have remained constant. Fluid inclusions within late-stage barite and amber calcite show markedly lower salinities and slightly lower temperatures of formation than the preceding calcite stage. Barite precipitation is probably the result of increased sulfate content brought in by a more dilute solution (see Figure 28). As mentioned previously, had zinc been transported as a sulfate, then barite would have been deposited much earlier. Calcite was

deposited in solutions of both high and low salinity and at various temperatures. Barite does, however, penetrate some calcite boundaries. Yet, the nearby dolomite rhombs remain unaffected. These observations highlight the complex relationship among the different coexisting mineral phases and suggest that pH did not increase appreciably during late stage gangue mineralization. Oxygen and carbon isotopes do not give conclusive evidence as to the source of the late, oxidized fluids. Meteoric influence is possible; more probable is the general evolution of the original ore fluid through time, with compositional changes affecting the deposition of minerals.

In summary, based on fluid inclusion and textural evidence, the results of this research are consistent with a single solution model in which base metals Zn (and lesser Pb) were transported together in the presence of reduced sulfur. Transport with partly oxidized sulfur is possible, yet the fine-grained ore texture expected upon deposition is not seen. Organic matter, however, is ubiquitous in the Gordonsville mine. Whether or not it was brought in with the ore fluid or was already present in the area of deposition is uncertain. These results give no indication as to whether reduced sulfur and metals were transported together as chloride complexes (Sverjensky, 1981,1984) or as organometallic complexes (McLimans, 1977; Giordano and Barnes, 1981; Barnes, 1983). Precipitation of fluorite and

main-stage calcite was brought about by temperature, and possibly, compositional changes in the ore fluid. Late-stage minerals, barite and amber calcite, record the influx of dilute, oxidized fluids with a possible meteoric component.

CHAPTER 7

CONCLUSIONS

1. The generalized sequence of ore and gangue mineralization is as follows: early, white calcite - sphalerite - galena - fluorite - main-stage, white to lavender calcite - barite - late-stage, clear to amber calcite. Petrographic and field evidence suggest that these minerals were, for the most part, in equilibrium with circulating fluids throughout the mineralization period.

2. Homogenization temperatures for ore and gangue minerals fall within the general range of 90° to 130°C. The slight decrease in fluid temperature after sphalerite deposition (≈6°C) may have been enough to cause the precipitation of fluorite. A further decrease in fluid temperature is suggested by inclusions in amber calcite (and barite?).

3. Freezing temperatures, which provide an estimate of fluid salinity, remained fairly constant through main-stage calcite deposition. Precipitation of barite and late-stage amber calcite, however, was marked by a large decrease in fluid salinity.

4. Carbon and oxygen isotope analyses of the three calcite stages show only minor variation, and all data fall in or

near the region of marine carbonates. This suggests that the slight decrease in fluid temperature and the marked decrease in fluid salinity during late-stage mineral precipitation is not necessarily due to an influx of meteoric water, although a meteoric component cannot be ruled out.

5. The consistency and narrowly defined range of paired homogenization and freezing temperatures for fluid inclusions in sphalerite suggest that the ore mineral was precipitated from one fluid rather than by the mixing of two or more fluids. Sulfur may have traveled with the metals in a partly oxidized state, or in a reduced state as chloride or organometallic complexes. Organic matter, abundant in mineralized zones, appears to have played a role in sphalerite precipitation.

6. Based upon fluid inclusion data, trace element data, and a lack of petrographic evidence proving otherwise, the three textural types of sphalerite (disseminated, massive, and vug-filling) are probably part of the same depositional phase. Field evidence suggests that the disseminated texture is mostly a function of host rock lithology.

7. Main-stage, white to lavender calcite and late-stage, clear to amber calcite could not be differentiated by the

trace elements analyzed (Sr, Mn, Fe, Mg), although they differ in color, formational temperatures and salinities.

8. Orange to white color regions in sphalerite, apparent in thin-section, may be due to variations in cadmium content. White areas contain the highest concentrations of cadmium (0.25 - 0.75 wt.%). The density and nature of solid, liquid, and vapor inclusions does not appear to influence color.

REFERENCES

REFERENCES

Anderson, G.M., 1975, Precipitation of Mississippi Valley-type ores: Econ. Geol., v. 70, p.937-942.

Anderson, G.M., 1983, Some geochemical aspects of sulfide precipitation in carbonate rocks, in G. Kisvarsanyi, et al., eds., Int'l. Conf. on Mississippi Valley Type Lead-Zinc Deposits Proceedings, Univ. of Missouri-Rolla, Oct., 1982, Univ. of Missouri-Rolla Press, p. 61-76.

Barnes, H.L., 1967, Sphalerite solubility in ore solutions of the Illinois - Wisconsin district: Econ. Geol. Mon. 3, p. 326-332.

Barnes, H.L., 1983, Ore-depositing reactions in MVT deposits, in G. Kisvarsanyi, et. al., eds, Int'l. Conf. on Mississippi Valley Type Lead-Zinc Deposits Proceedings, Univ. of Missouri-Rolla, Oct., 1982, Univ. of Missouri-Rolla Press, p. 77-85.

Barrett, T.J., and Anderson, G.M., 1982, The solubility of sphalerite and galena in NaCl brines: Econ. Geol., v. 77, p. 1923-1933.

Barton, Jr., P.B., 1967, Possible role of organic matter in the precipitation of the Mississippi Valley-type ores: Econ. Geol. Mon. 3, p. 326-332.

Beales, F.W., 1975, Precipitation mechanisms for Mississippi Valley-type ore deposits: Econ. Geol., v. 70, p. 943-948.

Bodnar, R.J., and Bethke, P.M., 1984, Systematics of stretching fluid inclusions I: Fluorite and sphalerite at 1 atmosphere confining pressure: Econ. Geol., v.79, p. 141-161.

Braun, E.R., 1983, Ore controls - - Middle Tennessee zinc district, in G. Kisvarsanyi, et al., eds., Int'l. Conf. on Mississippi Valley Type Lead-Zinc Deposits Proceedings, Univ. of Missouri-Rolla, Oct., 1982, Univ. Missouri-Rolla Press, p. 349-359.

Callahan, W.H., 1967, Some spatial and temporal aspects of the localization of Mississippi Valley-Appalachian type ore deposits: Econ. Geol. Mon. 3, p. 14-19.

Callahan, W.H., 1977, The history of the discovery of the zinc deposit at Elmwood, Tennessee - - concept and consequence: Econ. Geol., v. 72, p. 1382-1392.

Carpenter, A.B., Trout, M.L., and Pickett, E.E., 1974, Preliminary report on the origin and evolution of lead and zinc-rich oil field brines in Central Mississippi: Econ. Geol., v. 69, p. 1191-1206.

Churnet, H.G., 1979, The relationship between dolomitization and sphalerite mineralization in Lower Ordovician Upper Knox Group carbonate rocks of the Copper Ridge district, East Tennessee: Unpub. Ph.D thesis, Univ. Tennessee, Knoxville, 237 p.

Churnet, H.G., and Misra, K.C., 1983, Sphalerite mineralization and its relationship to carbonate facies boundaries, Copper Ridge district, East Tennessee, in G. Kisvarsanyi, et al., eds., Int'l. Conf. on Mississippi Valley Type Lead-Zinc Deposits Proceedings, Univ. of Missouri-Rolla, Oct. 1982, Univ. Missouri-Rolla Press, p. 360-372.

Churnet, H.G., Misra, K.C., and Walker, K.R., 1982, Deposition and dolomitization of Upper Knox carbonate sediments, Copper Ridge district, East Tennessee: Geol. Soc. Am. Bull., v. 93, p. 76-86.

Craig, L.E., 1982, Silicification and porosity development in Lower Ordovician Knox Group carbonates, Burkesville, Kentucky: Unpub. M.A. thesis, Univ. of Texas, Austin, 104p.

Craig, J.R., Solberg, T.N., and Vaughan, D.J., 1983, Growth characteristics of sphalerites in Appalachian zinc deposits, in G. Kisvarsanyi, et. al., eds., Int'l. Conf. on Mississippi Valley Type Lead-Zinc Deposits Proceedings, Univ. of Missouri-Rolla, Oct. 1982, Univ. of Missouri-Rolla Press, p. 317-327.

Crawford, M.I., 1981, Phase equilibria in aqueous fluid inclusions, in Hollister, L.S., and Crawford, M.I., eds., Short Course on Fluid Inclusions - Applications to Petrology: Calgary, Mineralog. Assoc. Canada, v. 6, p. 75-100.

DeGroodt, J.H., 1973, Determination of temperature of fluorite formation by fluid inclusion thermometry, Central Tennessee zinc district: Unpub. M.S. thesis, Univ. Tennessee, Knoxville, 75p.

Dietrick, R.V., Hobbs, C.R.B., Jr., and Lawry, W.D., 1963, Dolomitization interrupted by silicification: Jour. Sed. Petrology, v. 33, p. 646-663.

Ferguson, T.L., 1981, Petrographic and trace-element characterization of coarse crystalline carbonate minerals in fractures and breccia bodies and associated mineralization in the Right Fork area, Central Tennessee: Unpub. M.S. thesis, Univ. Tennessee, Knoxville, 80p.

Gaylord, W.B., and Briskey, J.A., 1983, Geology of the Elmwood and Gordonsville mines, Central Tennessee zinc district, in Tennessee Zinc Deposits Field Trip Guidebook, Virginia Polytechnic Inst. State Univ., guidebook 9, p. 116-151.

Gilbert, R.C, and Hoagland, A.D., 1970, Paleokarst phenomena and the post-Knox unconformity of middle Tennessee [abs.]: Geol. Soc. America Abstracts with Programs, v. 2, p. 558.

Giordano, T.H., and Barnes, H.L., 1979, Ore solution chemistry VI. PbS solubility in bisulfide solutions to 300°C: Econ. Geol., v. 74, p. 1637-1646.

Giordano, T.H., and Barnes, H.L., 1981, Lead transport in Mississippi Valley-type ore solutions: Econ. Geol., v. 76, p. 2200-2216.

Gorody, A.W., 1980, The Lower Ordovician Mascot Formation, Upper Knox Group, in north central Tennessee, Part II: Dolomitization and paleohydraulic history: Unpub. Ph.D. thesis, Rice Univ., 181p.

Grant, N.K., and Bliss, M.C., 1983, Strontium isotope and rare earth element variations in non sulfide minerals from the Elmwood - Gordonsville mines, central Tennessee, in G. Kisvarsanyi, et al., eds., Int'l. Conf. on Mississippi Valley Type Lead-Zinc Deposits Proceedings, Univ. of Missouri-Rolla, 1982, Univ. Missouri-Rolla Press, p. 206-210.

Haas, J.R., Jr., 1971, The effect of salinity on the maximum thermal gradient of a hydrothermal system at hydrostatic pressure: Econ. Geol., v. 66, p. 940-946.

Hall, W.E., and Friedman, I., 1963, Composition of fluid inclusions, Cave-in-Rock fluorite district, Illinois, and Upper Mississippi Valley zinc-lead district: Econ. Geol., v. 58, 886-911.

Hall, W.E., and Friedman, I., 1969, Oxygen and carbon isotopic composition of ore and host rock of selected Mississippi Valley deposits: U.S. Geol. Survey Prof. Paper 650-C, p. C140-C148.

Hannah, J.L., and Stein, H.J., 1984, Evidence for changing ore fluid composition: stable isotope analyses of secondary carbonates, Bonneterre Formation, Missouri: Econ. Geol., v. 79, p. 1930-1935.

Hanor, J.S., 1979, The sedimentary genesis of hydrothermal fluids, in Barnes, H.L., ed., Geochemistry of hydrothermal Ore Deposits, 2nd ed.: New York, John Wiley and Sons, p. 137-176.

Hanor, J.S., 1980, Dissolved methane in sedimentary brines: potential effect on the PVT properties of fluid inclusions: Econ. Geol., v. 75, p. 603-609.

Harris, L.D., 1969, Kingsport Formation and Mascot Dolomite (Lower Ordovician) of east Tennessee, in Papers on the Stratigraphy and Mine Geology of the Kingsport and Mascot Formations (Lower Ordovician) of East Tennessee: Tenn. Div. Geol. Rept. Inv. 23, p. 1-39.

Harris, L.D., 1971, A Lower Paleozoic paleoaquifer - the Kingsport Formation and Mascot Dolomite of Tennessee and southwest Virginia: Econ. Geol., v. 66, p. 735-743.

Hill, W.T., Morris, R.G., and Hagegeorge, C.C., 1971, Ore controls and related sedimentary features at the Flat Gap Mine, Treadway, Tennessee: Econ. Geol., v. 66, p. 748-756.

Hoagland, A.D., 1973, Appalachian zinc-lead and the deposits of middle Tennessee: Unpub. manuscript of oral presentation at the Geol. Soc. America, southeastern section meeting, Knoxville, Tennessee 1973, 12p.

Hoagland, A.D., 1976, Appalachian zinc-lead deposits, in K.H. Wolfe, ed., Handbook of Stratabound and Stratiform Ore Deposits, Vol. 6: New York, Elsevier, p. 495-534.

Hoagland, A.H., Hill, W.T., and Fulweiler, R.E., 1965, Genesis of the Ordovician zinc deposits in east Tennessee: Econ Geol., v. 60, p. 697-714.

Holland, H.D., and Malinin, S.D., 1979, The solubility and occurrence of non-ore minerals, in Barnes, H.L., ed., Geochemistry of hydrothermal Ore Deposits, 2nd ed.: New York, John Wiley and Sons, p. 461-508.

Jackson, S.A., and Beales, F.W., 1967, An aspect of sedimentary basin evolution: the concentration of Misissippi Valley-type ores during the late stages of diagenesis: Bull. Can. Pet. Geol., v. 15, p. 393-433.

Jewell, W.B., 1947, Barite, fluorite, galena, sphalerite veins of central Tennessee: Tennessee Div. Geology Bull. 51, 114p.

Jolly, J.L., and Heyl, A.V., 1968, Mercury and other trace elements in sphalerite and wall rocks from central Kentucky, Tennessee, and Appalachian zinc districts: U.S. Geol. Survey Bull. 1252-F, p. F1-F29.

Kearns, L.E., and Campbell, F.H., III, 1978, The Elmwood and Gordonsville zinc mines near Carthage, Tennessee: Mineralogical Record, v. 9, p. 213-218.

Kyle, J.R., 1973, Preliminary investigation of brecciation, alteration, and mineralization in the Upper Knox Group of Smith and Trousdale Counties, Tennessee: Unpub. M.S. thesis, Univ. Tennessee, Knoxville, 105p.

Kyle, J.R., 1976, Brecciation, alteration and mineralization in the Central Tennessee zinc district: Econ. Geol., v. 71, p. 892-903.

Larsen, R.L., 1978, A study of the cathodoluminescent properties and the trace element distribution of the gangue calcite (and other phases) at the Elmwood mine in Smith County, Tennessee: Unpub. M.S. thesis, Univ. Tennessee, Knoxville, 81p.

Leach, D.L., 1980, Nature of mineralizing fluids in the barite deposits of central and southeast Missouri: Econ. Geol., v. 75, p. 1168-1180.

McCormick, J.E., Evans, L.L., Palmer, R.A., and Rasnick, F.D., 1971, Environment of the zinc deposits of the Mascot-Jefferson City district, Tennessee: Econ. Geol., v. 66, p. 757-762.

McLaren, G.P., 1978, Minor elements in sphalerite and their implications for metallogenesis of carbonate hosted zinc-lead deposits of the Yukon Territory and adjacent district of Mackenzie: Unpub. M.S. thesis, Univ. British Columbia, 165p.

McLimans, R.H., 1977, Geologic, fluid inclusion and stable isotope studies of the Upper Mississippi Valley zinc-lead district, southwest Wisconsin, Unpub. Ph.D. thesis, The Pennsylvania State Univ., 175p.

McLimans, R.H., Barnes, H.L., and Ohmoto, H., 1980, Sphalerite stratigraphy of the Upper Mississippi Valley zinc-lead district, southwest Wisconsin: Econ. Geol., v. 75, p. 351-361.

Ohle, E.L., 1980, Some considerations in determining the origin of ore deposits of the Mississippi Valley type, Part II: Econ. Geol., v. 75, p. 161-172.

Ohmoto, H., and Rye, R.O., 1979, Isotopes of sulfur and carbon, in Barnes, H.L., ed., Geochemistry of hydrothermal Ore Deposits, 2nd ed.: New York, John Wiley and Sons, p. 509-567.

Pinta, M., ed., 1975, Atomic Absorption Spectroscopy: New York, John Wiley and Sons, 418p.

Plummer, L.N., 1971, Barite deposition in central Kentucky: Econ. Geol., v. 66, p. 252-258.

Potter, R.W., II, 1977, Pressure corrections for fluid-inclusion homogenization temperatures based on the volumetric properties of the system NaCl-H_2O: U.S. Geol. Survey J. Res., v. 5, p. 603-607.

Potter, R.W., II, Clynne, M.A., and Brown, D.L., 1978, Freezing point depression of aqueous sodium chloride solutions: Econ. Geol., v. 73, p. 284-285.

Richardson, C.K., and Holland, H.D., 1979, Fluorite deposition in hydrothermal systems: Geochim. Cosmochim. Acta, v. 43, p. 1327-1335.

Richardson, C.K., and Pinckney, D.M., 1984, The chemical and thermal evolution of the fluids in the Cave-in-Rock fluorspar district, Illinois: Mineralogy, paragenesis, and fluid inclusions: Econ. Geol., v. 79, p. 1833-1856.

Roedder, E., 1963, Studies of fluid inclusions II: Freezing data and their interpretations: Econ. Geol., v. 58, p. 167-211.

Roedder, E., 1971, Fluid inclusion evidence on the environment of formation of mineral deposits of the Southern Appalachian Valley: Econ. Geol., v. 66, p. 777-791.

Roedder, E., 1981, Origin of fluid inclusions and changes that occur after trapping, in Hollister, L.S. and Crawford, M.I., eds., Short Course in Fluid Inclusions - Applications to Petrology: Calgary, Mineralog. Assoc. Canada, p. 101-137.

Roedder, E., 1984, Fluid inclusions, in Ribbe, P.H., series ed., Reviews in Mineralogy, v. 12: Chelsea, Mich., BookCrafters, Inc., 644p.

Rye, R.O., and Ohmoto, H., 1974, Sulfur and carbon isotopes and ore genesis: A review: Econ. Geol., v. 69, p. 826-842.

Sangster, D.F., 1983, Mississippi Valley-type deposits: A geological melange, in G. Kisvarsanyi et. al., eds., Int'l. Conf. on Mississippi Valley Type Lead-Zinc Deposits Proceedings, Univ. of Missouri-Rolla, Oct. 1982, Univ. Missouri-Rolla Press, p. 7-19.

Seal, R.R., II, Cooper, B.J., and Craig, J.R., 1985, Anisotropic sphalerite of the Elmwood - Gordonsville deposits, Tennessee: Canadian Mineralogist, v. 23, p. 83-88.

Skinner, B.J., 1967, Precipitation of Mississippi Valley-type ores: a possible mechanism: Econ. Geol. Mono. 3, p. 363-370.

Spirakis, C.S., 1983, A possible precipitation mechanism for sulfide minerals in MVT lead-zinc deposits, in G. Kisvarsanyi, et al., eds., Int'l. Conf. on Mississippi Valley Type Lead-Zinc Deposits Proceedings, Univ. of Missouri-Rolla, Oct., 1982, Univ. Missouri-Rolla Press, p. 211-215.

Stagg, A.K., and Fischer, F.T., 1970, Upper Knox stratigraphy of middle Tennessee [abs.]: Geol. Soc. America Abstracts with Programs, v. 2, 693.

Steinberg, R.T., 1981, Geology and petrology of the Lost Creek barite mine, Union County, Tennessee: Unpub. M.S. thesis, Univ. Tennessee, Knoxville 78p.

Sverjensky, D.A., 1981, The origin of a Mississippi Valley-type deposit in the Viburnum trend, southwest Missouri: Econ. Geol., v. 76, p. 1848-1872.

Sverjensky, D.A., 1984, Oil field brines as ore-forming solutions: Econ. Geol., v. 79, p.23-37.

Taylor, M., Kesler, S.E., Cloke, P.L., and Kelly, W.C., 1983, Fluid inclusion evidence for fluid mixing, Mascot-Jefferson City zinc district, Tennessee: Econ. Geol. v. 78, p. 1425-1439.

Toland, W.G., 1960, Oxidation of organic compounds with aqueous sulfate: Journal Amer. Chem. Soc., v. 82, p. 1911-1916.

Wedow, H., Jr., and Marie, F.R., 1964, Statistical analysis of solution-collapse structures [abs.]: Geol. Soc. America Sp. Paper 76, p.262.

White, L., 1979, Middle Tennessee zinc: Jersey Mineire plans for growth at Elmwood - Gordonsville mine: Engineering and Mining Journal, v. 180, p. 66-76.

White, D.E., 1974, Diverse origins of hydrothermal ore fluids: Econ. Geol., v. 69, p. 954-973.

Winslow, K.R., and Hill, W.T., 1973, The Elmwood project: Mining Cong. Jour., v. 59, p. 19-24.

Ziebold, T.O., and Ogilvie, R.E., 1964, An emperical method for electron microanalysis: Analytical Chem., v. 36, p. 322-327.

Zimmerman, R.K., and Kesler, S.E., 1981, Fluid inclusion evidence for solution mixing, Sweetwater (Mississippi Valley-type) district, Tennessee: Econ. Geol., v. 76, p. 134-142.

APPENDIXES

APPENDIX A

Table A-1. Petrographic Descriptions of Samples Collected from the Gordonsville Mine.

Sample	Description
1a	Fine gr. dolostone frags. with rind of drusy qtz. and dolomite; matrix of main-stage cal. and sph.
1b	Fine-med. gr. dolostone frags. with fracture filling by dolomite, cal., sph., and qtz.; pyrite mobilized to edges of dol. frags.
4a	Silicified limestone containing remnant dolomite rhombs (partially replaced by silica); drusy qtz.; main-stage cal. and sph. matrix.
4b	Complex mixture of chert and dolomite; drusy qtz. and sph.
7a	Med. gr. dolostone consisting of zoned dolomite rhombs; drusy qtz., pyrite, barite matrix.
7b	Fine gr. dolostone frags. rimmed by drusy qtz.; med. gr., zoned dolostone; minor chert.
7c	Complex association between zoned dolomite rhombs, fine gr. dolostone, and drusy qtz.
11a	Med. gr. dolostone (zoned dolomite rhombs); drusy qtz. rims; bar. (with hydrocarbons); sph., main-stage cal. as matrix.
12a	Bar. and fluorite on earlier sph.; sharp boundaries.
12b	Dolostone (fine gr.) with drusy dolomite rind; py. mobilized to frag. edge.
17a	Med. gr. dolostone (with py.); dissem. qtz. grains; sph. matrix.

Table A-1. - (Continued)

Sample	Description
17b	Complex assemblage of chert and dolomite rhombs (some are zoned); minor replacement by sph.; sph. rich with hydrocarbons.
17c	Chert with med. gr., zoned dolomite rhomb inclusions; sph. matrix.
17d	Similar to 17c; with drusy qtz.
17e	Similar to 17c; silicification is prevalent process.
18a	Complex interaction between silicification and dolomitization; fine to coarse gr. dolomite rhombs.
18b	Similar to 18a.
20a	Fine gr. dolostone frag. and chert frag. broken up and cemented by drusy qtz., dolomite.
20b	Dolostone and chert frags. in matrix of coarse, zoned dolomite rhombs and drusy qtz.; py. common in dolostone.
21a	Silicified oolitic limestone - partially dolomitized; drusy qtz.
21b	Similar to 21a; sph. matrix and drusy dolomite.
22a	Hydrocarbon-rich sph.; associated with chert; dolomite rhombs and bar.
22b	Matrix of zoned dolomite rhombs and chert; minor sph.; v. minor py.
23a	Sph. and bar.; sharp, straight boundaries.
25a	Dolostone frag. with drusy qtz. followed by fl.
25b	Fluorite.

Table A-1. - (Continued)

Sample	Description
25c	Fluorite - barite boundary (sharp/straight).
26a	Silicified limestone frags. cemented by bar., sph., and drusy qtz.; some dolomitization of silicified limestone.
26b	Similar to 26a; bar. rich in hydrocarbons.
28a	Dolostone frag. with silica replacement; minor dissem. py.
28b	Dolostone frags. with drusy qtz. and dolomite; also sph. and bar.
29a	Assorted breccia frags. cemented by sph., bar., drusy qtz., and dol.
29b	Similar to 29a.
29c	Similar to 29a; late-stage qtz. veins cut chert frags.
37a	Partially dolomitized chert and other breccia frags. in matrix of sph., chert and dolomite rhombs.
37b	Assorted breccia frags. in matrix of sph., chert, dolomite rhombs and later main-stage cal.
45a	Dissem. sph. in matrix of chert and med. gr. zoned dolomite rhombs; main-stage cal. cement.
45b	Similar to 45a; contains amber (late-stage) cal.; silica replaces (original?) limestone.
45c	Similar to 45a and 45b.
49a	Breccia frags. with drusy qtz. and dolomite followed by fl., bar., and amber cal. growth.

Table A-1. - (Continued)

Sample	Description
49b	Fine gr. dolostone frag. with drusy qtz. and dolomite followed by fl. and bar. growth.
49c	Similar to 49a and 49b; complex matrix of zoned dolomite and silica between dolostone frags.
49d	Similar to 49c.
49e	Similar to 49c; zoned dolomite rhombs.
50a	Dolostone frags. with py.; drusy qtz.; sph. matrix.
50b	Similar to 50a.
52a	Fl. and bar. growth on assorted breccia frags.; drusy qtz. and dolomite.
52b	Similar to 52a.
52c	Similar to 52a.
53a	Assorted breccia frags.; matrix includes main-stage and late-stage cal., bar., and fl.
53b	Similar to 53a; contains sph.
53c	Similar to 53a.
55a	Amber cal. with bar. inclusions.
55b	Bar. with hydrocarbons.
55c	Fine gr. dolostone frags. with drusy qtz. and dolomite.
57a	Dolostone frag. in matrix of med. gr. zoned dolomite, silica, and sph.
57b	Dolostone frag. in matrix of zoned dolomite, silica, and sph.; sph. contains hydrocarbons.

Table A-1. - (Continued)

Sample	Description
57c	Similar to 57b; several breccia frags.
58a	Dolostone frags. with qtz. vein surrounded by drusy qtz. and sph.
59a	Silicified limestone breccia frags. associated with py.; matrix of zoned dolomite and argillaceous material; drusy qtz. and dolomite.
59b	Similar to 59a; some dolomitized breccia frags.
60a	Assorted breccia frags. in argillaceous matrix.
60b	Similar to 60a.
63a	Irregular silica masses rimmed by drusy qtz., bounded by sph.; zoned dolomite rhombs also common.
63b	Similar to 63a; no sph.; minor py.
63c	Similar to 63a; sph. replaces some of the silica.
65a	Sph. and amber cal.
65b	Minor bar. and amber cal.
66a	Fl. followed by bar.; mostly sharp boundaries; some intrusion of bar. blades into fl.
66b	Bar. and sph.; bar. rich in hydrocarbons; high porosity.
66c	Sph. rich in hydrocarbons.
67a	Brecciated dolostone with drusy qtz. rim; sph. matrix.
67b	Islands of drusy qtz. and dolomite in sph.; minor sph. replacement.

Table A-1. - (Continued)

Sample	Description
67c	Sphalerite.
70a	Matrix of zoned dolomite rhombs and very coarse drusy dolomite; sph. in voids.
70b	Similar to 70a; py. associated with matrix fill.
73a	Amber cal. and sph.
73b	Amber cal., bar., sph.; inclusion of bar. in amber cal.
73c	Amber cal.
78a	Fl., bar., sph.; inclusions of drusy dolomite in fl.
78b	Similar to 78a.
78c	Mostly fl.; minor bar. and hydrocarbons.
80a	Bar. and fl.
80b	Sph. and fl.
UN1a	Round "blebs" of dissem. sph. in chert matrix with zoned dolostone rhombs; minor erosion of dolomite boundaries by sph.

APPENDIX B

Table B-1. Homogenization and Freezing Temperatures for Sphalerite Samples from the Gordonsville Mine.

Sample Number	Sphalerite Type	Chip Number	Homogenization and Freezing Temperatures (°C)
23	massive	1	107.0, -21.9; 107.0, -21.9; 119.3, -22.3; 104.0, -22.0; 129.5, -21.2; 127.0, -21.2; 105.9, -21.7; 116.9, -21.7
		2	105.9, -21.7; 116.9, -21.7
25	massive	1	107.0, 145.0; 124.8; 109.0; 103.0; 115.7; 112.0
		2	112.0, -23.8; 135.8, -21.9; 130.4, -22.0; 134.5, -23.8; 116.0, -23.4; 132.0, -23.4; 119.2, -23.4; 134.0, -23.4; 134.0, -23.4
31	vug	1	115.0, -22.5; 123.0, -22.5; 123.0, -22.5; 111.0, -23.5; 96.0, -21.5; 96.0, -21.5; 100.5, -22.0
		2	115.0, -20.6; 104.0, -20.8; 102.0, -20.8; 108.5, -20.2
41	vug	1	109.3; 102.0, -22.8; 113.0; 115.5, -15.5; 105.0, -18.0; 105.0, -18.0; 117.8, -22.6; 95.0, -22.6; 108.5, -21.9; 108.5, -21.9; 126.0, -14.5; 128.5, -14.5; 106.0, -15.8; 110.0, -15.5
62	massive	1	120.0, -23.2; 105.0, -22.5; 115.0, -22.7
68	vug	1	121.5, -21.8; 120.5, -23.6; 111.8, -21.9; 115.2, -22.0; 119.1, -21.9; 111.5, -21.8; 120.0, -21.8; 118.0, -20.8; 119.0, -20.5; 129.5, -20.4; 117.5, -20.4; 120.0, -21.8; 120.0, -21.8
		2	125.2, -22.7; 125.0, -22.4; 122.3, -22.3; 133.0, -21.8; 123.0, -21.8
75	massive	1	108.5, -20.0; 118.0, -17.0; 111.4, -21.0; 114.0, -16.4; 110.0, -14.4; 114.2, -14.3; 116.0, -20.4; 117.0, -20.4

Table B-1. - (Continued)

Sample Number	Sphalerite Type	Chip Number	Homogenization and Freezing Temperatures (°C)
27A1	massive	1	137.5, -21.6; 125.0, -22.0; 121.6, -21.2; 128.0, -22.5; 112.0, -22.5
38A1	massive	1	138.0, -23.2; 123.6, -23.3; 123.6, -22.0; 107.1; 102.6; 102.6; 102.5; 102.5; 110.0, -22.7; 111.0, -22.5; 110.7, -22.8; 111.0, -21.8
71A1	massive	1	99.5, -19.5; 99.5, -18.5; 99.5, -20.0; 101.5, -18.8; 101.0, -22.1; 101.8, -21.6; 94.5, -22.1; 93.0, -21.7; 105.0, -21.6; 105.8, -18.7; 105.6, -21.6; 106.3, -21.6
75A1	massive	1	106.5, -15.3; 112.3, -21.3; 113.7, -18.0; 112.5, -16.2; 113.7, -16.2; 113.6, -16.2; 113.6, -16.2; 113.4, -17.0; 111.6, -15.8; 105.2, -16.0
81A1	massive	1	103.0, -20.0; 100.1, -18.0; 100.0, -18.0; 101.4, -18.0; 107.0
2-45	massive	1	102.8, -22.7; 96.0, -22.7; 105.9, -22.7; 106.0, -22.1; 110.0, -22.2; 127.9, -22.1; 112.0, -22.2; 118.5, -22.2; 128.3, -23.5; 121.0, -22.0
2-49	vug	1	107.0, -22.1; 118.0, -22.4; 118.0, -22.4; 129.5, -21.7; 126.9, -23.0; 132.2, -22.7; 113.5, -22.5; 120.5, -22.9; 119.6, -21.9; 123.2, -22.5
2-63	massive	1	117.2, -21.7; 107.5; 125.0, -16.0; -22.0; 121.0, -22.5; -17.9
		2	121.4, -21.4; 127.0, -21.4; 120.0, -21.4; 121.2, -21.4; 116.0, -22.0; 116.0, -22.2; 123.0, -21.6; 123.0, -21.6
2-69	massive	1	117.0, -18.9; 125.0, -18.5; 125.4, -18.5; 125.0, -18.5; 140.0, -18.6; 152.7, -18.4; 145.0, -21.0; 150.0, -21.0; 118.5, -24.0; 117.5, -20.9

Table B-1. - (Continued)

Sample Number	Sphalerite Type	Chip Number	Homogenization and Freezing Temperatures (°C)
2-79	dissem	1	115.2, -18.5; 116.0, -18.5; 115.3, -18.4
2-81	dissem	1	110.4, -20.8; 109.5, -18.4; 133.3, -18.0; 110.0, -14.0; 112.0, -14.5; 108.5, -15.5; 108.5, -15.6; 108.5, -16.6
2-83	dissem	1	106.0, -20.6; 106.0, -19.8; 106.8, -17.2; 124.7, -20.0; 127.0, -17.8

Table B-2. Homogenization and Freezing Temperatures for Fluorite Samples from the Gordonsville Mine.

Sample Number	Fluorite Chip	Homogenization and Freezing Temperatures (°C)
55	1	105.3, -16.2; 102.7, -16.2; 115.0, -18.5; 113.4, -18.0; 103.9, -19.6; 103.8, -18.5; 111.6, -15.6; 112.2, -15.8; 109.0, -19.5; 110.1, -18.5; 106.8, -18.9
81	1	106.0, -18.5; 105.5, -18.2; 115.4, -20.7; 100.5, -15.9; 116.2, -15.1; 108.6, -4.0; 116.2, -15.1; 111.0, -16.5; 110.0, -19.4; 110.0, -16.5; 116.3, -14.6
	2	113.3, -21.4; 114.1; 115.3, -16.0; 115.3, -17.7; 115.3, -18.0; 115.3, -17.7; 116.1, -15.6; 116.3, -15.6; 115.1, -16.0; 116.1, -15.6
86	1	93.8, -21.5; 95.8, -21.9; 91.5, -21.5; 99.2, -21.7; 92.0, -22.0; 101.7, -22.0; 95.6, -21.8
38A1	1	103.6, -22.0; 99.7, -21.8
48A1	1	98.4, -22.1; 92.3, -22.7; 104.2, -20.8; 99.5, -20.7; 94.0, -21.9; -10.9; 102.2, -15.7; 102.0, -21.2; 113.7, -21.2; 103.2, -21.3; 103.2, -21.3; 109.5, -20.5
2-22	1	122.7, -18.0; 116.8, -17.8; 116.5, -18.0; 118.2, -18.1; 113.0, -17.7; 114.0, -18.0; 117.9, -18.0; 118.5, -18.0; 118.3; -17.9; -17.8; -17.9
	2	112.2, -17.0; 112.4, -17.0; 112.5, -17.0; 117.4, -18.2; 115.6, -18.5; 115.5, -18.2; 115.8, -18.0; 116.7, -18.4; 117.8, -18.0
2-31	1	105.5; 107.5; -19.3; 104.4, -19.7; 104.5, -21.1; 103.9, -19.4; 105.2, -19.4; 104.0, -18.1; 106.0, -19.6; 107.5, -21.5; 107.6, -21.5
	2	113.4, -21.7; 113.6, -21.7; 113.1, -22.0; 117.5, -21.6; 110.5, -23.0; 104.8, -21.0; 103.6, -21.4; 101.0, -21.2; 103.5, -21.8; 116.7, -22.3

Table B-2. - (Continued)

Sample Number	Fluorite Chip	Homogenization and Freezing Temperatures (°C)
2-50	1	113.9, -17.2; 116.4, -13.2; 120.4, -13.0; 106.7, -6.6; 112.4, -12.0; 114.0, -10.0; 116.2, -15.0; 115.3, -14.9; 116.5, -15.3; 116.6, -15.2
	2	118.5, -15.1; 117.6, -15.5; 118.6, -15.2; 117.6, -15.2; 117.9, -15.3; 117.2, -15.8
2-52	1	118.5, -15.3; 117.1, -15.2; 112.0, -17.5; 105.6, -19.2; 114.6, -15.6; 114.6, -15.6; 115.3, -15.2; 114.8, -15.2; 112.7, -15.2; 113.2, -15.0; 114.9, -15.0; 115.3, -15.0
	2	110.5, -14.6; 121.0, -14.6; 111.0, -13.9; 114.8, -12.4; 113.7, -12.4; 112.6, -14.9; 113.0, -14.9; 114.1, -14.9; 115.1, -14.4; 115.2, -14.2; 115.2, -15.6

Table B-3. Homogenization and Freezing Temperatures for Calcite Samples from the Gordonsville Mine.

Sample Number	Calcite Stage	Chip Number	Homogenization and Freezing Temperatures (°C)
E-1	early	1	84.4, -17.0; 106.5, -18.5; 80.3, -20.2; 86.2, -19.5; 96.0, -19.5; 102.6, -16.0; 91.2, -20.5; 92.2, -17.3; 93.0, -19.2; 106.0, -21.0; 102.0, -21.0; 100.0, -19.0; 105.0, -20.7; 106.0, -20.7; 95.4, -16.7; 96.0, -18.5; 102.3, -20.2; 102.9, -20.2; 103.4, -19.8; 98.9, -18.8
16	main	1	141.0, -19.2; 145.0, -18.5; 129.0, -20.7; 132.0, -20.0; 144.5, -20.7; 147.1, -22.7; 142.3, -20.4; 150.0, -20.2; 148.4, -20.6; 132.0, -19.9
12	main	1	119.7, -16.4; 136.0, -15.1; 112.8, -15.9; 144.5, -21.0; 116.0, -20.5; 122.0, -19.3; 136.0, -20.5; 136.0, -21.0; 147.2, -16.0; 115.5, -18.0
35	main	1	120.4, -21.7; 120.4, -22.0; 139.5, -8.2; 158.0, -22.0; 157.0, -21.7; 144.9, -22.0; 135.5, -22.0; 133.0, -22.0
2-3	main	1	115.0, -21.2; 115.0, -21.0; 116.0, -21.3; 105.0, -21.3; 120.9, -21.3; 110.0, -20.9; 110.7, -21.2; 115.0, -20.9
2-22	main	1	155.0, -20.6; 142.9, -22.0; 157.9, -21.5; 128.0, -21.8; 154.2, -22.0
2-70	main	1	122.0, -21.8; 134.0, -24.0; 126.0, -20.5; 132.0, -17.0; 121.5, -18.0; 147.0, -21.6; 145.0, -21.6; 117.1, -23.0; 158.0, -23.0; 160.0, -23.0
2-72	main	1	101.6, -18.2; 108.4, -18.2; 111.2, -5.6; 113.5, -19.8; 128.6, -20.0; 108.4, -20.0
		2	134.2, -21.1; 116.5, -20.9; 122.4, -20.9; 129.0, -20.9; 107.5, -4.2

Table B-3. - (Continued)

Sample Number	Calcite Stage	Chip Number	Homogenization and Freezing Temperatures (°C)
2-72	main	3	137.5, -20.7; 156.5, -20.2; 112.5, -20.2; 151.0, -19.5
3-13	main	1	128.0, -20.2; 150.4, -14.1; 142.5, -20.5; 143.0, -20.2; 133.0, -18.8; 127.7, -20.3
19	late	1	110.3, -6.0; 105.0, -3.2; 115.5, -4.4; 87.9, -4.4; 85.5, -3.2; 95.5, -9.3; 95.5, -2.3; 99.9, -4.4; 103.2, -4.5
74	late	1	83.2; 97.0; 95.4; 105.0; 110.5; 102.4; 76.5; 85.9; 97.2; 102.3; 84.5; 108.3; 90.7; 115.0; 104.2; 106.0
2-19	late	1	77.2, -5.6; 85.8, -5.2; 94.0, -5.4; 95.5, -5.8; 95.0, -5.4; 92.1, -5.4; 92.1, -8.1; 92.1, -6.2; 94.3, -6.2; 94.3, -6.3; 94.8, -7.0
		2	77.9, -5.0; 89.4, -5.2; 97.5, -5.8; 98.0, -5.0; 102.0, -5.0; 98.5, -5.1; 94.5, -5.0; 97.5, -5.9; 88.9, -6.0; 86.8, -6.8; 88.0, -5.8
		3	102.0, -3.7; 106.0, -3.8; 112.7, -3.7; 82.0, -4.0; 82.0, -4.0; 88.0, -3.5; 111.5, -5.0; 70.6, -3.9; 105.5, -6.3; 97.4, -4.8; 98.4, -4.0; 99.5, -3.9
2-28	late	1	86.8, -6.2; 72.1, -6.2; 105.5, -3.0; 105.5, -3.0
2-54	late	1	85.0, -3.5; 95.2, -2.5; 105.5, -2.5; 78.5, -2.5; 94.4, -3.0; 108.3, -2.2; 108.3, -2.2; 100.4, -2.2
75A2	late	1	-3.6; -3.6; -3.6; -5.0; -3.3; -4.8; -3.7
		2	-4.5; -5.0; 5.0; -5.0; -3.0

Table B-4. Homogenization and Freezing Temperatures for Barite Samples from the Gordonsville Mine.

Sample Number	Chip Number	Homogenization and Freezing Temperatures (°C)
7A	1	-4.3; -4.8; -4.8; -4.3; -5.0; -5.0; -5.0; -5.6; -5.6
25	1	-4.5; -3.0; -3.0; -3.0; -4.0; -6.5; -6.5
27	1	-7.8
36	1	-6.1; -6.1; -2.4; -5.6; -5.6; -6.5; -8.6; -8.6; -8.6; -9.1; -9.1; -8.2; -8.2; -4.7
53	1	-4.5; -4.6; -4.4; -4.5
2-36	1	125.0, -3.8; 122.3, -4.0; 125.9, -4.0; 120.5, -5.3; 122.0, -6.0; 118.8, -3.2; 116.7, -4.1; 120.3, -6.3; 116.0, -5.1
	2	-3.3; -3.3; -4.3; -3.1; -2.0; -2.0; -2.0; -2.8
2-46	1	-7.4; -7.2; -5.5; -7.0; -7.3; -8.0; -4.0
2-60	1	124.2, -8.0; 120.5, -8.0
	2	-8.2; -7.0; -7.0; -9.3; -11.8; -11.0; -8.5; -8.5
2-69	1	-4.0; -4.0; -7.6; -3.6; -5.0

APPENDIX C

Table C-1. Fluid Inclusion Sample Numbers, Mineral Type, and Stope Numbers for Samples from the Gordonsville Mine.

Sample Number	Mineral Type	Stope Number
23	massive sphalerite	58-5
25	massive sphalerite	58-5
31	vug sphalerite	58-5
41	vug sphalerite	34S
62	massive sphalerite	28-2
68	vug sphalerite	73-5
75	massive sphalerite	73-5
27A1	massive sphalerite	58-5
38A1	massive sphalerite	34S
71A1	massive sphalerite	73-5
75A1	massive sphalerite	73-5
81A1	massive sphalerite	73-5
2-45	massive sphalerite	10N
2-49	vug sphalerite	10N
2-63	massive sphalerite	34-6
2-69	massive sphalerite	34-6
2-79	dissem sphalerite	40A
2-81	dissem sphalerite	40A
2-83	dissem sphalerite	40A
55	fluorite	31-3
81	fluorite	73-5
86	fluorite	73-5
38A1	fluorite	34-5
48A1	fluorite	31-3
2-22	fluorite	58-2
2-31	fluorite	73-5
2-50	fluorite	10N
2-52	fluorite	10N
E-1	early calcite	Elmwood
12	main-stage calcite	67
16	main-stage calcite	67
35	main-stage calcite	34S
2-3	main-stage calcite	58-2
2-22	main-stage calcite	58-2
2-70	main-stage calcite	34-6
2-72	main-stage calcite	34-6
3-13	main-stage calcite	29S
19	late-stage calcite	67
74	late-stage calcite	03-S
2-54	late-stage calcite	10N
2-19	late-stage calcite	58-2
2-28	late-stage calcite	73-5

Table C-1. - (Continued)

Sample Number	Mineral Type	Stope Number
75A2	late-stage calcite	03-S
7A	barite	67
25	barite	58-5
27	barite	58-5
36	barite	34-13
53	barite	31-3
2-36	barite	73-5
2-46	barite	10N
2-60	barite	34-6
2-65	barite	34-6

APPENDIX D

Table D-1. Microprobe Analyses (wt. %) of Traverses Across Sphalerite Samples from the Gordonsville Mine.

Sample/ Traverse/Point	Color	Fe	Zn	S	Cd	Fe/Cd
18-1-1	orange	.22	65.48	32.89	.08	2.75
18-1-2	orange	.27	66.77	33.33	.17	1.59
18-1-3	white	.43	65.66	33.33	.60	0.72
18-1-4	white	.36	66.50	32.97	.69	0.52
18-1-5	white	.44	65.88	32.73	.55	0.80
18-1-7	orange	.17	66.29	32.97	.21	0.81
18-1-8	orange	.28	66.43	33.27	.14	2.00
18-2-1	yellow	.41	66.69	33.50	.09	4.56
18-2-2	yellow	.18	66.13	33.52	.14	1.29
18-3-1	orange	.27	66.07	32.59	.30	0.93
18-3-2	orange	.27	65.70	32.90	.21	1.29
18-3-4	white	.38	65.81	33.20	.46	0.83
18-3-5	white	.39	65.08	33.16	.53	0.74
18-3-7	orange	.22	66.96	32.97	.05	4.40
18-4-1	orange	.25	66.04	32.59	.16	1.56
18-4-2	orange	.25	66.49	33.46	.00	--
18-4-3	white	.40	65.88	33.25	.47	0.85
18-4-4	white	.32	66.48	33.04	.52	0.62
18-4-5	yellow	.20	66.09	33.33	.00	--
18-4-6	orange	.25	66.78	33.07	.18	1.39
18-5-1	orange	.18	66.60	33.32	.06	3.00
18-5-2	orange	.27	67.02	33.05	.14	1.93
18-5-3	white	.46	66.46	33.64	.50	0.92
18-5-4	white	.40	65.79	33.13	.55	0.73
18-5-5	white	.53	65.51	32.96	.70	0.76
18-5-6	orange	.19	65.88	33.66	.04	4.75
18-5-7	orange	.29	66.53	33.64	.21	1.38
18-5-8	orange	.29	67.29	33.50	.05	5.80
18-6-1	orange	.27	66.16	33.93	.11	2.45
18-6-2	orange	.28	66.53	33.62	.08	3.50
18-6-3	white	.38	66.44	33.12	.62	0.61
18-6-4	white	.50	66.70	33.41	.68	0.74
18-6-5	white	.40	66.30	33.43	.63	0.63
18-7-1	orange	.29	66.82	33.66	.00	--
18-7-2	orange	.23	67.63	33.31	.27	0.85
18-7-3	white	.45	66.62	33.29	.57	0.79
18-7-4	white	.40	66.47	33.40	.63	0.63

Table D-1. (Continued)

Sample/ Traverse/Point	Color	Fe	Zn	S	Cd	Fe/Cd
18-7-5	white	.49	65.22	33.63	.63	0.78
18-7-6	white	.40	66.30	33.54	.70	0.57
18-7-7	orange	.24	66.73	33.23	.18	1.33
18-7-8	orange	.31	66.46	33.16	.00	--
41-1-2	yellow	.17	66.41	33.24	.00	--
41-1-4	orange	.18	67.09	31.53	.10	1.80
41-1-5	orange	.21	68.70	31.09	.00	--
41-1-6	yellow	.38	67.50	31.14	.30	1.27
41-1-7	white	.32	68.60	31.67	.37	0.86
41-2-1	yellow	.16	67.30	31.64	.04	4.00
41-2-3	yellow	.23	68.75	31.69	.27	0.85
41-2-4	orange	.25	67.30	31.10	.00	--
41-2-5	orange	.24	66.90	30.80	.04	6.00
41-2-6	yellow	.39	65.72	30.22	.20	1.95
41-2-7	yellow	.34	66.79	30.87	.15	2.27
41-3-2	white	.22	67.98	33.04	.47	0.47
41-3-3	white	.14	66.43	33.04	.36	0.39
41-3-4	white	.31	66.48	32.85	.48	0.65
41-3-5	orange	.44	66.57	33.36	.50	0.88
41-3-6	orange	.36	66.82	33.46	.36	1.00
41-4-1	yellow	.21	67.33	32.84	.00	--
41-4-2	white	.30	66.86	33.29	.52	0.58
41-4-3	white	.23	66.25	33.43	.29	0.79
41-4-4	yellow	.26	66.72	33.27	.20	1.30
41-4-5	orange	.20	66.50	33.41	.15	1.33
41-5-1	orange	.23	65.23	32.93	.20	1.15
41-5-2	yellow	.34	67.25	33.09	.27	1.26
41-5-4	orange	.35	66.93	32.89	.20	1.75
41-6-2	yellow	.20	66.70	33.53	.11	1.82
41-6-3	orange	.24	66.95	33.11	.00	--
41-6-4	orange	.16	66.87	33.09	.17	0.94
41-6-5	yellow	.27	68.45	32.40	.12	2.25
41-6-6	yellow	.17	67.14	33.12	.00	--
41-6-7	orange	.18	67.72	32.88	.05	3.60
41-7-2	yellow	.25	66.27	33.31	.00	--
41-7-3	yellow	.26	67.38	32.78	.28	0.93
41-7-4	yellow	.21	67.27	32.94	.00	--

Table D-1. (Continued)

Sample/ Traverse/Point	Color	Fe	Zn	S	Cd	Fe/Cd
23-1-1	orange	.25	67.12	32.39	.08	3.12
23-1-1'	orange	.25	67.75	32.82	.00	--
23-1-2	yellow	.20	66.02	32.20	.15	1.33
23-1-3	white	.34	63.82	32.76	.37	0.89
23-1-3A	white	.31	65.09	32.42	.42	0.76
23-1-4	orange	.27	66.38	32.87	.15	1.80
23-2-1	white	.41	67.32	31.23	.36	1.14
23-2-2	yellow	.37	66.11	32.46	.60	0.62
23-2-3	orange	.26	66.34	32.54	.36	0.72
23-2-4	orange	.32	65.84	32.63	.28	1.14
23-2-5	orange	.34	66.41	32.46	.28	1.21
23-3-1	orange	.42	66.14	31.48	.50	0.84
23-3-1'	white	.39	67.14	31.99	.57	0.68
23-3-2	yellow	.45	67.09	31.26	.54	0.83
23-3-3	yellow	.39	66.59	32.11	.62	0.63
23-3-4	orange	.41	66.87	31.41	.47	0.87
23-4-1	orange	.23	67.47	31.90	.05	4.60
23-4-2	white	.32	66.66	32.11	.63	0.51
23-4-3	yellow	.25	66.29	31.78	.13	1.92
23-4-4	orange	.26	66.71	32.74	.00	--
23-5-1	white	.38	66.58	31.61	.63	0.60
23-5-1'	yellow	.33	67.45	31.59	.41	0.80
23-5-2	white	.25	67.24	32.17	.51	0.49
23-5-2'	orange	.25	67.22	31.62	.36	0.69
23-5-3	orange	.20	67.34	32.18	.20	1.00
23-5-R	white	.38	66.57	31.75	.76	0.54
23-5-R	white	.39	66.35	32.13	.54	0.72
23-5-R	white	.33	66.84	31.82	.40	0.77
23-5-R	orange	.23	66.18	32.20	.03	7.67

VITA

Jeffrey Farrell Gratz was born in Chicago, Illinois on June 6, 1961. He attended grade school in Miami Beach, Florida and graduated from Miami Beach Senior High School in June 1979. The following September he entered Colgate University in Hamilton, New York. In May 1983 he received a Bachelor of Arts degree in Geology. In the fall of 1983 he began study toward a Master of Science degree in Geology at The University of Tennessee, Knoxville. This degree was awarded in March 1986.